Università degli Studi di Ferrara

DOTTORATO DI RICERCA IN
MEDICINA MOLECOLARE E FARMACOLOGIA

CICLO XXXI

COORDINATORE Prof. Di Virgilio Francesco

STUDY ON THE INTERACTION BETWEEN LRRK2 G2019S MUTATION AND PARKINSONIAN RISK FACTORS

Settore Scientifico Disciplinare BIO/14

Dottorando
Dott. Novello Salvatore

Tutore
Prof. Morari Michele

Anni 2015/2018

“I won't be impressed with science until I can download a waffle.”

-Sean Gabay

ABSTRACT

Parkinson's Disease (PD) is a neurodegenerative disorder characterized by the loss of dopaminergic neurons in the Substantia nigra pars compacta (SNc) and the presence of intracytoplasmic aggregates of α-synuclein, named Lewy Bodies. Mutations in the LRRK2 gene are the most common cause of late-onset autosomal dominant Parkinson's Disease (PD), with the G2019S being the most prominent reported. LRRK2-related PD patients are clinically indistinguishable from idiopathic PD patients, and presents an incomplete penetrance, a variable age of onset and a heterogeneous pattern of symptoms, suggesting that the increased kinase activity induced by the pathogenic LRRK2 mutations could not alone account for the clinical expression of this disorder. In keeping with clinical data, rodent models of LRRK2-associated PD lack a consistent parkinsonian phenotype, since in vast majority of studies they do not show overt degeneration of the nigrostriatal pathway or deposition of pathological α-syn aggregates. Therefore, genetic and environmental factors influencing LRRK2 penetrance and expressivity are an appealing field of research which can provide new insights into the etiology of PD. The main objective of this thesis was to investigate the interaction between the LRRK2 G2019S mutation and other risk factors of PD, such as ageing, environmental toxins and α-synuclein (α-syn). To achieve this goal, we employed LRRK2 G2019S Knock-in (KI) mice, which carry this mutant form of LRRK2 with the same levels of expression and brain distribution pattern of LRRK2 WT mice. We first sought to investigate the role of ageing in the dysfunctions of the nigro-striatal DA transmission associated with LRRK2 G2019S (Study I). Using a combination of ex vivo and in vivo experiments, we reported that aged (>12 month) G2019S KI mice display DAT and VMAT2 alterations, both in terms of protein levels and function, alongside an increase in levels of endogenous α-syn and its Serine129 phosphorylated form. In the second study of this thesis (Study II), we aimed to investigate the interplay between G2019S LRRK2 and A53T α-syn during ageing. Young (3-month-old) and aged (12-month-old) G2019S KI mice were injected in SNc with a recombinant adeno-associated viral vector (AAV) serotype 2/9 overexpressing the human A53T α-syn or green fluorescent protein (GFP) under the synapsin 1 promoter. We evaluated the motor phenotype and the neuropathology associated with α-synuclein overexpression, and assessed microglia morphology as a gross marker of neuroinflammation. G2019S LRRK2 did not worsen α-synucleinopathy in 3-month-old G2019S KI mice compared to WT mice, whether aged (12-month-old) G2019S KI displayed a greater reduction of the number of SNc dopaminergic neurons and an increased number of Proteinase K-resistant α-syn aggregates compared to WT mice. No impact of α-synuclein overexpression on microglia morphology was observed 3 months after virus injection. In the third part of this thesis (Study III), we investigated whether the increased LRRK2 kinase activity associated with the G2019S mutation alters the susceptibility to the parkinsonian neurotoxicant MPTP, which impairs the mitochondrial complex I and selectively destroys dopaminergic neurons. Under a subacute protocol of administration, MPTP was given to 3-month-old WT mice, to mice constitutively lacking LRRK2 (LRRK2 KO), to mice expressing the kinase-

dead mutation D1994S (KD) or the kinase enhancing mutation G2019S (G2019S KI). We found that the augmented kinase activity conferred by the LRRK2 G2019S mutation, increases mice susceptibility to MPTP, as shown by the greater number of nigro-striatal neuron degenerated after toxin administration, an effect which is accompanied by a greater number of striatal microglial cells. We then proceeded to test the neuroprotective properties of two kinase inhibitors, i.e. PF-06447475 and MLi-2. Once again, we concluded the study by assessing microglial number and morphology. Both compounds were able to rescue the increased susceptibility of G2019S KI mice to MPTP by enhancing the number of spared nigro-striatal dopamine neurons, although only MLi-2 was able to protect also striatal terminals. In striatum, different patterns of microglial morphology were induced by the two inhibitors, since only PF-06447475 was able to normalize the microglia number in in G2019S KI mice being MLi-2 ineffective. The present thesis provides novel information on the role of G2019S LRRK2 in experimental parkinsonism and possibly, PD etiopathogenesis, in particular replicating in a genetic model of PD the positive interaction of LRRK2 G2019S mutation with genetic (α-syn), physiological (aging) or environmental (MPTP) risk factors in PD. This study confirms the neuroprotective potential of LRRK2 inhibitors, strengthening the view that the increased kinase activity associated with the LRRK2 G2019S mutation is instrumental for LRRK2 toxicity. Finally, the present work supports the view that G2019S KI mice represent a model for presymptomatic/premotor PD, useful to study the interaction between genetic, intrinsic and environmental factors, or in other words, the interplay between “triggers, facilitators and aggravators” in the pathogenesis of PD.

Table of content

INTRODUCTION

Genetics of Parkinson's Disease

Differently from other neurodegenerative disorders, Parkinson's disease (PD) was believed to be a pathology without a genetic basis. This misconception was changed thanks to studies of molecular genetics seeking a genetic cause in different families in which PD followed a recessive or dominant inheritance pattern (Golbe et al., 1990). The turning point was reached in 1997 at the National Institute of Health in Bethesda (USA), where Polymeropoulos and colleagues identified PD-associated point mutations in the SNCA gene, encoding for the protein α-synuclein (α-syn) (Polymeropoulos et al., 1997). This study set the basis for further genetic studies in PD. This first key discovery led to the identification of mutations in genes linked to rare recessive forms of early-onset PD (EOPD), such as PARKIN, PINK1 and DJ-1 (Kitada et al., 1998, Valente et al., 2001, Bonifati et al., 2003). In 2004, two different group of studies identified that mutations in the *LRRK2* gene were cause of autosomal dominant PD (Paisan-Ruiz et al., 2004, Zimprich et al., 2004). As of today, 23 different loci and 19 genes have been linked to the disease (Fig.1), with 10 being autosomal dominant and 9 autosomal recessive (Deng et al., 2018).

Locus	Location	Gene	Protein	Inheritance
PARK1	4q22.1	SNCA	α-synuclein	AD
PARK2	6q26	PRKN	Parkin	AR
PARK3	1p13	PARK3 (Unclear)	Unclear	AD
PARK4	4q22.1	SNCA	α-synuclein	AD
PARK5	4p13	UCHL1	UCHL1	AD
PARK6	1p36	PINK1	PTEN induced putative kinase 1	AR
PARK7	1p36.23	PARK7	Parkinsonism associated deglycase	AR
PARK8	12q12	LRRK2	Leucine-rich repeat kinase 2	AD
PARK9	1p36.13	ATP13A2	ATPase 13A2	AR
PARK10	1p32	PARK10		Unclear
PARK11	2q37.1	GIGYF2		AD
PARK12	Xq21-q25	PARK12 (Unclear)		X-linked inheritance
PARK13	2p13.1	HTRA2		AD
PARK14	22q13.1	PLA2G6		AR
PARK15	22q12.3	FBX07		AR
PARK16	1q32	PARK16		Unclear
PARK17	16q11.2	VPS35		AD
PARK18	3q27.1	EIF4G1		AD
PARK19	1p31.3	DNAJC6		AR
PARK20	21q22.1	SYNJ1		AR
PARK21	20p13	TMEM230		AD
PARK22	7p11.2	CHCHD2		AD
PARK23	15q22.2 11p14.4	VPS13C RIC3		AR AD

Fig. 1: List of all known loci linked to PD with chromosomal location, name of the related gene, transcript and clinical phenotype associated with it. AR= autosomal recessive, AD= Autosomal dominant.

SNCA (PARK1/4)

Identification and mapping

In 1993, Ueda and colleagues described the second major peptidic component of amyloid plaques in Alzheimer's disease and named it NAC (non-Amyloid-β component) (Ueda et al., 1993). Subsequent studies were able to link the precursor of this protein to a class of protein highly enriched in the human brain maned synucleins (Chen et al., 1995). The term "synuclein" was coined by Maroteaux and collaborators, upon identification of a class of proteins located mostly in presynaptic endings and nuclei of the *Torpedo californica* and rat brain (Maroteaux et al., 1988). In 1996, Polymeropoulos and colleagues located a locus on the long arm of chromosome 4 linked to PD inheritance in an Italian family from Contursi Terme (Polymeropoulos et al., 1996). The following year, the same group identified the A53T point mutation in the SNCA gene (Polymeropoulos et al., 1997). At the same time, the group of MG Spillantini reported α-syn as the major component of Lewy bodies (LB), intracellular inclusions characteristic of PD brain (Spillantini et al., 1997) . The two alleles of the SNCA gene, PARK1 and PARK4, are located on chromosome 4q21.3-q22. PARK1 mutations have been linked to point mutations of α-syn, whereas PARK4 mutations are attributable to gene duplication or triplication. SNCA comprises six exons, the translational initiation codon is situated in exon 2, whereas the TAA stop codon can be found on exon 6. The full-length transcript is a 140-amino acid protein. Truncated transcripts have also been found. These minor isoforms, named NACP112, NACP126 and NACP98, are produced via alternative splicing of exon 3, exon 5 or both (Xia et al., 2001).

Protein Structure

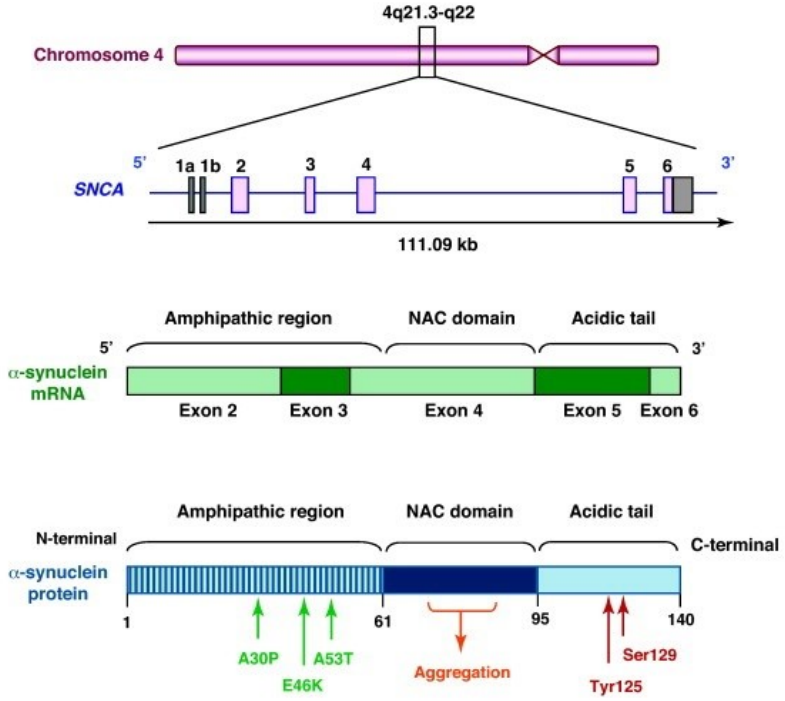

Fig. 2: Chromosomal localization of PARK1/4 loci, gene, mRNA and protein structure of α-synuclein. α-synuclein is a 140-aminoacid protein with an amphipathic region, an acidic tail and a central NAC domain. Common mutations occur in the amphipathic region of the protein, whereas post-translation modifications are located in the C-terminal region. Figure taken from (Venda et al., 2010).

Three regions form the α-syn protein: a N-terminal amphipathic region, a central hydrophobic domain and a C-terminal acidic tail. The N-terminal domain is composed of 61 residues and contains the highly conserved KTKEGV hexameric lipid-binding motif, similar to that found in the α-helical domain of apolipoproteins. This region can form amphiphilic α-helices which are able to bind cellular membranes. Residues from 61 to 95 are referred to as the NAC (Non Amyloid-β Component) domain, which confers the protein the ability to form β-sheets and may play a role in pathological aggregation of α-syn (Pfefferkorn et al., 2012). The C-terminal domain (residues 95-140) is a glutamate-rich region, which confers a negatively charged potential and, in addition to its low hydrophobicity, the tendency of this region to form a random coil structure. Furthermore, the acidic tail of α-syn is homologous with small heat shock proteins (HSPs), suggesting a protective role for α-syn in regulating the degradation process of certain proteins (Kim et al., 2004). The importance of the tertiary structure of α-syn becomes evident when considering its neurotoxic potential, although once again, reports are contrasting. The most widely accredited hypothesis describes the protein in equilibrium between a monomeric and oligomeric form (Burre et al., 2015). Under physiological conditions, unfolded monomeric α-syn assembles into more elaborate structures such as tetramers and protofibrils (Lashuel et al., 2002). If these forms are not rapidly degraded, they may lead to formation of highly neurotoxic mature fibrils. These complexes exert their toxic activity by binding to membranes and altering their integrity, or by destabilizing

proteostasis (Pieri et al., 2016). Furthermore, recent studies have suggested that fibrillar misfolded α-syn can spread cell-to-cell in a prion-like fashion and seed the aggregation of endogenous α-syn in healthy neurons, thus promoting cell death (Paumier et al., 2015).

Localization and function

α-syn is predominantly expressed in the brain and can be detected primarily in the substantia nigra (SN), hippocampus, globus pallidus, olfactory bulb and dorsal motor nucleus of the vagus (Taguchi et al., 2016). Still very little is known about α-syn physiological functions, despite the protein has been linked to a variety of activities, from neuronal differentiation to maintenance of polyunsaturated fatty acid levels, the most widely recognized being the regulation of neurosecretion and vesicle trafficking. In fact, through its chaperone activity, α-syn promotes the assembly and disassembly of the SNARE complex (composed by syntaxin-1, SNAP-25 and synaptobrevin-2) by interacting directly with the protein synaptobrevin-2 (Burre et al., 2010, Burre et al., 2014). In addition, α-syn has been implicated in the enhancement of vesicle clustering by inhibiting SNARE-mediated vesicle fusion and stabilizing docked vesicles at the presynaptic membrane (Larsen et al., 2006, Lai et al., 2014). Another interesting putative role of α-syn involves dopamine (DA). Indeed, synuclein negatively regulates short-term release of DA from synaptic vesicles, thus increasing the turnover of the DA pool (Abeliovich et al., 2000). Furthermore, α-syn controls the cytosolic levels of DA by interacting directly with the membrane DA transporter, DAT (Lee et al., 2001, Fountaine and Wade-Martins, 2007). A putative role of α-syn in mitochondrial function has also been proposed based on the finding that α-syn colocalizes at mitochondria-associated endoplasmic reticulum membrane (Guardia-Laguarta et al., 2014). Indeed, different studies consistently reported that α-syn effects mitochondrial calcium homeostasis by facilitating the physical interaction between the endoplasmic reticulum (ER) and mitochondria, (Cali et al., 2012, Guardia-Laguarta et al., 2014, Paillusson et al., 2017). Nonetheless, not all studies confirmed this finding (Paillusson et al., 2017). Endogenous α-syn has also been shown to be required for the normal activity of the respiratory chain complexes (Devi et al., 2008), its expression directly affecting mitochondrial fission (Nakamura et al., 2011). Similar studies showed that the A53T aberrant form induces mitochondrial fragmentation even at low levels (Pozo Devoto et al., 2017).

Mutations and toxicity

Genetic screenings of a large family from a village in south-western Italy, Contursi Terme, led to the identification of a point mutation in the SNCA gene, responsible for the onset of autosomal-dominant PD. All members of the Contursi kindred present a single base pair mutation at position 209 (from guanine to adenosine G209C), resulting in an alanine to threonine substitution in position 53 (A53T) (Polymeropoulos et al., 1997). In the last two decades many more mutations were identified such as:

- A guanine to cytosine substitution in position 88, resulting in an alanine to proline replacement as the 30th amino acid (A30P) in a German family (Kruger et al., 1998).
- A substitution of a guanine to an adenosine in the 152nd base pair, switching a glycine to an aspartate in position 51 (G51D), in four members of a French family (Lesage et al., 2013).
- A guanine to adenosine change in the 136th base pair, causing the exchange of a lysine with a glutamic acid in position 46 (E46K) in a Spanish family (Zarranz et al., 2004).
- A substitution of a histidine to glutamine at the 50th amino acid (H50Q), due to a replacement of a thymine to a guanine in position 150 (Proukakis et al., 2013).

Although the underlying mechanism remains to be elucidated, α-syn mutants display a greater propensity to form aggregates when compared to wild type (WT) forms (Flagmeier et al., 2016). Different studies showed that A53T, E46K and H50Q mutants display an accelerated rate of fibrillization in vitro (Conway et al., 1998, Narhi et al., 1999). This may be due to the fact that mutated α-syn lacks long-range interaction between the NAC domain and the flanking regions, translating into a higher inclination to form β-sheet structures and amyloid protofibrils (Coskuner and Wise-Scira, 2013). In contrast, it has been reported that other pathogenic mutations such as A30P, G51D and A53E, decrease the fibrillization rate of α-syn (Li et al., 2001, Fares et al., 2014, Ghosh et al., 2014). This discrepancy could be explained by the increased capability of the aberrant forms to form pre-fibrillar oligomers which are thought to be more toxic than fibrils derived from monomers (Winner et al., 2011). Furthermore, α-syn oligomers undergo continuous conformational changes and become more stable, compact and resistant to proteinase-K, inducing a higher degree of oxidative stress, before becoming fibrils (Cremades et al., 2012). The hypothesis that α-syn oligomers are more toxic than downstream fibrils is also supported by the evidence that injection of α-syn variants promoting oligomers formation as opposed to fibril formation into the rat brain causes a more severe degree of neurodegeneration (Winner et al., 2011). However, it has recently been shown that injection of human α-syn fibrils into the rat substantia nigra pars compacta (SNc) induces greater motor impairment along with a more severe nigro-striatal dopaminergic denervation (Peelaerts et al., 2015). Another interesting point is the possibility that there may exist different strains of α-syn which express different degree of aggregation and toxicity. The generation of these strains may be due to the various conformational states that monomeric α-syn can adapt following changes in physical-chemical conditions (pH, viscosity, ionic strength, and nature of ions, etc.)(Uversky, 2003). Each conformational variant of α-syn monomer exposes specific amino acid stretches that govern its ability to establish defined sets of intermolecular interactions. Such interactions lead to assemblies that display different intrinsic structures and have distinct amino acid exposed at their surfaces. The intermolecular interactions that stabilize α-syn monomers within the aggregate confer the ability of given α-syn assembly to incorporate additional monomers in a thermodynamically stable manner, and to grow in size. Importantly, the different

amino acid stretches exposed influence the partner proteins, receptors and lipids a given α-syn strain will interact with, also dictating its seeding propensity, resistance to cellular degradation, cytotoxicity and tropism for different cell subtype in the central nervous system (CNS). It then becomes evident that this can result in highly specific pathological and physiological properties of certain α-syn assembly. Although the debate about which form of α-syn is the most toxic still remains open, various pathways of α-syn toxicity have been proposed (Wang et al., 2014, Pozo Devoto et al., 2017) (Hoenen et al., 2016). Among these pathways, the impairment of synaptic-vesicle trafficking deserves special consideration. Large α-syn oligomers preferentially bind VAMP2 and disrupt SNARE complex assembly, thus impacting neurotransmitter release and synaptic-vesicle motility (Choi et al., 2013, Wang et al., 2014). Similar results are also achieved through the upregulation of α-syn expression (Nemani et al., 2010), which leads to a reduction in DA reuptake, DAT dysfunction, and ultimately, disrupting of DA turnover (Lundblad et al., 2012). In accordance with the recent hypothesis of mitochondria dysfunction being instrumental for PD onset, it has been suggested that α-syn toxicity might directly impact on mitochondrial homeostasis. This theory is supported by the finding that mice expressing the A53T mutant display increased mitochondrial DNA damage and mitophagy (Choubey et al., 2011, Chen et al., 2015). It is also possible that mitochondrial dysfunction is indirectly induced by α-syn via decreased levels of the mitochondrial biogenesis factor PGC-1α (Zheng et al., 2010) or by disrupting the interaction between this organelle and the ER. As a matter of fact, α-syn has been reported to alter the number of mitochondria-associated ER membrane (MAM), a subdomain of the ER tethered to mitochondria via a group of adaptor proteins which serve as a critical site for autophagosome biogenesis, mitochondrial fission and calcium homeostasis (Cali et al., 2012, Guardia-Laguarta et al., 2014). α-syn expression also disrupts endosomal trafficking and induces ER stress and early secretory-pathway dysfunction (Cooper et al., 2006). Perhaps one of the most widely accepted theory points to autophagy as the main factor behind α-syn toxicity. Indeed, α-syn overexpression alters the trafficking of the autophagic transmembrane protein ATG9, thus impacting the biogenesis of the autophagosome (Winslow et al., 2010). In addition, oligomeric and aberrant forms of α-syn, such as A53T and A30P, bind the lysosomal receptor LAMP2A more tightly than the WT form, thus preventing their own import inside the lumen of the lysosome and blocking cargo loading of other chaperone mediated autophagy (CMA) substrates (Cuervo et al., 2004). Furthermore, DA-modified forms of α-syn, such as DOPAL-bound α-syn or nitrated α-syn, also block CMA activity, which might explain the selective dopaminergic vulnerability in PD (Martinez-Vicente et al., 2008). Finally, an abundance of α-syn negatively impacts on lysosomal enzymatic activity, dampening the activity of glucocerebrosidase (GCase), cathepsin B, β-galactosidase and hexosaminidase (Mazzulli et al., 2011, Mazzulli et al., 2016, Wong and Krainc, 2016). It is possible that all these numerous pathways could contribute to the pathogenesis of PD in different moments of disease progression, with some appearing early on, i.e. in a presymptomatic

stage, and others later, in a symptomatic or complicated stage. Moreover, different pathways might be recruited to compensate for dysfunctions occurring in other compartments. With this concept in mind, in 2003, Hugo Braak and colleagues, based on the postmortem analysis of LB patterns in PD brains, proposed a staging of α-syn pathology into six phases. According to this theory, early pathology affects low brainstem nuclei and correlates with appearance of non-motor symptoms such as olfactory dysfunction, depression or REM sleep disturbances (Braak stages 1 and 2). Then the degeneration invades the mesencephalic SNc (stages 3-4) causing the onset of the classical motor symptoms (Braak et al., 2003a), and finally enters the telencephalic areas causing severe cognitive deficits and mood changes. Subsequently, Braak and colleagues developed a theory in which olfactory and gastric mucosae might be used by an unknown pathogen as entry routes to gain access to the central nervous system (CNS) and spread across the neuronal population (Braak et al., 2003b). Such pathogen was hypothesized to be composed of fragments of misfolded α-syn which infiltrates in the gut to the submucous plexus, travels trans-synaptically along the preganglionic parasympathetic fibers to the dorsal motor nucleus of the vagus nerve. Alternatively, α-syn fragments might reach the CNS via the olfactory epithelium and reach the olfactory bulb. Both the olfactory bulb and the dorsal motor nucleus of the vagus nerve where hypothesized by Braak and colleagues to be the initiation sites of the pathology in their first work.

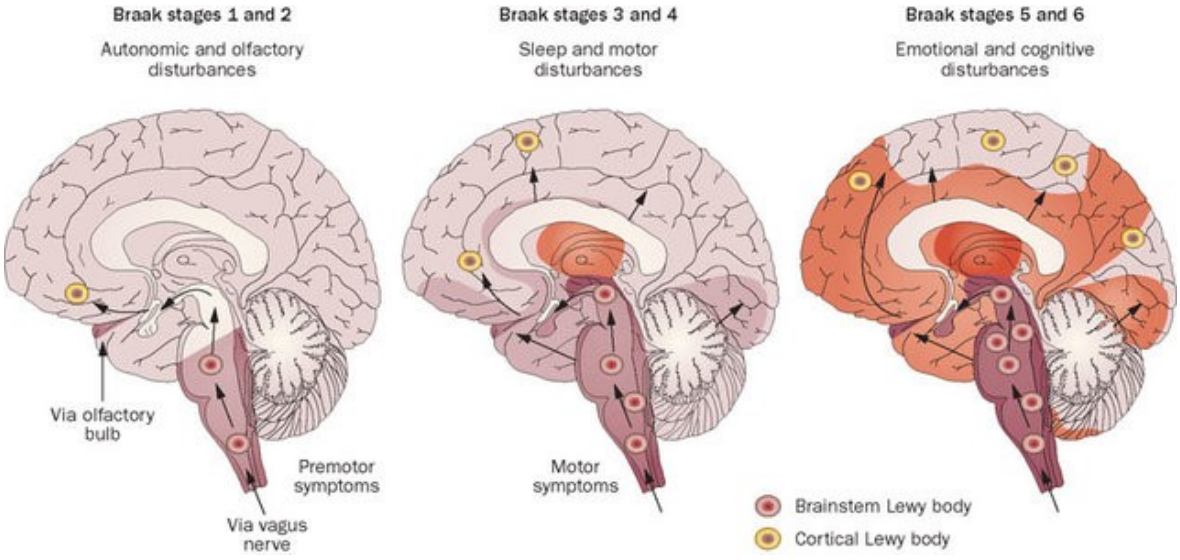

Figure 3: Schematic representation of α-syn staging postulated by Braak and colleagues. α-syn reaches the CNS via the vagus nerve and start to affect the brainstem nuclei and the olfactory bulb (Stage 1 and 2) with clinical manifestations only accountable to premotor symptoms such as autonomic alterations and anosmia. In Braak stage 3 and 4, α-syn aggregates reach the mesencephalon and motor symptoms, together with sleep behavior alterations, start to occur. In the late stage (5 and 6), LBs reach a whole brain localization, also affecting cortical areas, reaching the peak of symptoms manifestations. Figure taken from Petersen and collaborators.

This theory fueled the idea that α-syn spreading might follow a prion-like mechanism, an idea that found an apparent confirm a few years later when it was reported that 2-5% of healthy human foetal midbrain neurons therapeutically grafted into the striata of patients with advanced PD

developed Lewy pathology (Kordower et al., 2008). One of the main features of prions, acronym for proteinaceous infecting particles, is the ability to propagate both intercellularly and from organism to organism. Although there is no evidence that α-syn can transfer from one individual to another, hence the use of the term "prion-like", various works described the capability of α-syn to spread from cell to cell. Indeed, it has been demonstrated that after oligomerization, α-syn assemblies are released in the extracellular space via vesicles or through passive exocytosis and interact with membranous proteins which promote their uptake (Shrivastava et al., 2015, Mao et al., 2016). Once inside the cell, α-syn oligomers act as seeds, triggering the aggregation of endogenous cytosolic α-syn, through a yet unknown process. Then, they are transported anterogradely or retrogradely along the axon and directed mostly to the lysosomes (to be degraded) or to release areas thus spreading to anatomically connected areas (Lee et al., 2008, Lee et al., 2010a, Reyes et al., 2015).

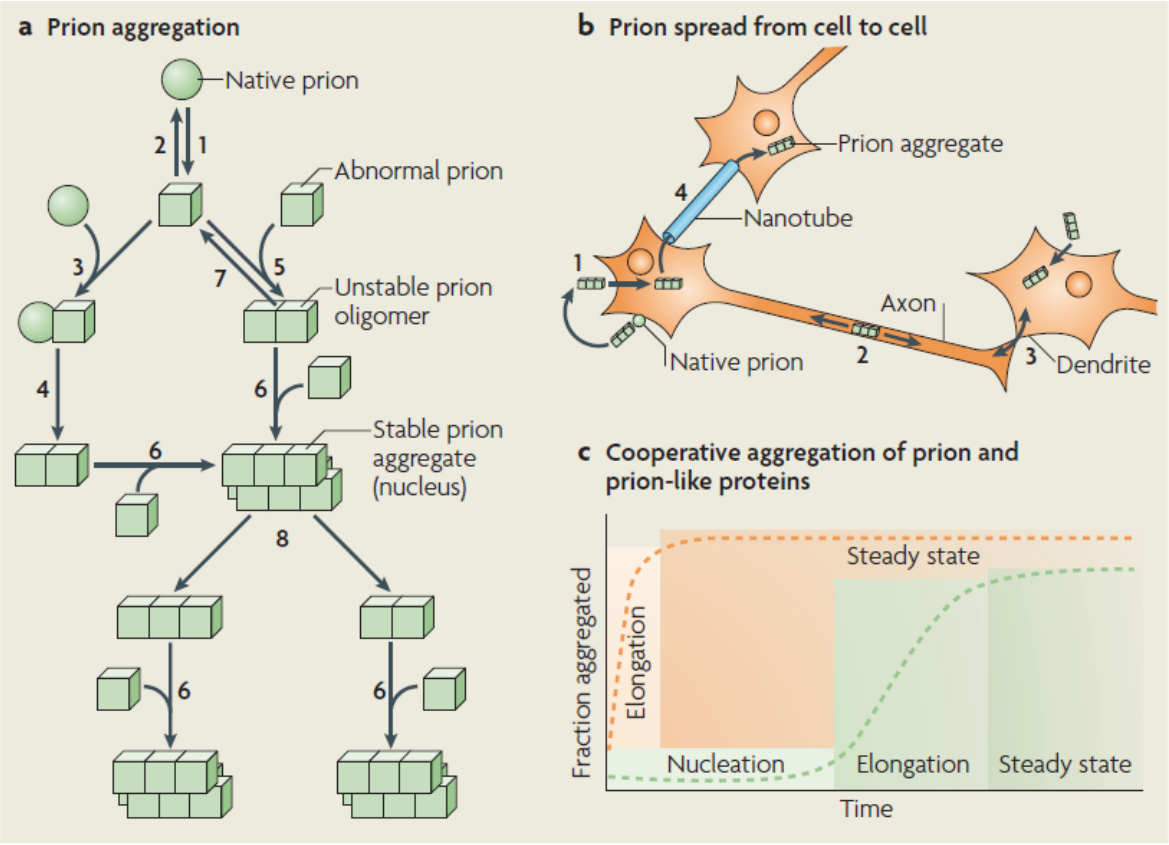

Fig. 4: Schematic representation of prion aggregation, aggregation states and cell-to-cell spreading. Picture taken form (Brundin et al., 2010)

To confirm this view, injections of preformed α-syn fibrils into the striatum lead to the generation of α-syn aggregates, with subsequent neurodegeneration of SN dopaminergic neurons that project to the striatum. Furthermore, the hypothesis that misfolded α-syn might prime and destabilize other strains of α-syn to trigger aggregation is supported by the evidence that injection of preformed fibrils does not trigger α-syn pathology in α-syn-null mutant mice (Luk et al., 2012). It is also

important to note that α-syn can spread beyond synaptic connections and anatomical pathways, suggesting that non-synaptic propagation mechanisms might exist (Sacino et al., 2014). One possible mechanism of diffusion involves circulating glial cells. For instance, aggregated tau, like α-syn, can be carried by microglia and transduced into cells in far areas, promoting aggregated protein propagation (Asai et al., 2015). Furthermore, this effect is reverted after depletion of microglial cells. Although direct evidence is still lacking, a role of microglia and other immune cells in a periphery-to-CNS propagation of aggregated α-syn cannot be ruled out. Indeed, the transmission of α-syn from the periphery is often accompanied by increased microglial activity and neuroinflammation, along with a leaky blood-brain barrier (BBB) (Breid et al., 2016).

Post-translational modifications

In order to better understand the physiological and pathological role of α-syn, it is important to note that it can undergo a plethora of post-translational modifications that directly modify its activity and capability to interact with certain proteins. Biochemical characterization of α-syn aggregates in LBs revealed the presence of small quantities of truncated forms of α-syn with molecular weight of 10-15 kDa derived from the C-terminus of the protein (Anderson et al., 2006). Other three truncated forms of α-syn have been identified in post-mortem tissues derived from Dementia with Lewy Bodies (DLB), multiple system atrophy (MSA) and PD patients: two C-terminal truncated regions (approximately between residues 102-125 and 83-110, respectively) and, finally, isoforms of N- and C-terminal, only detected in α-syn aggregates (Li et al., 2005). Quite interestingly, these isoforms have been found also in the healthy brain, suggesting that α-syn cleavage might occur at physiological level and could exert a specific activity (Li et al., 2005). These findings also suggest that the C-terminal truncated forms, which localize selectively into LBs or in insoluble aggregates, accumulate very rapidly and may act as nucleation points to accelerate the aggregation rate of the full-length protein (Oueslati et al., 2010). Although a specific protease has not yet been identified, various putative enzymes might be implicated in α-syn cleavage and production of truncated forms. For instance, neurosin (also known as kallikrein-6) is a trypsin-like protease that has been detected in LB (Iwata et al., 2003). In vitro experiments showed that cleavage of α-syn by neurosin generates a major residue of 1-80 amino acids, which does not aggregate, and three minor fragments: 1-97, 1-114 and 1-121. Quite interestingly the serine-129 (Ser129) phosphorylated form and the A53T and A30P deviants are resistant to proteolysis mediated by neurosin. The intracellular calcium-dependent protease calpain also cleaves WT α-syn or its mutants (A30P and A53T) at different sites in the NAC region, producing fragments that inhibit the aggregation of the full-length protein (Mishizen-Eberz et al., 2005). The major fragments that are generated consist of two residues of the N-terminal domain (58-140 and 84-140), and four of the C-terminal domain (1-57, 1-73, 1-75 and 1-83). Furthermore, following sequencing the N-terminal and using antibodies raised against the N-terminal truncated forms, another cleavage site of calpain has been identified, between residues 9 and 10. In fibrillar state, the calpain-mediated cleavage occurs exclusively in

the C-terminal region, between residues 114 and 122, probably due to this region remaining flexible and exposed to the action of proteases (Mishizen-Eberz et al., 2005). Fragments of calpain-cleaved α-syn have been identified in LB and Lewy neurites, also co-localized with activated calpain, suggesting a relationship between calpain-cleavage of α-syn and disease-linked aggregation (Dufty et al., 2007). Recently, the lysosomal enzyme cathepsin D has been reported to generate two forms of α-syn cleaved at the C-terminal region, of 12 and 10 kDa, respectively (Sevlever et al., 2008). Using specific antibodies against different epitopes of α-syn it has been showed that these fragments end approximately at 91-98 and 91-115 amino acids, respectively. Moreover, Sevlever and colleagues demonstrated that α-syn fragments generated by cathepsin D are the major component of the oligomeric species of α-syn that are produced under oxidative stress conditions (Sevlever et al., 2008). Levin and collaborators showed an increased aggregation rate of α-syn in vitro following proteolysis mediated by metalloproteases. Interestingly, higher concentrations of metalloproteases inhibit α-syn aggregation (Levin et al., 2009), probably due to an increased cleavage in the NAC region, essential for oligomerization and formation of α-syn fibrils (Oueslati et al., 2010). Numerous studies focused on the phosphorylation at serine residue 129 (pS129) and its possible implications on the neurodegeneration induced by α-syn (Oueslati et al., 2010) (Tenreiro et al., 2014b). Interestingly, only a small fraction (4%) of α-syn is constitutively phosphorylated at S129 in the brain at physiological level, whereas a dramatic increase (90%) is observed in patients affected by synucleinopathies (Fujiwara et al., 2002) as well as in animal models of PD (Neumann et al., 2002, Takahashi et al., 2003). These results strongly support the hypothesis that phosphorylation at S129 could play an important role over the normal function of α-syn, regulation of its aggregation, LB formation and neurotoxicity. Despite the great efforts made to identify the kinase responsible for α-syn phosphorylation, and to understand the consequences of such modification on the biophysical and biochemical properties of the protein, it is still a matter for debate how pS129 modulates α-syn physiological function or whether it exerts a protective or toxic effect on cell biology. It is interesting to note that the C-terminal tail of α-syn comprises most of the post-translational modification sites, such as phosphorylation (Tyr125, Ser129, Tyr133 and Tyr136), cleavage (Aspe115, Asp119, Prol120, Glu130 and Asp135) and ubiquitination (Lys96). The interaction between α-syn and vesicles of different lipid composition has been widely investigated (Snead and Eliezer, 2014). Recent studies focused their attention on the role of phosphorylation at S129 over the regulation of the interaction between α-syn and the membrane. However, in vitro evaluation of the effect of pS129 α-syn on the binding of α-syn to the vesicular membrane led to contrasting results. In fact, whether a study reported no effect (Visanji et al., 2011), two independent studies demonstrated that GRK-mediated phosphorylation or the S129E mutation, which mimics the phosphorylation state, diminish the affinity between α-syn and phospholipids (Pronin et al., 2000, Nubling et al., 2014). On the other hand, animal and cellular studies using phosphomimics reported an inhibitory effect of pS129 on the interaction between α-

syn and vesicles. A similar finding has been reported in a genetic model of PD, i.e. the rat injected with an adeno-associated virus (AAV) overexpressing α-syn, in which electron microscopy analysis revealed that most of the non-phosphorylatable S129A mutant α-syn is associated with membranes (Azeredo da Silveira et al., 2009). Collectively, these in vitro and in vivo data support the hypothesis of an inhibitory effect of phosphorylation at S129 on the binding between α-syn and phospholipidic membranes. Recently, a role for phosphorylated membrane-bound α-syn in the regulation of neurotransmitters uptake, in particular DA, has been described. In a *in vitro* assay, Hara and colleagues reported that GRK-mediated phosphorylation increases the capability of α-syn to accelerate DA uptake, without influencing the expression of DAT on the membrane (Hara et al., 2013). These data suggest that pS129 α-syn might play a crucial role in regulating the function of α-syn at the synapses. Nevertheless, it remains still unresolved how phosphorylated α-syn is able to modulate synaptic plasticity despite its low levels and short physiological half-life. Hirai and collaborators might have given a partial answer to this question by reporting how phosphorylation state is tightly bound to physiological stimuli such as stress conditions (Hirai et al., 2004). Different studies highlighted that the C-terminal region of α-syn interacts with metal ions, and that S129 can be found in close proximity to the binding sites of these ions (Liu and Franz, 2007, Bisaglia et al., 2009). In a recent study, Nubling and colleagues reported that mimicking phosphorylation with the S129E substitution facilitates oligomers formation in the presence of trivalent metallic ions such as ion and aluminium, when compared to WT protein (Nubling et al., 2014). While different post-translational modifications, in particular ubiquitination, sumoylation and phosphorylation at Tyr39, have been reported to regulate α-syn degradation through different proteolytic systems, little is known regarding the implications of phosphorylation at S129 on α-syn turnover. The first evidence of a cross-talk between pS129 and α-syn clearance has been reported by Chau and colleagues. They observed that inhibition of the ubiquitin-proteasome system (UPS) induces a significant increase in pS129 α-syn levels in human neuroblastoma cells (Chau et al., 2009). A following study confirmed these findings and reported that also inhibition of the autophagic-lysosomal pathway (ALP) induces a massive accumulation of pS129 α-syn both in rat cortical neurons and in human neuroblastoma cells. Researchers observed that half-time of pS129 α-syn was significantly shorter than the non-phosphorylated form (1h against 4h), suggesting that α-syn in its phosphorylated state is selectively targeted to degradation (Machiya et al., 2010). More recently, Oueslati and colleagues reported that overexpression of Polo-like kinase 2 (PLK2), the main kinase responsible for α-syn phosphorylation in the brain, increases α-syn turnover via autophagic pathway (Oueslati et al., 2013, Bergeron et al., 2014). This cellular process is unique to the family of synucleins and is governed by kinase activity of PLK2 and through direct interaction between PLK and α-syn.

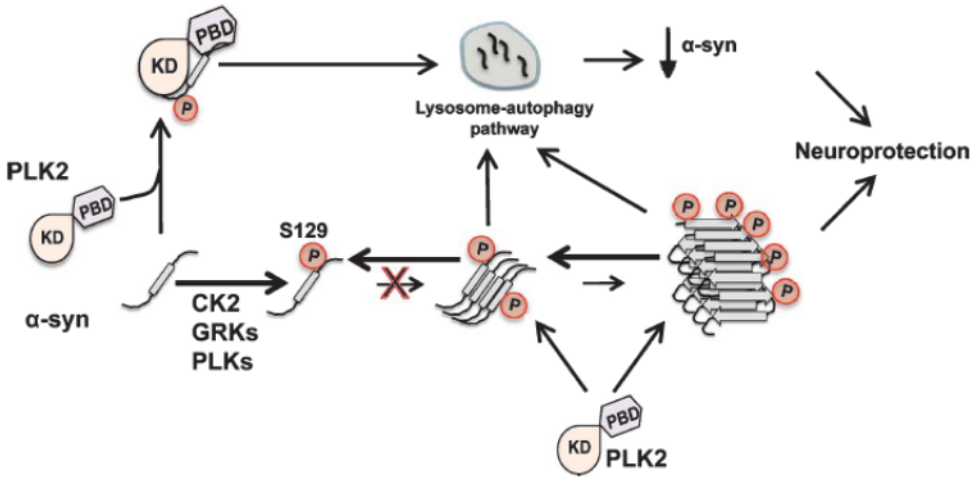

Fig. 5: Regulation of α-syn degradation mediated by PLK2 phosphorylation. (Oueslati et al., 2010)

A similar observation has been reported in a yeast PD model where the S129A substitution compromises α-syn clearance via the ALP system (Tenreiro et al., 2014b). Although the physiological interaction between PLK2 and α-syn remains elusive, different lines of evidence converge to suggest a synergistic role of these two proteins in the regulation of synaptic transmission and in cellular response to oxidative stress (Matsumoto et al., 2009, Burre, 2015). The identification of a PLK2 pathway for α-syn clearance offers the opportunity for the development of new selective therapeutic strategies aimed to reduce the levels of toxic α-syn in PD patients (Oueslati, 2016). The ability of the C-terminal tail of α-syn to interact with different proteins raised the question on how phosphorylation at S129 might regulate this interaction. McFarland and collaborators first answered this question using aimed functional proteomic assays. In their study, they demonstrated that non-phosphorylated α-syn mainly interacts with proteins related to the mitochondrial electron transport chain, although phosphorylated α-syn showed more affinity for cytoskeletal and presynaptic proteins implicated in synaptic transmission and vesicular trafficking (McFarland et al., 2008). In a recent study, Yin and colleagues demonstrated that the C-terminal region is implicated in the interaction between α-syn and Rab GTPases (Rab8a), small proteins which regulate vesicular trafficking. The authors reported that pS129 promotes α-syn-Rab8a interaction and modulates its toxicity (Yin et al., 2014). The abnormal accumulation of pS129 in the brain of patients affected by synucleinopathies, and the increase of its levels during ageing, the major risk factor of PD, suggest that this post-translational modification might represent a key factor in the pathogenesis of PD and related disorders. However, the exact implications of phosphorylation at S129 on α-syn aggregation and on its toxicity in vivo is still debated. Among the kinases responsible for α-syn phosphorylation, we find casein kinases, GRK, LRRK2 and PLK2. Two independent groups studied the effect of GRK2 and GRK6 overexpression on α-syn toxicity (Chen and Feany, 2005, Sato et al., 2011). In both studies, GRK overexpression was associated with an increase of pS129 α-syn levels and cell death. These observations suggest that GRK-mediated phosphorylation exacerbates its toxicity in vivo. Instead, an opposite outcome

resulted from a recent study, (Oueslati et al., 2013) where AAV-mediated overexpression of PLK2 in rat mesencephalon induced a 3-fold increase in pS129 α-syn levels in the infected neurons, which was accompanied by a significant attenuation of α-syn-induced dopaminergic cell loss.. At the molecular level, the same study demonstrated that PLK2 overexpression ameliorated α-syn clearance via ALP, suggesting that the PLK-mediated neuroprotective effect could be attributed to a decrease of the protein levels below the toxic threshold (Oueslati 2013). The discrepancy between the PLK2 and GRK effects on α-syn toxicity might be due to the superior ability of PLK2 in phosphorylating α-syn in vivo (Salvi et al., 2012). The role of pS129 on α-syn aggregation has been widely studied in vitro, with data supporting the hypothesis of an inhibitory effect of this post-translation modification on α-syn fibrillogenesis (Paleologou et al., 2008, Oueslati et al., 2010). Nevertheless, it remains to be clarified how pS129 controls α-syn aggregation and seeding in vivo. In cell cultures, adding exogenous α-syn or pre-formed fibrils (PFF) induces the formation of intracellular aggregates with close resemblance to LB (Luk et al., 2009, Volpicelli-Daley et al., 2011). This cellular process is governed by a nucleation-dependent mechanism in which PFF and α-syn offer the support to the assembly of soluble monomers of α-syn, ultimately resulting in highly ordered protein aggregates (Oueslati et al., 2014). Luk and colleagues were able to demonstrate *in vitro* that phosphorylation is not required for the formation of intracellular inclusions since S129A overexpressing cells treated with PFF presented intracellular inclusions similar to WT cells (Luk et al., 2009). Taken together these data suggest that phosphorylation is not a limiting step in α-syn aggregation and seeding in vivo and raise the question of whether the accumulation of pS129 represent an early or late event in the pathogenesis of synucleinopathies.

LRRK2 (PARK8)

Identification and mapping

In 2002, Funayama and colleagues identified and mapped a novel PARK locus (PARK8) on the short arm of chromosome 12 (12p11.2-q13.1) in a Japanese family with a dominantly-inherited form of parkinsonism similar to late-onset PD (Funayama et al., 2002). Two years later, PARK8 correlation to PD pathogenesis was confirmed by two independent studies describing families carrying mutations in the leucine-rich repeat kinase 2 (*LRRK2*) gene (Paisan-Ruiz et al., 2004, Zimprich et al., 2004). Zimprich and collaborators described pathogenic amino acid substitution p.R1441C and p.Y1699C in a family from Nebraska and in a German-Canadian family. At the same time, Paisan-Ruiz and colleagues, through genetic linkage in families with late-onset parkinsonism, described a substitution of a cytosine to a guanine in position 4321, which results in the p.R1441G mutation in both familial and sporadic PD patients from the Basque region of northern Spain, together with the p.G2019S mutation in families from Norway, Ireland, Poland, and the United States. The following year, Funayama's group identified the p.I2020T mutation as causative of the disease in the original Sagamihara pedigree in Japan (Funayama et al., 2005). As of today, more than 80 variants of LRRK2 protein have been reported, among which only seven

(p.N1437H, p.R1441G, p.R1441C, p.R1441H, p.Y1699C, p.G2019S and p.I2020T) have been confirmed to be pathogenic. The G2019S mutation located on the 42nd exon is the most common, with a frequency of 1-2% in sporadic PD and 4% in familial PD cases (Gasser, 2009).

Protein structure and mutations

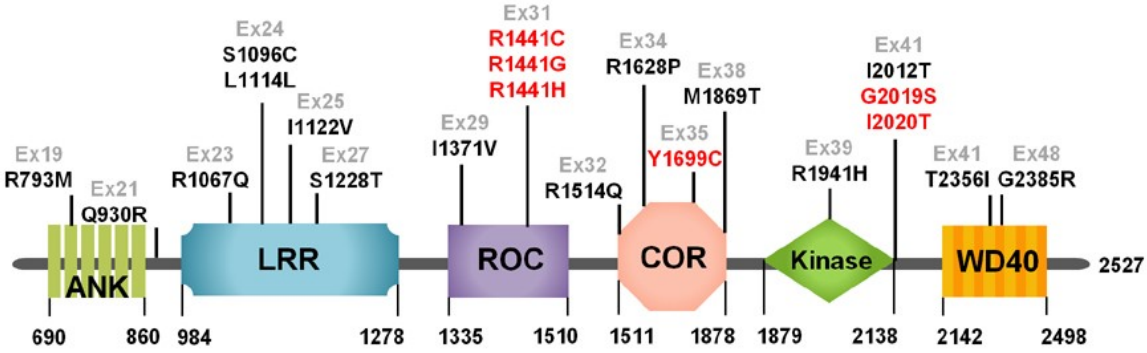

Fig. 6: LRRK2 protein structure with localization on exomes and protein of the most common mutations. Picture taken from (Hyun et al., 2013).

The *LRRK2* gene comprises 51 exons coding for a multidomain cytoplasmic protein of 2527 amino acids, also named LRRK2, which belongs to the Roco superfamily of proteins, a novel family of Ras-like G-proteins (Bosgraaf and Van Haastert, 2003). Also named dardarin, from the basque word *dardara*, which means tremors, LRRK2 comprises a central GTPasic Ras-of-complex (ROC) and a kinase domain surrounded by various protein-protein interaction domains, including armadillo repeats (ARM), ankyrin repeats (ANK), the namesake leucine-rich repeats (LRR) domain, a C-terminal of Roc (COR) and a WD40 domain (Mills et al., 2014). The pathogenic mutations of LRRK2 are clustered around the central catalytic core of the protein, with two mutations in the kinase domain (G2019S and I2020T), three in the Roc Domain (R1441C/G/H) and one in the COR domain (Y1699C). Furthermore, two variants located in the COR domain (R1628P) and in the WD40 domain (G2385R), have been identified as risk factors for sporadic PD (Cookson, 2010, Cookson and Bandmann, 2010). Given the difficulty to isolate sufficient high-quality recombinant LRRK2, advancement in understanding the structure of this protein has come from works with related Roco proteins from bacteria and *Dictyostelium discoideum* (Gotthardt et al., 2008, Gilsbach et al., 2012). Roco proteins include a Roc domain, with a high homology to proteins of the Ras superfamily, and possess all five G motifs that are required for guanine nucleotide binding. Roc can always be found in tandem with the COR domain, a 300-400-long amino acids peptide with no significant homology to the other domains. In vertebrates, only four Roco proteins have been identified: LRRK1, LRRK2, death-associated protein kinases-1 (DAPK1) and malignant fibrous histiocytoma amplified sequences with leucine-rich tandem repeats 1 (MASL). Roco proteins can be classified into three groups based on domain topology (Bosgraaf and Van Haastert, 2003). The MASL protein can be attributed to a group of Roco proteins

commonly found in metazoans, prokaryotes and plants, where the RocCOR tandem is always preceded by an LRR domain. The second Roco group comprises the two human LRRK proteins, which are also present in *D. discoideum* and metazoans, and display an N-terminal LRR and a C-terminal kinase domain in addition to the RocCOR tandem. Finally, the last group is characterized by the presence of a tumor-suppressor DAPK domain. Although, the exact function of the Roc domain of LRRK2 has not yet been cleared, it has been reported that the G-domain of LRRK2 acts as a GTP-binding protein which regulates the activity of the kinase domain (Taymans, 2012, Biosa et al., 2013). The G-domain contains five highly conserved G1-G5 motifs, which are responsible for nucleotide binding. The G1 motif, also called p-loop, is essential for the binding of the α- and β-phosphate of the nucleotide, as well as for the interaction with a magnesium-ion in the nucleotide binding pocket. The G-proteins oscillate between an active GTP- and inactive GDP-bound state through a switch mechanism that works via nucleotide binding and hydrolysis (Vetter and Wittinghofer, 2001). It is interesting to note that only the GTP-bound G-protein displays high affinity for effector proteins. Studies of the Roc G-domain are slowed by the lack of the crystal structures, with only two available that encompass the Roc G-domain: one structure of the LRRK2 Roc domain and one of the Roc-COR tandem of the Roco protein from *Chlorobium tepidum* (Deng et al., 2008, Gotthardt et al., 2008). Interestingly, the structure of the Roc domain in LRRK2 revealed a mirrored dimer in which the G-domain of two LRRK2 proteins are linked to form a constitutive dimer. Kinases play a key role in the regulation of cellular mechanisms via the transfer of γ-phosphate of ATP to a target protein. There are three subtypes of kinases: serine/threonine kinases, which represent the vast majority, tyrosine kinases, and a small group of kinases classified as atypical (Endicott et al., 2012). Roco proteins, and in particular LRRK2, are serine/threonine specific kinases. The architecture of LRRK2 kinase domain consists of a two-lobed kinase structure with an adenine nucleotide in the nucleotide-binding pocket. The lobe in the N-terminal region is smaller and is composed of anti-parallel β sheets and contains the conserved αC-helix. The C-terminal lobe mostly contains α-helices and comprises an activation loop which expresses the conserved N-terminal DFG motif. Between the two lobes resides a gap housing the ATP binding site, which together with the activation loop forms the catalytic site of the kinase. The aspartic acid in the DFG motif makes contact with all three ATP phosphates either directly or via coordination of a magnesium ion. The DFG can assume two states: a DFG-in (active) and a DFG-out (inactive) conformation.

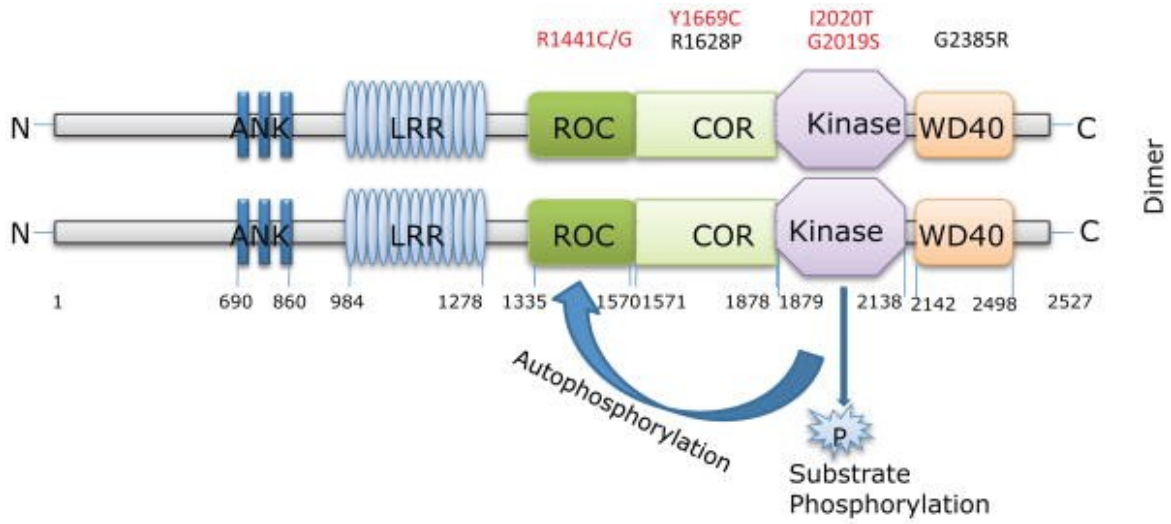

Fig. 7: LRRK2 dimerization increases the activity of the kinase domain, which is exacerbated by the presence of pathogenic mutations. Figure taken from (Kumar and Cookson, 2011)

In most kinases, the switch between an inactive and active state often involves autophosphorylation of residues in the activation loop. This modification modifies the orientation of the activation loop and alters the interaction with substrates and the affinity for ATP (Kornev et al., 2006). It has been shown that LRRK2 undergoes autophosphorylation in various residues that lie in the activation loop (Lobbestael et al., 2012). Moreover, multiple LRRK2 autophosphorylation sites have been identified outside of the activation loop, more precisely in the Roc domain, and it has been reported that either mutations of these residues or pharmacological blockade of kinase activity results in an increased neurite outgrowth (MacLeod et al., 2006, Herzig et al., 2011, Yao et al., 2013). Taken together, these data suggest that LRRK2 phosphorylation events are crucial for both the intramolecular activation mechanism as well for downstream signaling. Beside the central core, LRRK2 harbors the ARM, ANK and LRR domains in its N-terminus, whereas a WD40 domain is present in the C-terminus (Cardona et al., 2014). All these domains can be often found in signaling proteins and serve as protein-protein interaction sites. In particular, the ARM domain consists of a 42-amino acid long tandem repeat that form a super-helical bundle (Tewari et al., 2010). ANK contains seven repetitive motifs which form helix-loop-helix structures that end in a loop or hairpin (Mosavi et al., 2004). The LRR domain consists of a 11-amino acid long motif that form a parallel β-sheet ending with a α-helix. Studies have shown that the LRR domain of LRRK2 is essential for its function in vivo but not in vitro, and specifically for the kinase activity (Iaccarino et al., 2007, van Egmond and van Haastert, 2010). These data suggest that LRR influences the specificity of the protein via interaction with a downstream target or an upstream activator. Finally, the WD40 domain displays a highly hydrophilic surface and is involved in membrane binding. Indeed, altering this domain makes LRRK2 unable to dimerize, reduces its kinase activity and a misplaces the protein (Jorgensen et al., 2009). In addition, the novel G2385A mutation (and PD risk factor) located in this domain, results in an impaired kinase activity and abolished 14-3-3 binding to the N-

terminus, indicating the relevance of this domain in the intramolecular regulation of LRRK2 activity (Rudenko et al., 2012). Noticeably, it has been demonstrated that LRRK2 kinase activity is essential to its neurotoxic effect (Greggio et al., 2006). In particular, the G2019S mutation has been consistently associated with an at least two-fold increase of the kinase activity (West et al., 2005, Jaleel et al., 2007). This mutation is located in the DFG motif and was resolved with structural analysis of the ROCO protein homolog of LRRK2 in *D. discoideum*. The discoideum equivalent for the human G2019S mutation is the G1179S which does not cause any change in the overall structure of the protein, although the new serine in position 1179 can now interact with the arginine in position 1077 and form a salt bridge, which stabilizes the activation loop in its active conformation. The Arg1077 in the *D. discoideum* corresponds to Gln1918 in LRRK2, and when the Gln1918Ala substitution is introduced, which prevents the formation of the salt bridge, kinase activity returns to levels comparable to WT form (Gilsbach et al., 2012). LRRK2 I2020T displays slightly decreased kinase activity in some assays and increased in others (Jaleel et al., 2007, Gilsbach et al., 2012). The localization of this substitution per se does not explain how it may hinder kinase activity. As a matter of fact, the side-chain of the threonine is oriented to the solvent and does not interfere with the active state of the domain. This discrepancy was explained by Ray and collaborators noting that different substrates yield different levels of kinase activity, meaning that the threonine in this substitution may alter the interaction with some substrates but not with others (Ray et al., 2014). It has also been speculated that nontoxicity of this mutation might not be related to a variation of its kinase activity but more likely to an increased cellular degradation (Ohta et al., 2010). It is also possible that LRRK2 I2020T might work in tandem with LRRK2 WT resulting in an increased kinase activity, analogous to what has been shown for B-RAF mutations (Wan et al., 2004). Alternatively, this mutation might indirectly affect kinase activity by altering intramolecular interactions with other domains. The RocCOR GTPase domain mutation R1441H displays an increased GTP-binding activity due to slowed GTP hydrolysis and increased affinity for GTP (Liao et al., 2014). When small GTPases are in GTP-bound state they bind kinases and activate them. Then, it is possible that via intramolecular interactions, the GTPasic domain of LRRK2 impacts its kinase activity (Reynolds et al., 2014). Finally, the C-terminal region of LRRK2 can interact with its catalytic domain, and abolishing this interaction either via deletion of the C-terminus or introduction of the G2385 PD risk factor results in a dampened kinase activity (Rudenko et al., 2012). Despite all the different lines of evidence pointing to a detrimental effect of an enhanced LRRK2 kinase activity for the cell, it is yet to be clarified which interactors and which pathways are involved.

Cellular functions

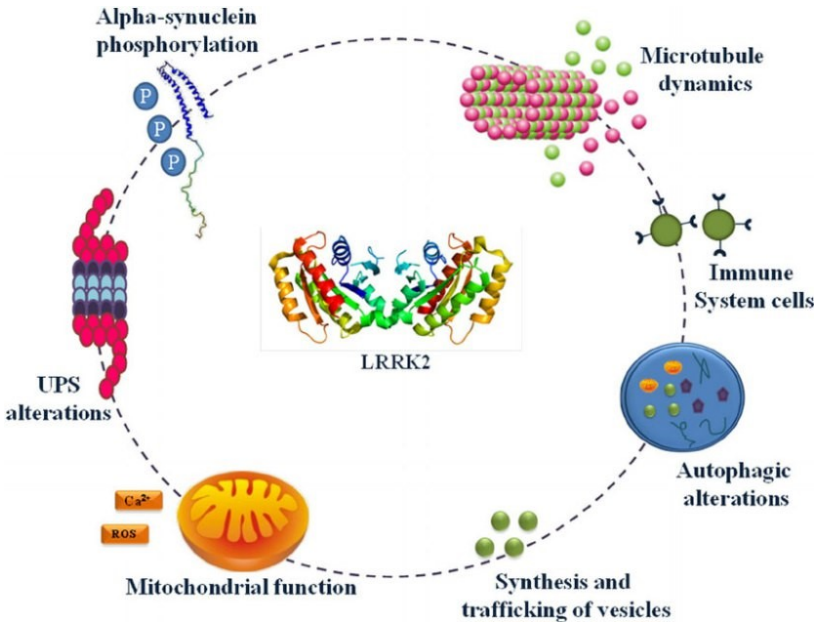

Fig. 8: schematics of cellular functions implicated in LRRK2 physiology. (Esteves et al., 2014)

LRRK2 is expressed in most brain regions, in great abundance in the hippocampus, cortex, striatum, cerebellum, olfactory bulb and, in small quantities, in the SNc (Santpere and Ferrer, 2009). Furthermore, it can be detected in high levels in the periphery, in particular in liver, kidneys, heart and lungs. At the cellular level, LRRK2 can be found mainly in the cytoplasm, but also associated with membranous and vesicular structures (Biskup et al., 2006) such as the membranes of mitochondria, ER, Golgi, endosomes and synaptic vesicles (Cookson and Bandmann, 2010). This particular distribution might indicate an involvement of LRRK2 in membrane trafficking as also suggested by results obtained in different transgenic mice models (Johnson and Wade-Martins, 2011). Although the physiological function of LRRK2 still remains to be fully elucidated, there is evidence of its involvement in different cellular processes, such as regulation of transcription (Kanao et al., 2010), translation (Imai et al., 2008), apoptosis (Ho et al., 2009) and mitochondrial activity (Smith et al., 2005). It is often difficult to discriminate whether the changes observed when expressing the mutant form of LRRK2 are due to a loss-of-function or a gain-of-function effect, although most studies fit with the latter hypothesis. Multiple in vitro studies suggest that LRRK2 interacts with cytoskeletal proteins causing reorganization and alteration of neuronal processes (Gillardon, 2009, Habig et al., 2013). This hypothesis is supported by the evidence that either overexpression or knock-down of WT cause neurite retraction whether overexpression of LRRK2 mutants causes excessive neurite outgrowth in neuronal cultures (MacLeod et al., 2006). LRRK2 might modulate the cytoskeleton through binding with both actin and microtubules either directly or via interaction with microtubules-associated proteins (Kett and Dauer, 2012). Indeed, anomalies in neurites outgrowth and ramification were the first cellular phenotypes to be associated with mutations in the LRRK2 gene. It was initially proposed that these morphological changes might be

a consequence of an ongoing apoptotic processes, however, further studies highlighted that this was due to an interaction between LRRK2, actin and tubulin (Wallings et al., 2015). Of the different isoforms of tubulin, studies in rodents pointed out that LRRK2 preferentially phosphorylates β-tubulin, a component of microtubules, at Thr107, thereby facilitating its disassembly (Gillardon, 2009, Parisiadou and Cai, 2010). Moreover, transgenic mice overexpressing LRRK2 display Golgi fragmentation due to microtubules alteration. This process does not imply neurotoxicity per se, but destabilizes the equilibrium between the ER and Golgi in the regulation of synthesis and secretion of cellular products (Parisiadou and Cai, 2010). In addition, animal models expressing LRRK2 G2019S and R1441G display higher levels of phosphorylated tau, which binds tubulin and promotes its incorporation in microtubules. Furthermore, in its phosphorylated state, tau causes disruption of microtubules, thus impacting the entire cytoskeletal network. LRRK2 also phosphorylates moesin, a member of the ezrin/radixin/moesin (ERM) protein family, which mainly serves to anchor the actinic cytoskeleton to plasmatic membrane. It has been shown that LRRK2 binds and phosphorylates endogenous tubulin, facilitating β-tubulin polymerization in the presence of microtubules-associated proteins (MAP) (Gillardon, 2009). Nevertheless, it is unclear if mutations in the GTPase and kinase domain influence cytoskeleton dynamics in the same way (Wallings et al., 2015). Drosophila studies suggested a possible involvement of LRRK2 in different forms of vesicular trafficking, such as synaptic vesicles recycling or interaction with the retromer and lysosomal trafficking. Indeed, LRRK2 has been reported to phosphorylate endophilin A, a protein required for vesicle endocytosis (Matta et al., 2012). In addition, increasing the phosphorylation of these proteins, for example as a consequence of LRRK2 pathogenic mutations, results in a dampened endocytosis. Finally, LRRK2 might be involved in regulation of the retromer, a complex of proteins which mediates trafficking of proteins from endosomes to the trans-Golgi network (TGN) (MacLeod et al., 2013). Indeed, it has been demonstrated that LRRK2 interacts with the vacuolar protein sorting 35 ortholog (VPS35), a component of the retromer complex whose mutations are cause of autosomal dominant PD, in order to mediate synaptic vesicle endocytosis through the endosomal pathway (Inoshita et al., 2017). Furthermore, VPS35 overexpression ameliorates motor activity and increases lifespan of Drosophila expressing either the I2020T or Y1699C LRRK2 mutants (Linhart et al., 2014). Considering that VPS35 levels and activity are not altered in brain tissue from G2019S LRRK2 or idiopathic PD patients (Tsika et al., 2014), it can be assumed that LRRK2 effect does not solely rely on a direct interaction with VPS35, but affects a converging pathway that involves the action of a third player. Indeed, it has been demonstrated that LRRK2 interacts with Rab7L1 modulating the sorting of CI-MPR, in a similar fashion to the pathogenic VPS35 mutation (MacLeod et al., 2013), and that VPS35 D620N mutation enhances the LRRK2-mediated phosphorylation of Rab8A, Rab10 and Rab12 in mouse embryonic fibroblasts (Mir et al., 2018). Taken together, these data suggest a Rab-mediated LRRK2-VPS35 interaction in regulating synaptic vesicle endocytosis. Another important putative

role of LRRK2 is the regulation of the ALP. As a matter of fact, murine models with impaired autophagy display cerebral anomalies such as formation of ubiquitin-positive inclusions and presynaptic accumulation of α-syn and LRRK2, supporting the idea that autophagy contributes to PD pathogenesis (Friedman et al., 2012). Although the precise mechanism on how LRRK2 regulates the ALP, and how this relates to PD onset are yet unknown. It is however clear that LRRK2 mutations significantly impact the autophagic machinery. A 2008 study investigated the relationship between LRRK2 and autophagy using immortalized cell lines expressing both WT and mutant LRRK2. This study showed alterations in the autophagic vesicles following transfection of LRRK2 G2019S (Plowey et al., 2008). Furthermore, analyzing the LRRK2-related phenotype, i.e. neurite retraction, researchers were able to demonstrate crucial alterations in the autophagic machinery such as LC3 or ATG7, thus suggesting a LRRK2 implication in macroautophagy. It has been postulated that the molecular basis behind this mechanism relies on calcium levels, NAADP, MEK/ERK pathways, and the interaction with BCL2 (Moran et al., 2010, Gomez-Suaga et al., 2012, Su et al., 2015). Another compelling cellular activity of LRRK2 involves mitochondria. Indeed, about 10% of cytosolic LRRK2 can be found to be associated with the mitochondrial outer membrane, suggesting that it may play a role in mitochondrial activity and dysfunction (Biskup et al., 2006). In addition, fibroblasts from patients carrying G2019S mutation display abnormal mitochondrial morphology (Mortiboys et al., 2010). Similarly, overexpression of WT LRRK2 in SHSY5Y cells causes mitochondrial fragmentation, which is enhanced by the R1441C and G2019S mutations (Wang et al., 2012), together with mitochondrial uncoupling, reduction of membrane potential and increase of oxygen consumption (Papkovskaia et al., 2012). A possible explanation to such morphological anomalies was provided by showing that LRRK2 overexpression recruits Dynamin-like protein 1 (DLP1), a regulator of mitochondrial fission, thus inducing fragmentation of the mitochondrial network, mitochondrial clearance and consequent increase of oxidative stress (Niu et al., 2012). Potentially corroborating these findings, DRP1 inhibition reverses mitochondrial fragmentations both in HEK cells and fibroblasts carrying G2019S mutation (Su and Qi, 2013). These observations suggest that LRRK2 might be responsible for mitochondrial homeostasis through a DLP1-dependent mitochondrial quality control. Another interesting LRRK2 cellular interactor is represented by the 14-3-3 family of adapting proteins, which encompasses seven isoforms, with each member binding its substrates at phosphoserine/threonine motifs (Jones et al., 1995, Yaffe et al., 1997). The main molecular functions of these proteins are to stabilize specific conformations, regulate enzymatic activity and subcellular localization of given substrates. As of today, more than 200 proteins have been identified to interact with 14-3-3, among which receptors, enzymes, structural and cytoskeletal proteins, small G proteins and their regulators, scaffolding molecules, proteins involved in the control of apoptosis and protein-kinases such as LRRK2 (Fu et al., 2000, Yaffe, 2002, Mackintosh, 2004). It has been recently demonstrated that LRRK2 binds to different isoforms of 14-3-3 (Dzamko et al., 2010), and that LRRK2 mutations abolish this

interaction (Li et al., 2011), causing LRRK2 accumulation in the cytoplasmic pools. Indeed, 14-3-3 proteins play a role in stabilizing LRRK2 structure and protecting ser910/935 residues from dephosphorylation (Rudenko and Cookson, 2010). An interesting aspect which has recently gained much interest is the potential role of LRRK2 in the immune system (Dzamko and Halliday, 2012). LRRK2 variants have been identified as risk factor for diseases with an inflammatory basis such as Crohn's disease and leprosy (Barrett et al., 2008, Fava et al., 2016). The pathogenic mechanism appears to be the same: LRRK2 sequestrates the NFAT transcription factor, thus preventing its translocation to the nucleus and the transcription of proinflammatory cytokines. A prolonged inflammatory response is triggered when LRRK2 expression or turnover are altered due to genetic variance (Barrett et al., 2008, Fava et al., 2016). It has been previously reported that LRRK2 is expressed in microglial cells and astrocytes, however only in 2010 it was discovered that LRRK2 expression is finely regulated by inflammatory signals in myeloid cells, suggesting a potential role as a regulator of the immune response (Gardet et al., 2010). As a further evidence that LRRK2 might regulate the activity of immune cells, it has been demonstrated that LRRK2 protein levels rise in immune cells following inflammatory processes. LRRK2 might control the antigen presentation in human monocytes, process that is altered in PD patients. In vitro studies showed that pharmacological blockade of LRRK2 kinase activity using the LRRK2 kinase inhibitor LRRK2-IN-1 reduces the expression of CD14, CD16 and MHC-II in monocytes. A study from Gardet and collaborators in peripheral blood mononuclear cells (PBMC) demonstrated that lymphocytes B show the highest expression of LRRK2, followed by monocytes and dendritic cells (Gardet et al., 2010). Aimed studies confirmed that LRRK2 is highly expressed in human CD19 lymphocytes and CD14/16 monocytes. Lower levels were detected in CD3 T lymphocytes (Thevenet et al., 2011), microglial cells and resident macrophages, both in human (Miklossy et al., 2006) and adult mice brain (Gillardon et al., 2012). Treating human PBMC with IFN-γ induces a significant increase in LRRK2 mRNA and consequently its protein levels in CD19 B lymphocytes, CD11b monocytes and CD3 T lymphocytes (Gardet et al., 2010). In addition, LRRK2 expression is also upregulated in microglial cells following treatment with the bacterial toxin Lipopolysaccharides (LPS) (Moehle et al., 2012). Another interesting hint about LRRK2 involvement in the immunity signaling cascade comes from the observation that LRRK2 is directly phosphorylated after activation of Toll-like receptors (TLR) (Dzamko and Halliday, 2012). As a matter of fact, pathogen-mediated activation of TLR induces the expressions of cytokines such as TFN-α and IL-6 under the regulation of the NF-kB signaling cascade (Kawai and Akira, 2011). Finally, LRRK2 is phosphorylated on the residues Ser910 and Ser935 by the IkB kinase complex, a component of the NF-κB signal transduction cascade. Another interesting proof that relates LRRK2 to the immune system comes from a study of Liu and colleagues (Liu et al.,2011) where the Drosophila LRRK2 orthologue controls the nuclear translocation of NFAT1. NFAT1 orchestrates the expression of a multiple number of proinflammatory cytokines such as IFN-γ, IL-1 and TNF-α,

and LRRK2 negatively regulates NFAT1 activity. LRRK2 may act as transcriptional regulator of immunity-related pathways, such as by modulating the activity of transcription factors as NFAT1 and NF-kB (Russo et al., 2015). It is still unclear whether pathogenic LRRK2 mutations act as a gain or loss of function. Assuming the latter implies that aberrant proteins act as dominant negative mutants, recruiting and impairing the WT functional proteins. A putative mechanism comes from the dimeric nature of LRRK2 (Greggio et al., 2008) and from the fact that mutant LRRK2 displays a greater tendency to oligomerization (Greggio et al., 2006). The heterodimer might in fact compromise the LRRK2-dependent inhibition of the nuclear translocation of NFAT1 with a subsequent increase in its transcriptional activity and cytokines production. Elevated levels of cytokines might activate microglia thus establishing positive feedbacks of regulation cycles that lead to a prolonged inflammatory state.

LRRK2-related pathology and kinase inhibitors

From a clinical point of view, LRRK2- related PD is indistinguishable from sporadic PD, although LRRK2 patients are less likely to manifest hyposmia, REM sleep alterations, non-motor symptoms, dementia and visual hallucinations than noncarriers (Healy et al., 2008). Moreover, these patients present a more benign course, and a slower progression of the pathology. From the neuropathological point of view, LRRK2 pathology is heterogeneous and could include the presence of LB and other pathological hallmarks of dementia with LB (DLB), multiple system atrophy and corticobasal degeneration. It is interesting to note that there are contrasting results regarding the male to female ratio of LRRK2-related PD. Some studies report a similar gender distribution among LRRK2 carriers (Alcalay et al., 2013), whereas some report a greater penetrance in men, like in idiopathic PD (Nabli et al., 2015) or in women (Marras et al., 2011). As of today, the main therapy for PD is limited to control symptoms via palliative therapies, and all available drugs, such as L-DOPA, dopamine agonists, COMT and MAO-B inhibitors, are aimed to compensate for the lack of DA, thus ameliorating patients' quality of life. Furthermore, surgical alternatives have been implemented in patients with motor fluctuations an L-dopa-induced dyskinesia, such as pallidotomy and thalamotomy, or more recently deep brain stimulation. Since the most common genetic variants of LRRK2 result in a, increased activity of the kinase domain, which is instrumental for LRRK2 toxicity, it has been postulated that pharmacological blockade might represent a viable tool for disease-modifying therapies in PD. The kinase inhibitors that have been developed differ in terms of selectivity, potency and brain permeability. To quantify the ability of these compounds to inhibit LRRK2, kinase activity assays based on its autophosphorylative or heterophosphorylative process as well as phosphorylation of putative substrates have been developed. Initially, myelinic basic protein was employed as a generic kinase substrate; a specific artificial substrate, named LRRKtide (RLGRDKYKTLRQIRQ), containing a repeated amino acidic pattern of a physiological substrate for LRRK2, namely the 558

phosphorylation site of moesin, was later developed (Jaleel et al., 2007). The first compounds to be identified as LRRK2 inhibitors were Rho Kinase inhibitors, which however non-specifically inhibited LRRK2 with similar potency of Rho kinase (Nichols et al., 2009). The first patent for a selective kinase inhibitor for LRRK2 was deposited in 2009 by Novartis. It was a dihydroindolic sunitinib analogue, which displayed a 1.2 μM IC_{50} against LRRK2. Another interesting compound from the same class is GW5074, which displays an IC_{50} of 9 nM against LRRK2, and neuroprotective effects in vivo and in vitro in models of neurodegeneration induced by LRRK2 overexpression (Lee et al., 2010b). Despite this evidence, these compounds showed a low selectivity profile and high overall toxicity, thus compromising their employment in a chronic therapy for PD (Deng et al., 2012). Alessi's group was the first to identify what is considered the first potent and selective LRRK2 inhibitor: LRRK2-IN-1 (Deng et al., 2011). LRRK2-IN-1 has been identified after the synthesis of over 50 analogues through biochemical and cellular assays. This compound is capable of blocking the kinase activity of LRRK2 WT and LRRK2 G2019S with a IC_{50} of 13 nM and 6 nM, respectively. Furthermore, it is able to rapidly suppress LRRK2 activity in vivo by inducing LRRK2 dephosphorylation at Ser910 and Ser935, thus resulting in loss of interaction with 14-3-3 and accumulation of LRRK2 in fibrillary aggregates (Dzamko et al., 2010). Drug concentration assays for LRRK2-IN-1 displayed a half-life of 4,5 hours and 49,4% bioavailability in mice. Nevertheless, based on the evaluation of LRRK2 phosphorylation at Ser910 or Ser935, LRRK2-IN-1 showed an unsatisfying brain penetrance. Moreover, it displayed a significant off-target activity, such as on ERK5 (Deng et al., 2013), DCLK1 (Weygant et al., 2014) and Brd4 (Hatcher et al., 2017). All these data precluded the clinical advancement of this compound. In 2012, researchers from GlaxoSmithKline (GSK) patented a new class of kinase inhibitors with an arylbenzamidic core. The most interesting compound was GSK2578215A which displayed an IC_{50} of 10,9 nM against LRRK2 WT and 8.9 nM against LRRK2 G2019S in HEK293 transfected cells (Reith et al., 2012). It was also observed that this compound was able to inhibit LRRK2 Ser910/935 phosphorylation in kidney and spleen lysates with similar potency to IN-1. Nevertheless, GSK2578215A did not exhibit dephosphorylation at Ser935 at the central level despite a total brain to plasma ratio of 1,4. This discrepancy could be explained by inadequate free drug levels in the brain relative to the cellular potency. The lack of central target engagement halted further pre-clinical and clinical development of this compound. Researcher from Pfizer considered to employ a pyrrolopyrimidine scaffold to synthesize potent and selective LRRK2 inhibitors with favorable CNS penetrance. Among these, PF-06447475 showed great potency of LRRK2 inhibition, showing an IC_{50} of 3 nM against LRRK2 WT and 11 nM against LRRK2 G2019S (Henderson et al., 2015). It also displayed a selectivity profile of 32/449 kinase at 1 μM with less than 30% of inhibition compared to control. Further in vivo studies using 3, 10, 30 and 100 mg/Kg PF-06447475, subcutaneously twice a day, confirmed the high central bioavailability of PF-06447475 with a 60-80% reduction of phosphorylation at Ser935 90 minutes after

administration, and an unbound drug IC_{50} estimated to be 8 nM in brain and 11 nM in kidney in WT mice. It is interesting to note that the compound was found to be 10-fold less potent in causing LRRK2 dephosphorylation at S935 and S1292 in BAC-transgenic G2019S mice, reaching 80% reduction only at the 100 mg/Kg dose (Henderson et al., 2015). Importantly, however, PF-06447475, displayed less peripheral toxicity when compared to other kinase inhibitors. MLi-2 is one of the latest compounds synthetized by Merck that display high potency and LRRK2 selectivity. The heterocyclic indazole group confers the compounds a high affinity for LRRK2 ATP-binding site over a wide range of kinases, receptors and ionic channels (Fell et al., 2015). Oral administration of MLi-2 in WT mice causes a dose-dependent dephosphorylation of Ser935, reaching its maximum (90%) at the 10 mg/kg dose. In vitro studies pointed out an IC_{50} of 0.76 nM with good oral bioavailability and permanence time. Furthermore, in vivo studies with an acute or subchronic treatment in mice led to dose-dependent reduction of LRRK2 kinase activity, both at the central and peripheral level. MLi-2 treatment is well tolerated, with no adverse effects on weight, food intake or motor behavior. A recent publication of Fuji and collaborators showed that most of LRRK2 kinase inhibitors display significant lung toxicity (Fuji et al., 2015). Mli-2 and PF-06447475, however, displayed a good tolerability after chronic administration (Daher et al., 2015), with a higher potency and selectivity compared to the two kinase inhibitors employed by Fuji and colleagues, GNE-0877 and GNE-7915. Nonetheless, in vivo study revealed that MLi-2, despite showing prolonged kinase inhibition, over a 15-weeks period, did not halt or slowed the behavioral and neurochemical parkinsonian-like phenotype in the MitoPark mouse model (Fell et al., 2015).

Interaction between LRRK2 and α-synuclein

Mutations in the *SNCA* and *LRRK2* genes can cause autosomal dominant PD and have been identified as genetic risk factors for sporadic PD (Nalls et al., 2014). The finding that phosphorylated α-syn is a major component of LB (Anderson et al., 2006) and that LRRK2 mutants display increased kinase activity (Henry et al., 2015) suggest that these two genetic risk factors may interact and contribute to α-syn aggregation and/or spreading. LRRK2 mutations carriers which present the SNCA single nucleotide polymorphism rs356219-G, which regulates SNCA expression in PD-related brain regions, display an earlier age of onset of the pathology, reinforcing the concept that SNCA variants might play a permissive role in LRRK2-related pathology (Botta-Orfila et al., 2012). This concept also seems to be supported by studies in animal models expressing LRRK2 G2019S and/or α-syn aberrant forms. Indeed, inhibition LRRK2 expression in transgenic mice overexpressing A53T α-syn abolished α-syn accumulation and slowed the progression of neuropathology (Lin et al., 2009). Furthermore, mice overexpressing LRRK2 G2019S under the CaMKII promoter display an increase in α-syn aggregation (Xiong et al., 2017). Moreover, selective overexpression of LRRK2 G2019S in the SNc causes neurodegeneration and aggregation of endogenous α-syn (Xiong et al., 2018). Similar findings were also reported in models of acute induction of α-syn overexpression via viral vector or injection of preformed fibrils.

Daher and collaborators reported that AAV-injection of α-syn in BAC G2019S rats induces a greater loss of DA neurons compared to LRRK2 WT animals (Daher et al., 2015). Despite this great wealth of evidence, the molecular basis of how LRRK2 and α-syn interact to trigger or worsen PD pathology still remain elusive. Various mechanisms have been put forward. For instance, LRRK2 might impact the synthesis, levels of post-translational modification and handling of α-syn. Indeed, G2019S-LRRK2 overexpressing rats display higher levels of pSer129 α-syn in the striatum (Volpicelli-Daley et al., 2016). Furthermore, Kondo and colleagues showed that co-transfecting cells with both α-syn and LRRK2 G2019S induces the formation of α-syn aggregates and α-syn-containing vesicles (Kondo et al., 2011). Similar findings have been obtained by Schapansky and collaborators, reporting that primary cortical neurons derived from LRRK2 G2019S KI mice display an accumulation of endogenous, detergent-insoluble α-syn which is rescued by pharmacological blockade of LRRK2 kinase activity (Schapansky et al., 2018). Interestingly, knocking-down α-syn ameliorates LRRK2 G2019S-induced neurotoxicity, whereas genetic or pharmacological inhibition of LRRK2 kinase activity only mildly affects LRRK2 toxicity in PD patient-derived induced pluripotent cells (Skibinski et al., 2014). Taken together, these results suggest that LRRK2 can hasten α-syn accumulation and regulate the cellular localization of such aggregates. Nevertheless, it still remains to be elucidated which intracellular pathways are affected by a direct or indirect interaction between LRRK2 and α-syn. The 14-3-3 chaperone-like protein family has been consistently shown to interact with both LRRK2 and α-syn, as well as being a component of LB (Xu et al., 2002, Berg et al., 2003, Nichols et al., 2010). 14-3-3 proteins are known to exert an anti-apoptotic action in the cell, therefore sequestration of 14-3-3 to LB by α-syn binding might prevent this effect (Slone et al., 2015). In addition, disruption of 14-3-3 binding to LRRK2 alters LRRK2 cellular localization, hyper-activates LRRK2 kinase activity and alters exosome release (Dzamko et al., 2010, Mamais et al., 2014). Another intracellular pathway which entwines LRRK2 and α-syn toxicity sees mitochondria at the center of it. Indeed, both endogenous and exogenous α-syn have been shown to localize to mitochondria (West et al., 2005, Biskup et al., 2006), and inhibit TOM20, thereby impairing mitochondrial protein import (Chinta et al., 2010, Subramaniam et al., 2014, Di Maio et al., 2016). Furthermore, this association of α-syn with mitochondria is particularly high in the striatum, SNc and cortex of PD brains (Devi et al., 2008). In addition, both LRRK2 and α-syn seem to induce mitochondrial fragmentation and functional defects, probably through the interaction with the mitochondrial protein DLP1 which regulates mitochondrial fission and degradation (Su and Qi, 2013, Ryan et al., 2018). In this regard, another major pathway which links α-syn and LRRK2 is autophagy. Indeed, α-syn is degraded through CMA via recognition of the KFERQ motif and its aberrant forms impair autophagy by tight binding to the LAMP2A, thus inducing compensatory activation of macroautophagy (Cuervo et al., 2004, Xilouri et al., 2009). Also, LRRK2 has been shown to be degraded by CMA and to localize to autophagic vacuoles, amphisomes and lysosomes (Alegre-Abarrategui et al., 2009,

Dodson et al., 2012, Orenstein et al., 2013). In addition, LRRK2, and in particular G2019S LRRK2, has been shown to be a negative regulator of autophagy, thus suggesting that it may impact α-syn aggregates handling and degradation (Alegre-Abarrategui et al., 2009). Finally, both proteins interact with Rab7, a regulator of autophagosome and lysosome trafficking, positioning and fusion events which also regulates clearance of α-syn aggregates and LRRK2 localization (Dodson et al., 2012, Dinter et al., 2016). Another suggestive mechanism in which LRRK2 modulates α-syn toxicity relies on the putative role of these two proteins in neuroinflammation. PD has been linked to neuroinflammation since analysis of PD brain disclosed reactive microglia and the presence of pro-inflammatory cytokines (Mogi et al., 1996, Hunot et al., 1999). LRRK2 has been found to be expressed in microglia after activation of resident microglial cells following LPS injection, other than being implicated in many inflammatory diseases such as Chron's disease and a type of inflammatory bowel syndrome (Barrett et al., 2008, Moehle et al., 2012). Supporting this concept, LPS injection in transgenic mice overexpressing mutant LRRK2 causes a more profound neuroinflammation and loss of SNc DA neurons compared to controls (Kozina et al., 2018). On the other hand, also α-syn aggregates have been linked to neuroinflammation. Indeed, misfolded α-syn can activate TLR2 and TLR4 triggering neuroinflammation (Daniele et al., 2015, Gustot et al., 2015). These data suggest that either aberrant LRRK2 potentiates α-syn-mediated immune response or LRRK2 triggers an abnormal immune response which induces α-syn aggregation and strengthens the immune response in a feedforward mechanism. Whatever the mechanism, the role of LRRK2 kinase activity has been established since pharmacological blockade of LRRK2 kinase activity in LRRK2 G2019S transgenic rats attenuates neuroinflammation and neurodegeneration induced by AAV-α-syn injection (Daher et al., 2015).

AIM OF THE STUDY

The inheritance pattern of familial PD cases greatly varies depending on the gene that is altered (Schulte and Gasser, 2011). Even in the case of a dominantly inherited gene, an enormous clinical variability can be observed, with some carriers manifesting a mild pathology and others even not showing any symptoms at all (Kestenbaum and Alcalay, 2017). This different penetrance could be explained on the basis of the multifactorial nature of PD, meaning that a set of risk factors must be present in order to trigger the pathology. Mutations in the *LRRK2* gene are the most common monogenic cause of PD, contributing up to 40% of familial PD cases in certain populations (Healy et al., 2008). Most, if not all, LRRK2 mutations that cluster within the GTPase and kinase domains result in an increased kinase activity (Greggio et al., 2006, West et al., 2007, Ray et al., 2014). In particular, the G2019S mutation located in the catalytic core of the protein induces around a twofold increase in its kinase activity, which is required to exert its neurotoxic effect (Yao et al., 2010). Nevertheless, LRRK2-related pathology presents an incomplete penetrance, a variable age of onset and a heterogeneous pattern of symptoms, suggesting that the increased kinase activity induced by the pathogenic mutations could not alone account for the clinical expression of this disorder. In keeping with clinical data, rodent models of LRRK2-associated PD lack a consistent parkinsonian phenotype, since in vast majority of studies they do not show overt degeneration of the nigrostriatal pathway or deposition of pathological α-syn aggregates (Volta and Melrose, 2017). Therefore, genetic and environmental factors influencing LRRK2 penetrance and expressivity are an appealing field of research which can provide new insights into the etiology of PD. The main objective of this thesis was to investigate the interaction between the LRRK2 G2019S mutation and other risk factors of PD, such as ageing, environmental toxins and α-syn. In the first study (Study I) of this thesis we sought to investigate the role of ageing in the dysfunctions of the nigro-striatal DA transmission associated with LRRK2 G2019S. To achieve this goal, we assessed the integrity of the nigro-striatal DA neurons in young (3-month-old) and aged (>12-month-old) G2019S KI mice via Western blot and immunohistochemical analysis. We then proceeded to evaluate the status of the dopaminergic terminals, in particular measuring DA release, the expression and function of proteins involved in membrane (DAT) and vesicular (VMAT2) DA uptake, and, finally, the levels of endogenous α-syn and its Serine129 phosphorylated or 3,4-dihydroxyphenylacetaldehyde (DOPAL)-bound forms, which are considered markers of synaptic damage. In the second part of this study we aimed to investigate the interplay between G2019S LRRK2 and A53T α-syn during ageing. Young (3-month-old) and aged (12-month-old) G2019S KI mice were injected in the SNc with a recombinant adeno-associated viral vector (AAV) serotype 2/9 overexpressing the human A53T α-syn or green fluorescent protein (GFP) under the synapsin 1 promoter. We then evaluated the motor phenotype, nigrostriatal pathway integrity and synucleinopathy at 20 weeks (3-months cohort) or 12 weeks (12-month cohort) after virus injection. Furthermore, as neuroinflammation and microglia have been implicated in the pathophysiology of many neurodegenerative disorders,

we also analyzed microglial morphology. In the third study of this thesis (Study III), we investigated whether the increased LRRK2 kinase activity associated with the G2019S mutation alters the susceptibility to the neurotoxicant MPTP, which impairs the mitochondrial complex I and selectively destroys dopaminergic neurons. Under a subacute protocol of administration, MPTP was given to 3-month-old WT mice, to mice constitutively lacking LRRK2 (LRRK2 KO), or expressing the kinase silencing mutation D1994S (KD) or the kinase enhancing mutation G2019S (G2019S KI). The integrity of the nigro-striatal pathway was assessed by immunohistochemical analysis. We then proceeded to test the neuroprotective properties of two kinase inhibitors, i.e. PF-06447475 (Henderson et al., 2015) and MLi-2 (Fell et al., 2015). Once again, we concluded the study by assessing microglial number and morphology.

MATERIALS AND METHODS

Animals

Male homozygous LRRK2 G2019S KI, LRRK2 KO and KD mice backcrossed on a C57BL/6J strain were employed in the present study. LRRK2 KO mice were obtained through a collaboration with Prof. Matthew Farrer and Dr. Heather Melrose from Mayo Clinic (Jacksonville, FL, USA), whereas G2019S KI and KD animals were obtained through a collaboration with Novartis Institutes for BioMedical Research, Novartis Pharma AG (Basel, Switzerland) Male non-transgenic WT mice were either littermates obtained from the heterozygous breeding or from homozygous breeding. Animals were housed in the vivarium of the University of Ferrara, in a humidity and temperature-controlled environment under regular lighting conditions (12 hours light/dark cycle) with ad libitum access to food and water. Experimental procedures involving the use of animals were approved by the Ethical Committee of the University of Ferrara and the Italian Ministry of Health (licenses 171/2010-B and 318/2013-B). Adequate measures were taken to minimize animal pain and discomfort and to limit the number of animals employed.

Behavioral Tests

In order to assess different motor functions, a battery of three validated behavioral tests, i.e. the bar, drag and rotarod test, were employed as previously described (Marti et al., 2005, Viaro et al., 2013) with experimenters unaware of genotype and treatment. The different tests allow to measure different aspects of the parkinsonian phenotype, such as the absence or poverty of movement (akinesia, measured with the bar test), the slowness of movement and difficulty to adjust body posture (bradykinesia, evaluated with the drag test), poor coordination, balance, gait and motivation to run (assessed via the rotarod test). The three tests were performed in the same sequence (bar, drag and rotarod) when used in the same experimental design.

Bar test

In the bar (or catalepsy) test (Sanberg et al., 1988), which measures the ability of the animal to respond to an externally imposed static posture, mice were gently placed on a table with the forepaws on three blocks of increasing heights (1.5, 3 and 6 cm respectively). The time (in seconds) that each paw spent on each block (i.e. the immobility time) was recorded, up to a maximum of 20 seconds (cut-off time). Akinesia was calculated as the total time spent on the different blocks by each forepaw. Since values between the right and left forepaws do not different significantly, they were pooled together.

Drag test

The drag test, modification of the “wheelbarrow” test (Schallert et al., 1979), evaluates the ability of the animal to balance its body posture with the forelimbs, in response to an externally applied dynamic stimulus, such as backward dragging (Marti et al., 2005). Each animal was gently lifted

from the tail allowing the forepaws to rest on the table, and then dragged backwards at a constant speed of around 20 cm/s for a fixed distance of 100 cm. The number of steps made by each forepaw was counted by two different observers with five to seven determinations collected for each animal. As for the bar test, values between the right and left forepaw did not differ significantly, so data were pooled together.

Rotarod test

This test analyses the ability of the rodents to run on a rotating cylinder of 8 cm of diameter, and provides information on different motor parameters such as coordination, gait, balance, muscle tone and motivation to run (Rozas et al., 1997). The fixed-speed rotarod test was employed according to a previously described protocol (Marti et al., 2005, Viaro et al., 2013). Briefly, mice were tested in a stepwise mode at increasing speeds (usually from 5 to 45 rpm with increases of 5 rpm; 180 s each), and the total time spent on the rod was calculated (in sec).

Immunohistochemistry

Mice were deeply anesthetized with isoflurane and transcardially perfused with Phosphate Buffer Solution (PBS) and then with 4% paraformaldehyde in PBS (0.1 M, pH 7.4). Brains were removed, transferred to a 30% sucrose solution in PBS for cryoprotection and then stored at −80 °C.

TH, iba-1, α-syn and pSer129 α-syn immunohistochemistry

Fifty micrometer free-floating sections of striatum (AP from +1.0 to −1.25 from bregma) and SNc (AP from −3.16 to −3.52 from bregma) (Paxinos and Franklin, 2004) were rinsed 3 times in PBS, incubated for 30 min at room temperature with a blocking solution (PBS + BSA 1:50 + Triton X100 0.3%) and then incubated with a rabbit polyclonal antibody raised against TH (ab112; 1:750 in BSA 1% PBST; Abcam, Cambridge, UK), total α-syn (ab52168; 1:200 in BSA 1% PBST; Abcam, Cambridge, UK), pSer129 α-syn (ab51253; 1:250 in BSA 1% PBST; Abcam, Cambridge, UK), human α-syn (hα-syn) (ab138501; 1:150 in BSA 1% PBST; Abcam, Cambridge, UK) or ionized calcium binding adaptor molecule 1 (iba-1) (ab178846; 1:2000 in BSA 1% PBST; Abcam, Cambridge, UK) overnight at room temperature. Sections were then rinsed 3 times in PBS and incubated for 1 h with an anti-rabbit HRP-conjugated secondary antibody (ab6721, 1:500 in BSA 1% PBST; Abcam, Cambridge UK), washed again and revealed by a DAB substrate kit (ab64238, Abcam, Cambridge, UK). Sections were mounted on gelatinized slides, dehydrated with a solution of Chloroform/100% Ethanol 1:1 and coverslipped for further analysis.

Stereology and neuron counting

Stereological analysis was performed counting TH-positive neurons (phenotypic marker) and cresyl violet stained cells (structural marker) in SNc, according to an unbiased stereological sampling method based on optical fractionator stereological probe (Larsen et al., 1998). A Leica DM6B motorized microscope (Leica Microsystems, Milan, Italy) coupled with a Stereo

Investigator software (MBF Europe, Delft, The Netherlands) was used. Counting was performed on at least 5 consecutive 50 μm thick slices, magnified at 63×.

TH quantification in striatum

Images of mice striata were taken at 2.5× magnification with a Leica DM6B motorized microscope, and optical densitometry analyzed off-line as grey level with ImageJ (Rueden et al., 2017) using the corpus callosum as background.

Quantification of α-syn and pSer129 α-syn expression

To quantify the levels of expression of α-syn, pSer129 α-syn, hα-syn, the semi-stereological method described by Bourdenx et al. (Bourdenx et al., 2015) was employed. This method has been rigorously standardized; in fact, all serial striatal slices for each animal were taken, marked, put in the same well and exposed to DAB for 1 min (according to the data sheet of Abcam DAB substrate Kit). After being mounted, slides were scanned using a Leica DM6B motorized microscope and the representative surface of the staining in each SN and striatal section was determined using a color threshold, then the area was sampled (probes of 50 × 40 μm, space 150 × 120 μm). The Cavalieri principle was applied to evaluate the representative volume of α-syn or pSer129 α-syn expression for each SN. The SN volume obtained from the α-syn staining was used to calculate the pSer129 α-syn expression as a percentage, thus allowing the comparison between groups.

Iba-1 analysis

Three consecutives sections were mounted on a coverslip and images were acquired using a Leica DM6B motorized microscope, and later analyzed with ImageJ software. Iba-1+ cells were binarized and number of cells and area of surface occupied in pixels^2 were quantified in order to compare the different treatments.

Western blot analysis

Mice were anesthetized, sacrificed by cervical dislocation, and brains collected. Striata were solubilized and homogenized in lysis buffer (RIPA buffer, protease and phosphatase inhibitor cocktail) and centrifuged at 13,000 rpm for 15 min at 4 °C. Supernatants were collected and total protein levels were quantified using the bicinchoninic acid protein assay kit (Thermo Scientific). Thirty micrograms of protein per sample were separated by SDS-PAGE, transferred onto polyvinyldifluoride membrane and tested for the following primary antibodies: rabbit anti-tyrosine hydroxylase (TH) (Merck Millipore, AB152, 1:1000), rabbit anti-DAT (Sigma Aldrich, D6944, 1:1000), rabbit anti-VMAT2 (Sigma Aldrich, V9014, 1:300), rabbit anti-VMAT2 (Miller Lab, Emory University, 1:1000), rabbit anti-pSer129 α-syn (Abcam, ab51253, 1:1000), rabbit anti pSer1292 LRRK2 (Abcam, ab203181, 1:300). Appropriate horseradish peroxidase-linked secondary antibodies (Merck Millipore, goat anti-rabbit IgG HRP-conjugate 12–348, 1:4000 or goat anti-rat IgG HRP-conjugate AP136P, 1:5000) were then used and immunoreactive proteins

were visualized by enhanced chemiluminescence (ECL) detection kit (Pierce™ BCA Protein Assay Kit, Thermo Scientific or ECL+, GE Healthcare). Images were acquired and quantified using the ChemiDoc MP System and the ImageLab Software (Bio-Rad). Membranes were then stripped and re-probed with rabbit anti-GAPDH antibody (Thermo Scientific, PA1-988, 1:1000), rabbit anti-LRRK2 (Abcam, ab133474, 1:300) or rabbit anti-α-syn antibody (Abcam, ab52168, 1:1000). Data were analyzed by densitometry and the optical density of specific target protein bands was normalized to the corresponding housekeeper protein levels.

Antibody	Code	Dilution
TH	Ab112	1:750 IHC
Total α-synuclein	Ab52168	1:200 IHC, 1:1000 WB
pSer129 α-synuclein	Ab51253	1:200/250 IHC, 1:1000 WB
Human α-synuclein	Ab138501	1:150 IHC
IBA-1	Ab178846	1:2000 IHC
Anti-rabbit HRP-conjugate	Ab6721	1:500 IHC
TH	Ab152	1:1000 WB
DAT	D6944	1:1000 WB
VMAT2	V9014	1:300 WB
VMAT2	Miller's lab	1:1000 WB
LRRK2 pSer1292	Ab203181	1:300 WB
Anti-rabbit HRP-conjugate	Millipore 12-348	1:4000 WB
Anti-rat HRP-conjugate	AP136P	1:5000 WB
GAPDH	PA1-988	1:1000 WB
LRRK2	Ab133474	1:300 WB

Table 1: List of antibodies employed in the different studies with their code and dilution.

Study I

Experimental design

For behavioral studies, twelve-month-old mice were acutely administered i.p. with the VMAT2 inhibitor reserpine at the doses of 1 or 2 mg/kg (Volta et al., 2010), or with the DAT inhibitor GBR-12783 at the dose of 6 mg/kg. Microdialysis experiments were carried out in the dorsolateral striatum of 19-month-old G2019S KI mice and with age-matched WT littermates. For immunohistochemical and biochemical analysis 3-month-old and 12-month old G2019S KI and age-matched WT were employed.

In vivo microdialysis

Two concentric microdialysis probes (1 mm Cuprophane membrane with a 6 kDa cut-off; AgnTho's, Stockolm, Sweden) were stereotaxically implanted under isoflurane anesthesia in both

dorsal striata (coordinates from the bregma: AP +0.6, ML ±2.0, DV −2.0) (Paxinos and Franklin, 2004). Twenty-four hours after implantation, probes were perfused (2.1 µl/min) with a modified Ringer solution (in nM CaCl2 1.2; KCl 2.7; NaCl 148 and MgCl2 0.85) and samples were collected every 20 min (Bido et al., 2011) (Mabrouk et al., 2010, Volta et al., 2010) after a 6 h wash-out period. Experiments were run at 24 and 48 h after implantation, and treatments were randomized. GBR-12783 and Nov-LRRK2-11 were administered at 20 mg/kg (i.p.) and 10 mg/kg (i.p.), respectively. At least three baseline samples were collected before drug treatment. At the end of the experiments, animals were sacrificed by isoflurane overdose, and the correct placement of the probes was verified histologically.

Neurochemical analysis using LC-MS

DA, HVA, DOPAC and 3MT concentrations in dialysates were analyzed using a benzyolation derivatization LC-MS method described by Song and collaborators (Song et al., 2012). Briefly, 5 µl dialysate samples were derivatized by adding 2.5 µl of 100 mM sodium tetraborate, 2.5 µl of 2% benzoyl chloride in acetonitrile, and 2.5 µl of a stable 13C benzoylated isotope internal standard mixture for improved quantitation. A Thermo Fisher Accela UHPLC (Waltham, MA) system automatically injected 5 µl of the sample onto a Waters (Milford, MA) HSS T3 reverse phase HPLC column (1 mm X 100 mm, 1.8 µm). Mobile phase A consisted of 10 mM ammonium formate and 0.15% formic acid. Mobile phase B was pure acetonitrile. Analytes were detected by a Thermo Fisher TSQ Quantum Ultra triple quadrupole mass spectrometer operating in multiple reaction monitoring (MRM) mode. Run times were approximately 6 min and all analytes could be detected well above quantification limits (data not shown).

Synaptosomes preparation

Mice were anesthetized and sacrificed by cervical dislocation. Striata from each mouse were homogenized in ice-cold 0.32 M sucrose (pH 7.4) with a Teflon-glass homogenizer and centrifuged at 9,500 g for 10 min at 4 °C. The supernatant was then centrifuged at 10,000 g for 20 min at 4 °C, and the pellet processed for release experiments or DA uptake assay.

Release experiments

The pellet was resuspended in 1.5 ml of pre-oxygenated Krebs solution (in mM: NaCl 118.5, KCl 4.7, CaCl2 1.2, MgSO4 1.2, KH2PO4 1.2, NaHCO3 25, glucose 10, ascorbic acid 0.05, disodium EDTA 0.03, pH 7.4) and incubated with 50 nM [3H]-DA (specific activity 40 Ci/mmol; Perkin-Elmer, Boston, MA, USA) for 25 min at 36.5 °C (Marti et al., 2003). At the end of the incubation, 12 ml of pre-oxygenated Krebs were added, then 1 ml aliquots of the suspension (~0.35 mg protein) were injected into nylon syringe filters maintained at 36.5 °C and superfused (0.4 ml/min) with pre-oxygenated Krebs. Under these superfusion conditions, spontaneous [3H]-DA efflux is essentially unaffected by reuptake (Marti et al., 2003). Sample collection (every 3 min) was

initiated after a 20 min period of filter washout. Radioactivity in the samples and in the filters was measured using a Perkin Elmer Tri Carb 2810 TR scintillation counter.

DA uptake assay

The pellet was resuspended in ice-cold uptake buffer (in mM: NaCl 125, KCl 5, MgSO4 1.5, CaCl2 1.2, KH2PO4 1.5, glucose 10, HEPES 25, pargyline 0.1, ascorbic acid 0.5, pH 7.4) and incubated for 5 min at 37 °C with 20 nM [^{3}H]-DA isotopically diluted with varying concentrations of unlabeled DA to obtain final DA concentrations in the 20–2000 nM range. Non-specific DA uptake was evaluated in the presence of 5 μM GBR-12783. The reaction was terminated by filtering the assay mixture through Whatman GF/B glass fiber filters using a Brandel cell harvester (Brandel Instruments, Unterföhring, Germany). The filter-bound radioactivity was counted using a Perkin Elmer Tri Carb 2810 TR scintillation counter. Specific DA uptake, defined as the difference between DA accumulated in the absence and in the presence of GBR-12783, was expressed as pmol/mg protein/min. Protein concentration was determined using a Bio-Rad method with bovine albumin as standard reference. Kinetic parameters (V_{max} and K_m) were determined using Prism 5.0 (GraphPad Software Inc., San Diego, CA).

DOPAL-bound α-syn analysis

DOPAL-bound α-syn was revealed using ABPA resin (Sigma Aldrich, A8530) pulldown. Five-hundred micrograms total protein were incubated with 50 μl of the resin overnight at 4 °C shaking. The resin was then pelleted, the supernatant removed, and the resin was washed twice with PBS/acetonitrile and water. Protein was collected from the resin by adding 20 μl Laemmli buffer and processed as described above using the anti-α-syn antibody. The band intensity was quantified by Image J software and the pull-down protein was compared with the total lysate.

VMAT2 activity assay

Mice were anesthetized and decapitated. Whole brains were homogenized in ice-cold buffer (4 mM HEPES, 0.32 M sucrose, pH 7.4) and centrifuged at 1,000 g for 10 min at 4 °C. Supernatants were centrifuged at 20,000 g for 20 min at 4 °C, the resulting pellets were resuspended in 1.6 ml of resuspension buffer (0.32 M sucrose, pH 7.4) and subjected to osmotic shock by 10 up-and-down strokes in 6.4 ml of ice-cold water followed by addition of 1 ml of 250 mM HEPES and 1 M potassium tartrate, pH 7.4, to restore osmolarity. Samples were then centrifuged at 20,000 g for 20 min at 4 °C, and supernatants were centrifuged at 120,000 g for 2 h at 4 °C. Final pellets containing synaptic vesicles were resuspended in assay buffer (100 mM potassium tartrate, 25 mM HEPES, 0.1 mM EDTA, 0.05 mM EGTA, 1.7 mM ascorbate, 2 mM ATP disodium salt, pH 7.4) and incubated for 5 min at 37 °C with 20 nM [^{3}H]-DA isotopically diluted with varying concentrations of unlabeled DA. Non-specific DA uptake was evaluated in the presence of 10 μM tetrabenazine. The reaction was terminated by filtering the assay mixture through 0.5% polyethylenamine-soaked

Whatman GF/B glass fiber filters using a Brandel cell harvester. The filter-bound radioactivity was counted using a Perkin Elmer Tri Carb 2810 TR scintillation counter.

Study II

Experimental design

Motor activity of 3-month-old and 12-month-old G2019S KI mice and age-matched WT mice was assessed for one week prior to surgical procedures. After viral injection, behavioral tests were performed every 4 weeks up the end of the observation time. After 12 (12-month-old cohort) or 20 (3-month cohort) weeks animals were sacrificed, and brains extracted for immunohistochemical analysis.

AAV2/9-hα-syn vector production and injection

Recombinant AAV2/9-hα-syn vectors driven by the synapsin-I promoter were produced, purified and characterized as already described (Bourdenx et al., 2015). Briefly, vectors were transfected into HEK-293 T/17 cells (ATCC, Teddington, UK) for three times using a polyethylenimine solution. Seventy-two hours after transfection, cells were re-suspended in lysis buffer (150 mM NaCl, 50 mM Tris-HCl pH 8.5), and then lysed using a freeze-thaw cycle (−80 °C/+37 °C). The obtained supernatant was purified by iodixanol gradient step centrifugation, and finally aliquoted and kept in stock at −80 °C. Nine 3-month-old and ten 12-month-old G2019S KI mice, and equal numbers of age-matched WT mice, received a bilateral SNc stereotaxic injection of AAV2/9-hα-syn (2.35×10^{13} genome containing particles/µl; 1 µl), under isoflurane anesthesia (Arcuri et al., 2016). As a control, nine 3-month-old and ten 12-month-old G2019S KI mice, and equal numbers of age-matched WT mice, received a bilateral SNc stereotaxic injection of AAV-GFP. Virus was injected with a glass syringe at a flow rate of 0.5 µl/min and was left in place for additional 4 min to prevent backflush. Coordinates from bregma were (in mm): antero-posterior −3.3; medio-lateral ±1.25; dorso-ventral −4.6 from dura (Paxinos and Watson).

Treatment with proteinase K (PK)

Tissue sections were incubated for 5 min with PK (ab64220; Abcam, Cambridge, UK) at room temperature. At the end of the incubation, sections were rinsed in PBS and processed as described above using rabbit polyclonal antibody for pSer129 α-syn (ab51253; 1:200 in BSA 1% PBST; Abcam, Cambridge, UK).

Study III

Experimental design

In the first part of the study, 8-10 G2019S KI, LRRK2 KO, D1994S KD and an equal number of age-matched mice were treated with MPTP 30 mg/Kg i.p. or saline for seven days. At the end of the treatment, animals were sacrificed, brains extracted for immunohistochemical analysis. In the second experimental set, G2019S KI mice were trained for one week with the bar, drag and rotarod

tests until their performance became reproducible, and baseline motor activity was recorded. Then, mice were treated with PF-06447475 (10 mg/kg b.i.d., s.c.) or saline for 9 days. On the third day of treatment, animals were administered with either 30 mg/Kg MPTP or saline up to the 9th day. On the 10th day, motor activity in the bar, drag and rotarod tests was evaluated, after which animals were sacrificed by cervical dislocation, and tissues extracted for further analysis. In the third part of this study, the neuroprotective potential of LRRK2 inhibitors was evaluated in MPTP-treated G2019S KI and LRRK2 WT mice adopting a "clinically-drive" approach. Mice were treated with either MPTP or saline for 7 days, and starting from the 4th day, also with PF-06447475 (10 mg/kg b.i.d., s.c.), MLi-2 (10 mg/kg b.i.d., i.p.) or saline for the next 10 days. At the end of treatement, animals were sacrificed, perfused and brains collected for further analysis

Data presentation and statistical analysis

Study I. Data are expressed as percentage of baseline (behavioral experiments) or absolute values and are mean ± SEM (standard error of the mean) of n mice. Statistical analysis of drug effect was performed by one-way conventional or repeated measure (RM) analysis of variance (ANOVA) followed by the Newman-Keuls test for multiple comparisons, or by two-way ANOVA followed by the Bonferroni test for multiple comparisons. The Student t-test, two tailed for unpaired data, was used to compare two groups of data. P-values <0.05 were considered to be statistically significant.

Study II. Motor performance in the drag and rotarod test was presented as absolute values (calculated as number of steps or time on rod in sec) and analyzed by two-way RM ANOVA followed by the Bonferroni test. All the other data were analyzed by one-way ANOVA followed by the Bonferroni test. Data obtained from stereological counting were expressed as absolute values (number of cells), density of striatal TH terminals was expressed as absolute data (mean absolute value of grey scale between the two striata), density of α-syn aggregates was expressed as area of threshold, data from iba-1+ cells were expressed as absolute value and as area occupied in pixel^2. P values<0.05 were considered to be statistically significant.

Study III. Data are expressed as absolute values (calculated as time on bar, number of steps or time on rod in sec) and are mean ± SEM of n mice. Statistical analysis of drug effect was performed by one-way conventional ANOVA followed by the Bonferroni test for multiple comparisons, or by three-way ANOVA followed by the Newman-Keuls test for multiple comparisons. Data obtained from stereological counting were expressed as absolute values (number of cells), density of striatal TH terminals was expressed as absolute data (mean absolute value of grey scale between the two striata. data from iba-1+ cells were expressed as absolute value and as area occupied in pixel^2. The Student t-test, two tailed for unpaired data, was used to compare two groups of data. P values <0.05 were considered to be statistically significant.

Drugs

GBR-12783 dihydrochloride and reserpine were purchased from Tocris Bioscience (Bristol, UK). Nov-LRRK2-11 was obtained from Novartis Institutes for BioMedical Research, Novartis Pharma AG (Basel, Switzerland). MPTP, PF-06447475 and MLi-2 were purchased from Carbosynth (Compton, Berkshire, UK). GBR-12783 and Nov-11 were dissolved in 3% DMSO and saline. MPTP was dissolved in slaine. PF-06447475 and MLi-2 were dissolved in 2% DMSO and 30% hydroxypropyl β-cyclodextrin. Reserpine was dissolved in 1% glacial acetic acid, distilled water and pH brought to 4.5 with NaOH.

RESULTS

Study I: presynaptic dopaminergic dysfunctions in aged G2019S KI

Experiment I: evaluation of nigrostriatal dopaminergic pathway and LRRK2 activity

The nigro-striatal DA pathway is intact in G2019S KI mice

To confirm that the G2019S KI mice under study possess enhanced LRRK2 kinase activity, we monitored LRRK2 autophosphorylation levels at Ser1292 using Western blotting. We found that pSer1292 levels were ~8-fold higher in the striatum of 12-month-old G2019S KI mice compared to age-matched WT littermates (Fig. 9), indicating a clear-cut gain of kinase activity in the presence of the G2019S mutation.

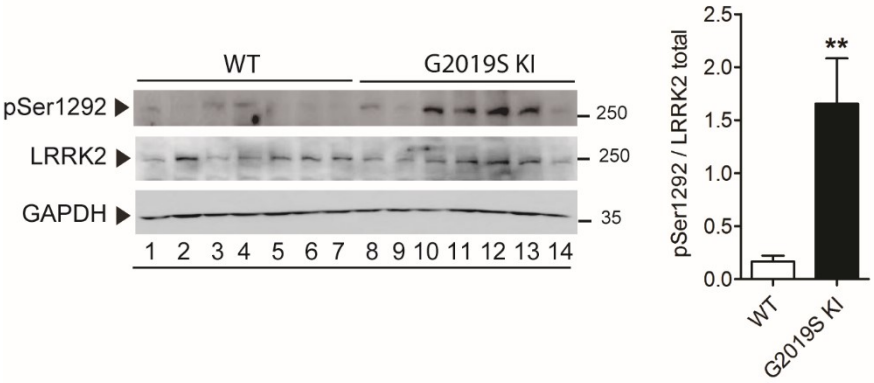

*Fig. 9: Phosphorylation levels of LRRK2 at Ser1292 (pSer1292) are elevated in G2019S knock-in (KI) mice. Striatal pSer1292 and total LRRK2 levels were measured by Western blotting in 12-month-old G2019S KI mice and age-matched WT controls. Representative blots (left) and quantification (right) are shown. Data are expressed as pSer1292 LRRK2/total LRRK2 and are means ± SEM of 7 animals per group. Statistical analysis was performed with the Student t-test, two tailed for unpaired data. **p < 0.01, different from WT.*

We next investigated the possibility that the G2019S mutation compromises the integrity of nigro-striatal DA neurons (Fig. 10). No differences in nigral DA cell number or density of striatal TH-positive terminals were detected between 12-month-old (Fig. 10A and 10B, respectively) or 19-month-old (data not shown) G2019S KI and WT mice. Likewise, striatal TH levels were similar between genotypes in 12-month-old animals (Fig. 10C).

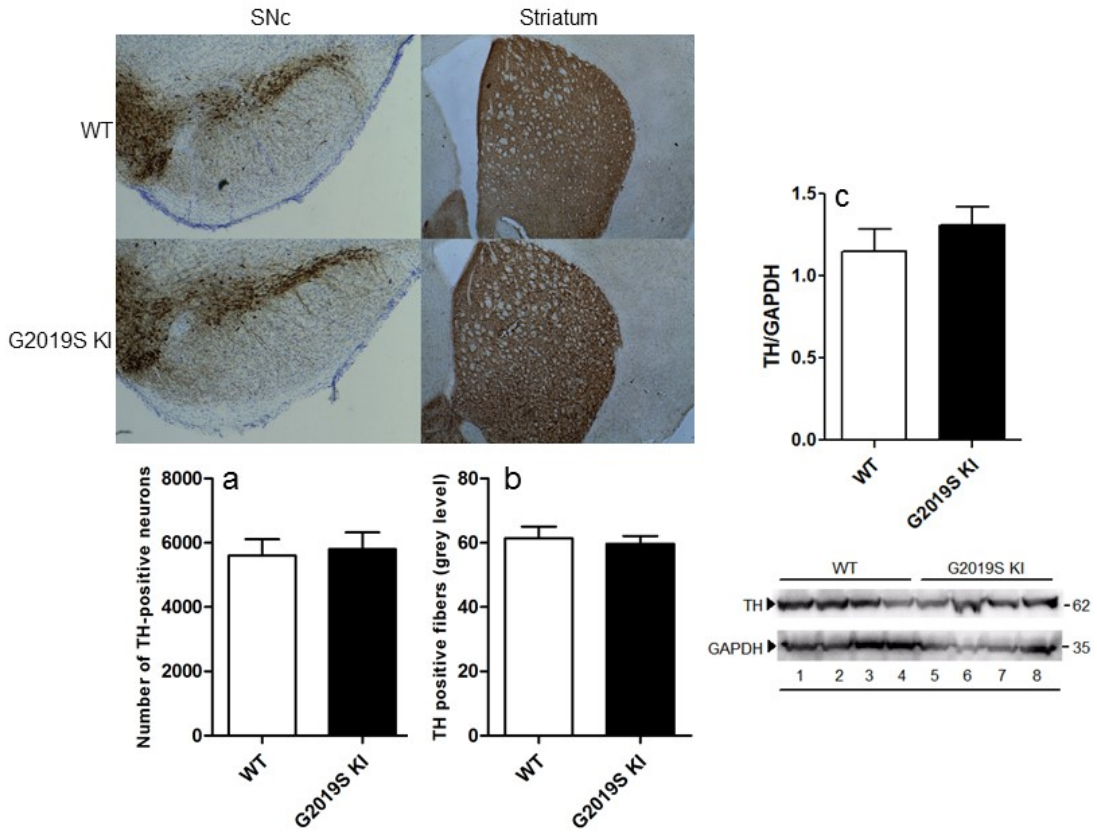

Fig. 10: The integrity of nigro-striatal dopaminergic neurons is preserved in G2019S KI mice. Stereological count of nigral DA neurons (a) and density of tyrosine hydroxylase (TH) positive striatal nerve terminals (b), with representative images, in 12-month-old G2019S KI mice and age-matched WT littermates. Western blotting analysis of striatal TH levels in 12-month-old G2019S KI mice and age-matched WT controls (c). Data are expressed as absolute values and are means ± SEM of 8 (a-b) and 4 (c) animals per group.

Striatal DA release is preserved in G2019S KI mice

Genotype	DA	DOPAC	HVA	3-MT	DOPAC/DA	HVA/DA	3-MT/DA
WT	0.28 ± 0.06	47.31 ± 15.98	82.39 ± 21.44	0.99 ± 0.51	247.63 ± 112.25	242.30 ± 36.65	2.96 ± 0.87
G2019S KI	0.36 ± 0.06	22.12 ± 5.63	54.74 ± 11.63	0.42 ± 0.082	48.65 ± 10.39	114.00 ± 36.50*	1.14 ± 0.24*

*Tab. 1: Basal dialysate levels (nM) of DA and its metabolites DOPAC, 3-MT and HVA monitored using in vivo microdialysis in the dorsal striatum of 19-month-old G2019S knock-in mice (G2019S KI) and wild-type littermates (WT). *p < 0.05, significantly different from WT. The metabolite/DA ratios are also reported. Data are means ± SEM of 11–15 determinations per group and were analyzed using the Student t-test, two-tailed for unpaired data.*

To investigate whether the exocytotic properties of DA terminals were affected by the G2019S mutation (Fig. 11), synaptosomes obtained from the striatum of 12-month-old mice were depolarized with a sequence of three 90-sec pulses (18 min away) of 10 mM or 20 mM K^+ (Fig. 11A). No differences in spontaneous [^{3}H]-DA efflux (Fig. 11A) and K^+-evoked [^{3}H]-DA overflow (Fig. 11A, B) were observed between G2019S KI mice and aged-matched WT controls, both after a

single or repeated pulse, suggesting that enhanced LRRK2 kinase activity is not associated with changes of striatal DA release.

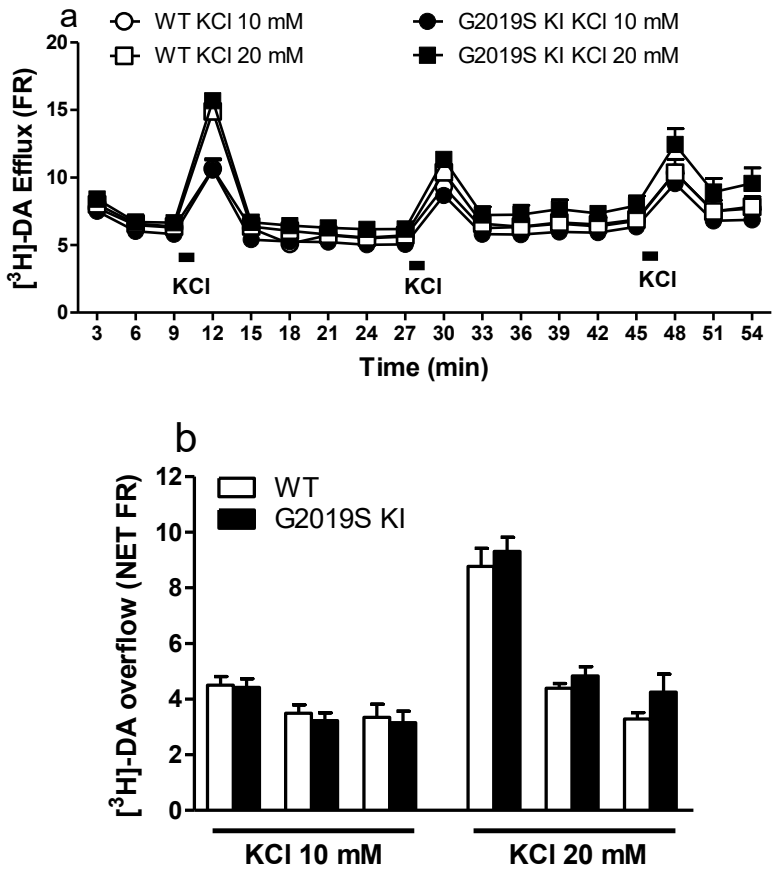

Fig 11: Dopamine (DA) release is preserved in G2019S KI mice. [3H]-DA preloaded synaptosomes obtained from the striata of 12-month-old G2019S KI mice and age-matched WT littermates were continuously superfused with Krebs and stimulated with 3 pulses (90 s) of 10 mM or 20 mM K+ (18 min apart). DA release has been expressed as fractional release (FR; i.e. tritium efflux expressed as percentage of the tritium content in the filter at the onset of the corresponding collection period; a), or NET FR (i.e. K+-evoked tritium overflow as percent of the tritium content in the filter at the onset of the corresponding collection period; b). Data are means ± SEM of 9 determinations per group.

Consistently, in vivo microdialysis revealed no significant differences in dialysate levels of DA and DA metabolites (DOPAC, HVA and 3-MT) between 19-month-old G2019S KI mice and WT littermates (Tab. 1), although a trend for higher DA and lower metabolites levels in G2019S KI mice was observed. Indeed, significant reductions of HVA/DA and 3-MT/DA ratios in G2019S KI mice were found, the reduction of DOPAC/DA ratio being close to significance (p=0.067; Tab. 1), suggesting a slower DA metabolism in G2019S KI mice Microdialysis also revealed that the LRRK2 kinase inhibitor Nov-LRRK2-11 (10 mg/kg, i.p.), which normalizes motor performance in G2019S KI mice (Longo et al., 2014), did not affect striatal DA release in any genotypes (Fig. 12A), suggesting the motor phenotype of G2019S KI mice did not rely on greater DA release.

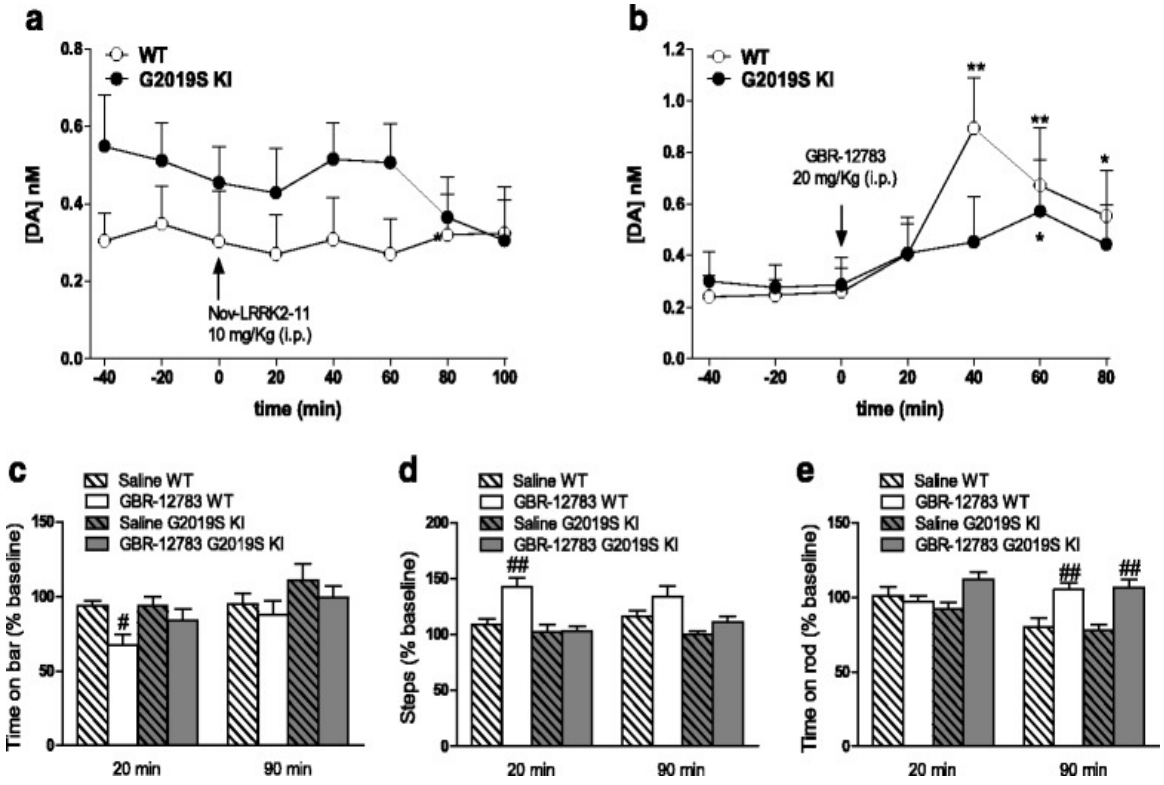

*Fig. 12: Acute blockade of LRRK2 kinase activity does not affect striatal dopamine (DA) levels whereas acute DAT blockade evoked blunted neurochemical and behavioral responses in G2019S KI mice in vivo. Microdialysis was performed in the dorsolateral striatum of 19-month-old G2019S KI mice and with age-matched wild-type (WT) littermates (WT) (a, b). Mice were then challenged with the LRRK2 kinase inhibitor Nov-LRRK2-11 (10 mg/kg, i.p.) or the DAT blocker GBR-12783 (20 mg/kg, i.p.). Dialysate levels of DA are expressed as absolute values (nM) and are mean ± SEM of 5 WT and 6 G2019S KI mice (a), or 6 WT and 9 G2019S KI mice (b). Motor responses of 12-month-old mice to GBR-12783 (6 mg/kg, i.p.) or saline administration (c-e). Motor activity was assessed using the bar (c), drag (d) and rotarod (e) tests, before (baseline) and after (20 and 90 min) drug administration, and was expressed as percentage of performance at baseline. Data are means ± SEM of 12–17 (WT) or 13–17 (G2019S KI) mice per group. Statistical analysis was performed using one-way RM ANOVA (a-b) or conventional ANOVA (c-e) followed by the Newman–Keuls test for multiple comparisons. *p < 0.05, ** p < 0.01 significantly different from baseline values; # p < 0.05, ## p < 0.01 significantly different from saline.*

Experiment II: ex vivo analysis of DAT and VMAT2 levels and activity

Age-dependent dysfunction of DAT in G2019S KI mice

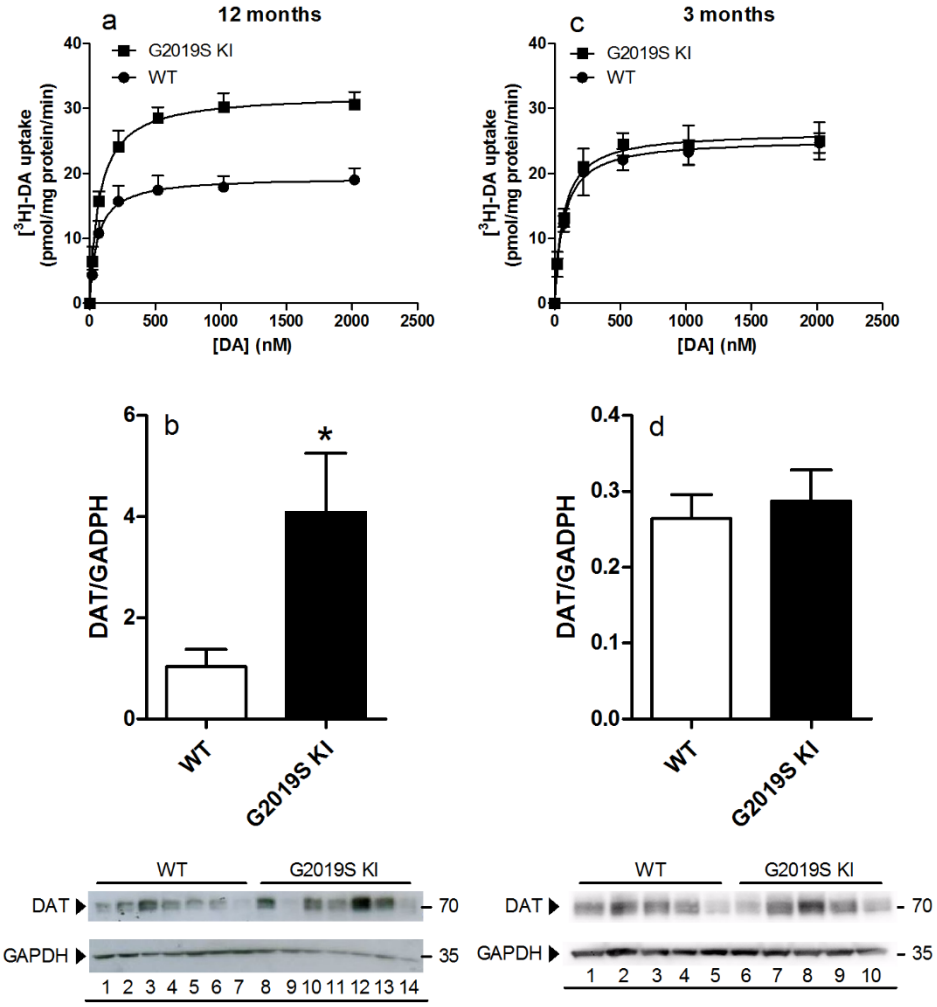

*Fig. 13: Age-dependent dysfunction of DAT expression and function in G2019S knock-in (KI) mice. Kinetic analysis of [3H]-DA uptake in synaptosomes (a, c), and Western blotting analysis of DAT protein levels (and representative blots) (b, d) were performed in the striata of 12-month-old (a, b) and 3-month-old (c, d) G2019S KI mice in comparison with age-matched WT controls. Values are expressed as mean ± SEM of n = 4 (uptake) or n = 3 (Western blotting) independent experiments performed in duplicate. Statistical analysis was performed using the Student t-test, two-tailed for unpaired data. *p < 0.05, different from WT.*

Since extracellular DA levels strongly rely on DAT activity, we investigated whether the trend for an increase in extracellular DA levels observed in G2019S KI mice was associated with changes in DAT activity. Microdialysis showed that striatal DA levels were elevated in both genotypes after administration of the DAT blocker GBR-12783 (20 mg/Kg, i.p) (Fig. 12B). However, the response in WT mice was more rapid and larger (maximum ~3-fold over basal) compared to that in G2019S KI mice that was delayed and blunted (~2-fold over basal) (Fig. 12B). To confirm dysfunctional DAT activity, we monitored motor performances following GBR-12783 administration. As previously reported (Longo et al., 2014), G2019S KI mice were more active ($p<0.001$) in the bar and drag tests (18.29±1.62 sec and 13.67±0.47 steps, respectively; n=60) compared to WT littermates (31.57±1.65 sec and 9.92±0.39 steps, respectively; n=58). Conversely, rotarod

performance was similar in G2019S KI and WT mice (837.58±21.73 and 872.2±31.89 sec, respectively). GBR-12783 (6 mg/Kg) reduced the immobility time (Fig. 12C) and increased the stepping activity (Fig. 12D) in WT but not G2019S KI mice, while causing a delayed increase in rotarod performance in both genotypes (Fig. 12E). We then investigated DAT expression and function in striatal synaptosomes from 12-month-old mice (Fig. 13A, B). Analysis of DA uptake kinetics (Fig. 13A) revealed a significant 63% increase of maximal transport rate (V_{max}) in striatal synaptosomes from G2019S KI mice (33.1±1.4 pmol/mg prot/min) with respect to WT mice (20.2±1.1 pmol/mg prot/min; $p<0.01$), without changes in the DA affinity for the transporter (K_m 76.3±8.5 nM vs 67.9±9.0 nM in G2019S KI and WT mice, respectively). Consistent with higher V_{max}, Western blot analysis showed that DAT protein levels were ~4-fold higher in G2019S KI than WT mice (Fig. 13B). To investigate whether these changes were age-dependent, experiments were replicated in younger animals (Fig. 13C, D). No differences were observed in [^{3}H]-DA uptake kinetics between 3-month-old G2019S KI mice (K_m 66.2±10.1 nM, V_{max} 26.5±1.7 nM) and age-matched WT controls (K_m 70.5±10.6 nM, V_{max} 25.3±0.6 nM) (Fig. 13C). Likewise, protein levels were similar between genotypes at this age (Fig. 13D).

Age-dependent dysfunction of VMAT2 in G2019S KI mice

Since the DAT/VMAT2 ratio is a vulnerability factor in DA neurons (Miller et al., 1999b), we next investigated whether VMAT2 was also dysfunctional in G2019S KI mice (Fig. 14). First, the VMAT2 blocker reserpine was administered (1 mg/Kg, i.p.) to 12-month-old mice (Fig. 14A-C). G2019S KI and WT mice showed similar increases of immobility time 24 hr after reserpine administration, although G2019S KI mice were also affected at 48 hr (Fig. 14A). Conversely, reserpine reduced stepping activity (Fig. 14B) and rotarod performance (Fig. 14C) selectively in WT mice, both at 24 hr and 48 hr after administration. Higher reserpine doses (2 mg/Kg), however, caused similar motor impairments in both genotypes (data not shown). We then measured VMAT2 uptake activity in a preparation of whole-brain synaptic vesicles (Fig. 14D). VMAT2 affinity for DA (K_m) was similar between 12-month-old G2019S KI mice and WT controls (356.3±25.2 vs 333.6±31.0 nM, respectively), although V_{max} was significantly higher in G2019S KI mice (52.7±2.4 vs 43.2±2.2 nM, respectively; $p<0.05$). Striatal VMAT2 protein levels were then analyzed, comparing a commercially available (Fig. 14E) with an in-house validated (Cliburn et al., 2016) antibody (Fig. 14F). Both antibodies revealed a ~50% reduction of VMAT2 levels in G2091S KI mice. Finally, VMAT2 activity and protein levels were measured in 3-month-old mice (Fig. 14G-I). As for DAT, no differences between genotypes were observed at this age.

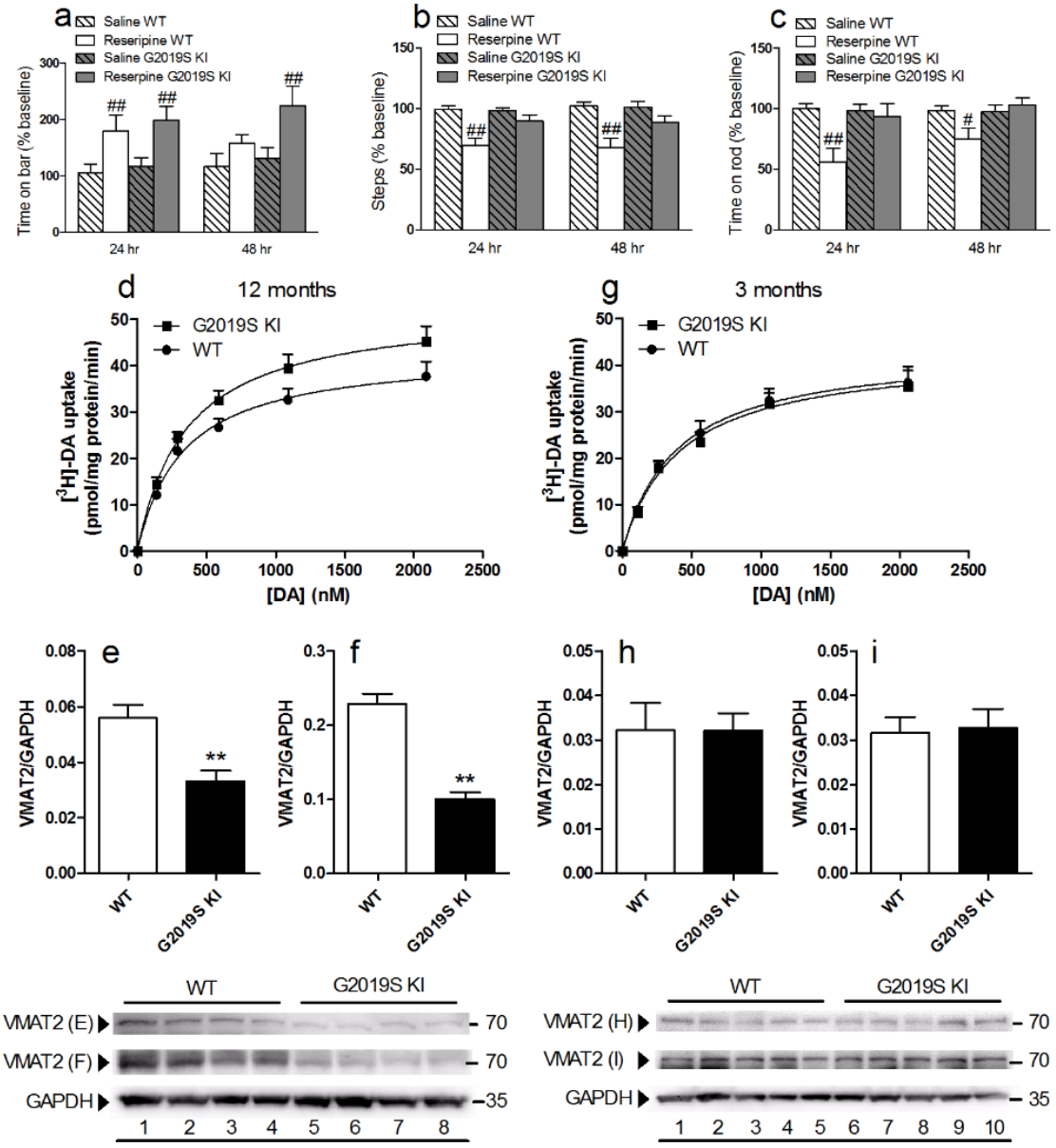

*Fig. 14: Age-dependent dysfunction of VMAT2 expression and function in G2019S KI mice. Motor activity in 12-month-old G2019S KI mice and wild-type (WT) littermates treated with reserpine (1 mg/kg, i.p.) or saline, and challenged in the bar (a), drag (b) and rotarod (c) tests, before (baseline) and after (24 and 48 h) drug administration. Motor performance was expressed as percentage of performance at baseline. Data are means ± SEM of n = 14–15 mice per group and were analyzed using conventional ANOVA followed by the Newman–Keuls test for multiple comparisons. # $p < 0.05$, ## $p < 0.01$ significantly different from saline. Kinetic analysis of [3H]-DA uptake in whole-brain vesicles and Western blotting of VMAT2 levels in the striata from 12-month-old (d-f) or 3-month old (g- i) G2019S KI mice and WT littermates. In Western blotting, two different anti-VMAT2 antibodies were used, one commercially available (e, h; Sigma) and another developed by Miller lab (f, i) (see Methods). Data are expressed as mean ± SEM of 4 mice (d- f), 3 mice (g) or 5 mice (h, i) per group, performed in duplicate. Statistical analysis was performed by the Student t-test, two-tailed for unpaired data. **$p < 0.01$, different from WT*

Experiment III: evaluation of α-synuclein and its modified forms

Age-dependent increase of pSer129 α-synuclein in G2019S KI mice

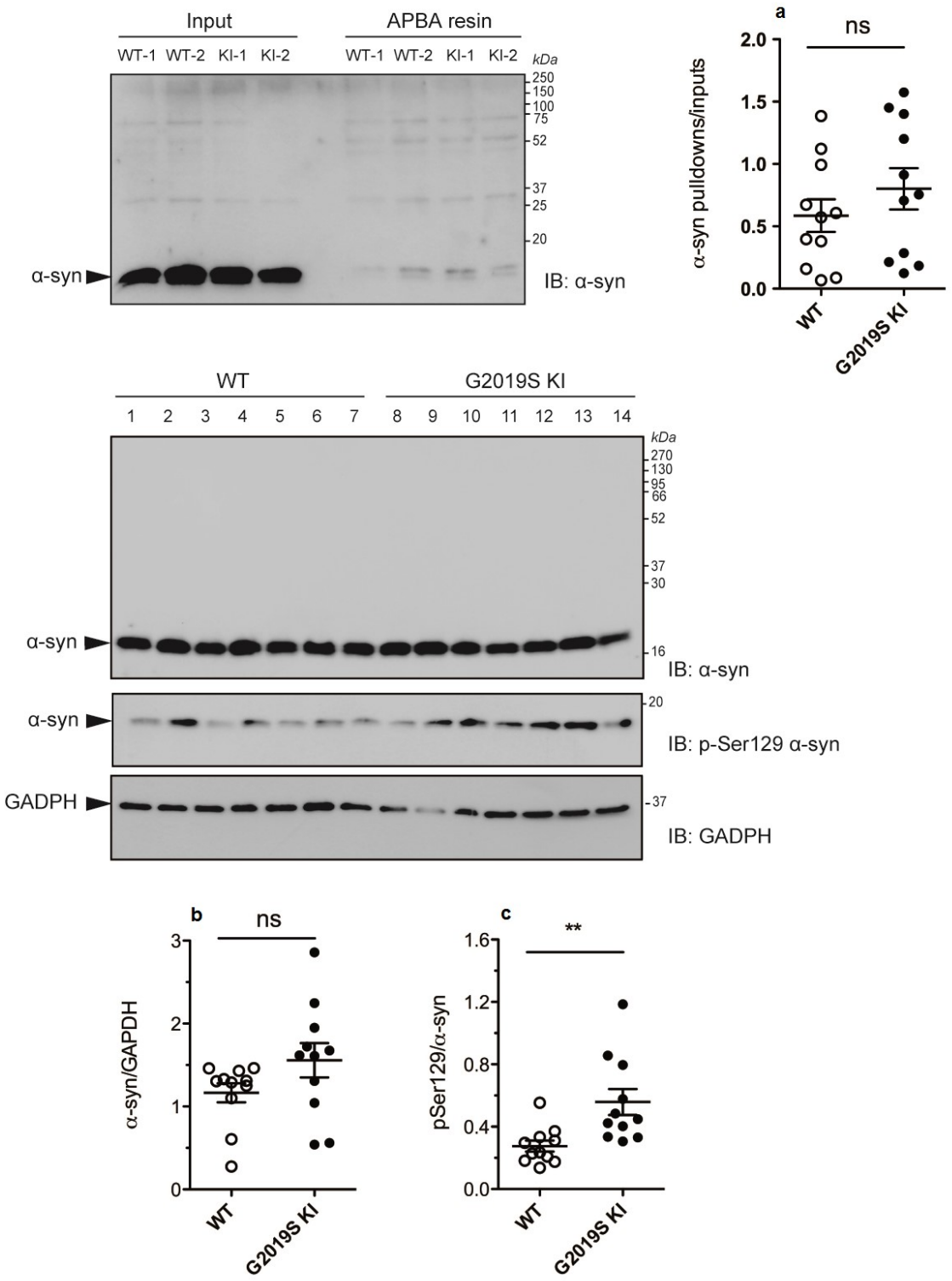

*Fig. 15: DOPAL-modified α-synuclein (α-syn) levels are unchanged whereas Ser129-phosphorylated α-synuclein (pSer129 α-syn) levels are elevated in G2019K KI mice. Relative quantification and representative blots of DOPAL-bound α-syn pull-down with aminophenylboronic acid (APBA) resin of striata from 12-month-old G2019S KI mice and age-matched WT controls (a). In the same preparation, pSer129 α-syn levels (c) were quantified relatively to α-syn levels (b). Data are expressed as mean ± SEM of n = 11 mice per group. Statistical analysis was performed by the Student t-test, two tailed for unpaired data. **p < 0.01 different from WT*

An increase of DAT activity (Masoud et al., 2015) can lead to an increased cytosolic DA levels and buildup of byproducts of DA metabolism which are toxic for the cell. Among these, DOPAL (Mattammal et al., 1995, Burke, 2003, Panneton et al., 2010), which is known to covalently bind to α-syn at lysine residues (Follmer et al., 2015, Werner-Allen et al., 2016). We therefore measured DOPAL-bound α-syn levels in the striatum of 12-month-old G2019S KI mice compared to WT controls (Fig. 15A). No significant difference between genotypes was found. We then investigated pSer129 α-syn levels (Fig. 15B,C), since this posttranslational modification of α-syn is thought to influence α-syn aggregation and is highly represented in intracellular inclusions and Lewy Bodies (Fujiwara et al., 2002, Saito et al., 2003, Anderson et al., 2006). Total endogenous α-syn levels were not different between genotypes (Fig. 15B) whereas pSer129 α-syn levels were ~2-fold higher in the striatum of G2019S KI mice (Fig. 15C). To study the localization of α-syn and pSer129 α-syn, immunohistochemistry was employed in striatal slices from 12-month-old mice (Fig. 16). α-syn and pSer129 α-syn inclusions were revealed in striatal neurons of both genotypes, seemingly at the cell body level. Endogenous α-syn levels did not differ between genotypes (Fig. 16A), while pSer129 α-syn inclusions were significantly higher in the striatum of G2019S KI mice compared to WT controls (Fig. 16B). We next confirmed that such increase was age-dependent, since no difference in striatal α-syn or pSer129 α-syn levels was observed between 3-month-old G2019S KI mice and WT controls (Fig. 16C, D).

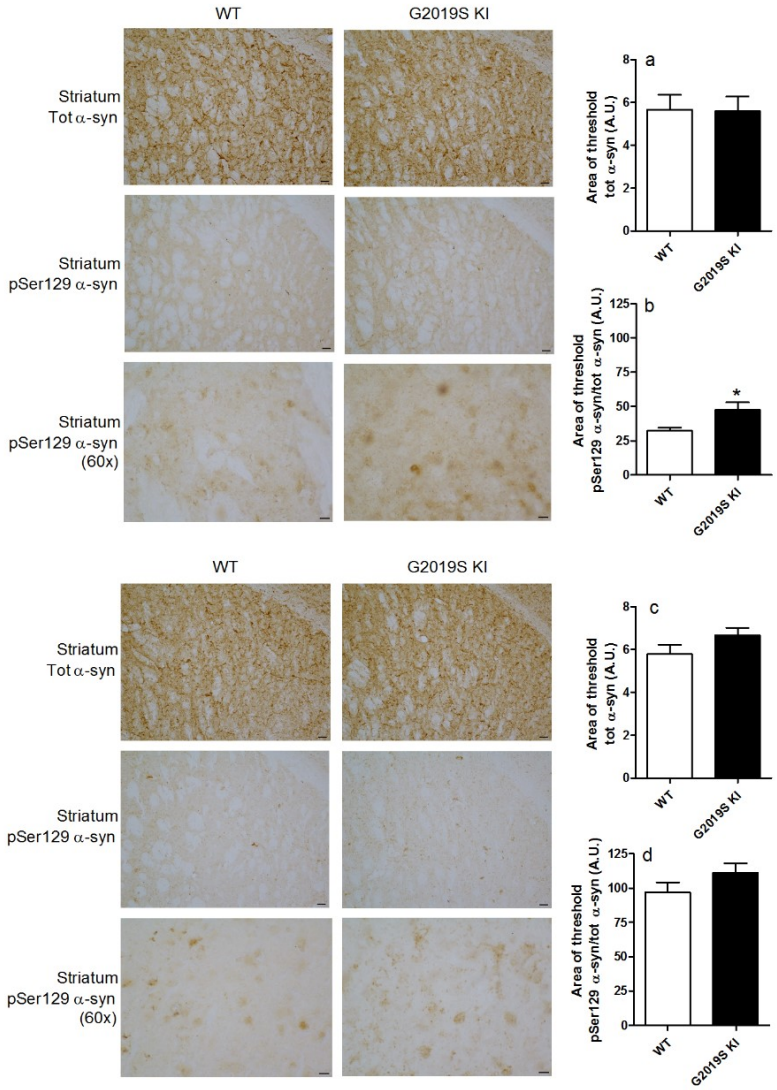

*Fig. 16: Age-dependent overload of Serine129-phosphorylated α-synuclein (pSer129 α-syn) in G2019S knock-in (KI) mice. Representative microphotographs and relative quantifications of α-syn and pSer129 α-syn immunostaining in the striatum of 12-month-old (a, b) and 3-month-old (c, d) G2019S KI mice and WT controls. Data are expressed as mean ± SEM of 8 (a, b) or 6 (c, d) mice per group. Statistical analysis was performed by the Student t-test, two tailed for unpaired data. *p < 0.05 different from WT.*

Study II: impact of LRRK2 G2019S mutation on α-synuclein neuropathology

Experiment I: injection of AAV2/9-hα-syn in 3-month-old mice

G2019S KI mice were injected with AAV2/9-hα-syn to verify whether the increase of LRRK2 kinase activity accelerates hα-syn-induced neuropathology. Mice injected with hα-syn displayed progressive motor deficits in the drag test whereas mice injected with GFP showed relatively stable performance over the 20-week observation period (treatment effect $F_{3,5} = 20.04$, $p < 0.0001$; time effect $F_{5,145} = 21.23$, $p < 0.0001$; time x treatment interaction $F_{15,145} = 2.38$, $p = 0.0005$). Stepping was significantly reduced starting from 8 weeks after virus injection with stable levels attained after 12 weeks onwards (−40% from baseline) (Fig. 17A). The time-courses of stepping activity of G2019S KI and WT mice injected with AAV2/9-hα-syn were superimposable, indicating no genotype susceptibility. Stereological analysis revealed a similar number of DA

neurons in SNc of GFP-injected G29019S KI and WT mice (4883 ± 176 vs 5112 ± 320; Fig. 17A). AAV2/9-hα-syn injected G29019S KI and WT mice had a similar ~50% loss of DA neurons in SNc (Fig. 17B). Consistently, optical density of TH+ striatal nerve terminals revealed that AAV2/9-hα-syn injected G29019S KI and WT mice had 60–70% loss of striatal TH signal, again without difference between genotypes (Fig. 17C).

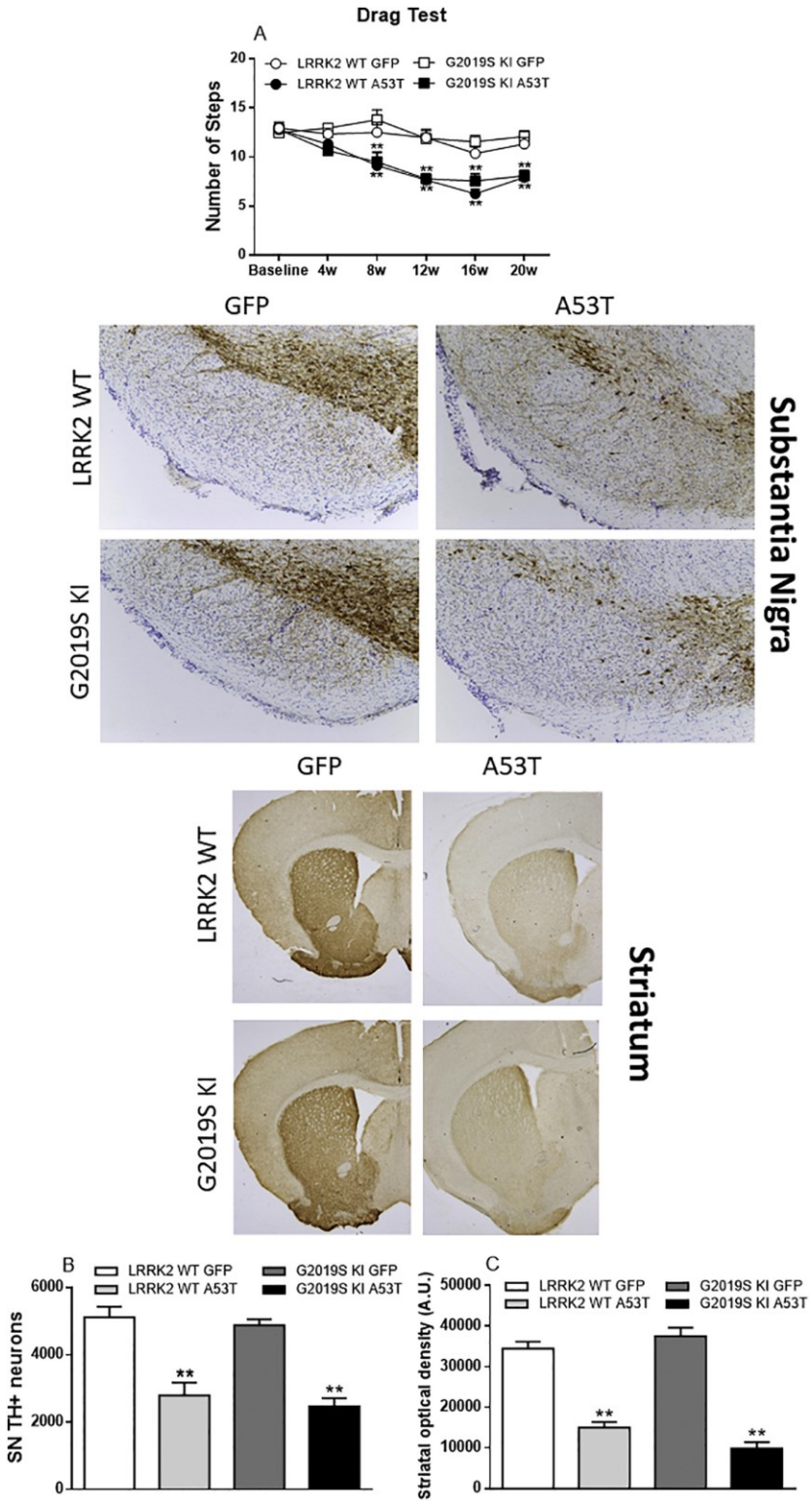

*Fig. 17: Behavioral impairment and nigrostriatal degeneration associated with hα-syn overexpression in 3-month-old mice. AAV2/9-hα-syn or AAV2/9 GFP (as a control) were injected bilaterally in the SNc of G2019S KI and WT mice. Stepping activity was evaluated using the drag test at baseline and 4, 8, 12, 16 and 20 weeks after surgery (A), stereological quantification of nigral dopamine neurons (B) and analysis of density of striatal tyrosine hydroxylase (TH) positive terminals (C) were performed after 20 weeks. Representative images of SNc and striatum are also given. Data are expressed as number of steps (A), number of nigral neurons (B) and optical density (grey scale arbitrary units, C) are means ± SEM of 7 (G2019S KI GFP), 8 (LRRK2 A53T WT) and 9 (LRRK2 WT GFP and G2019S KI A53T) mice per group. Statistical analysis was performed by two-way RM ANOVA followed by the Bonferroni test for multiple comparisons (A) or one-way ANOVA followed by the Bonferroni test for multiple comparisons (B–C). **p < 0.01 different from respective GFP controls.*

Evaluation of AAV2/9 injection efficiency in 3-month-old mice

The efficiency of AAV2/9 injections was evaluated by the expression patterns of hα-syn (Fig. 18). As expected, only mice injected with AAV2/9-hα-syn showed a significant hα-syn labelling in SNc. Strong labelling was also detected in striatum, indicating the diffusion of hα-syn from SNc to anatomically connected areas. No difference in hα-syn load between genotypes was found in SNc or striatum (Fig. 18A, B).

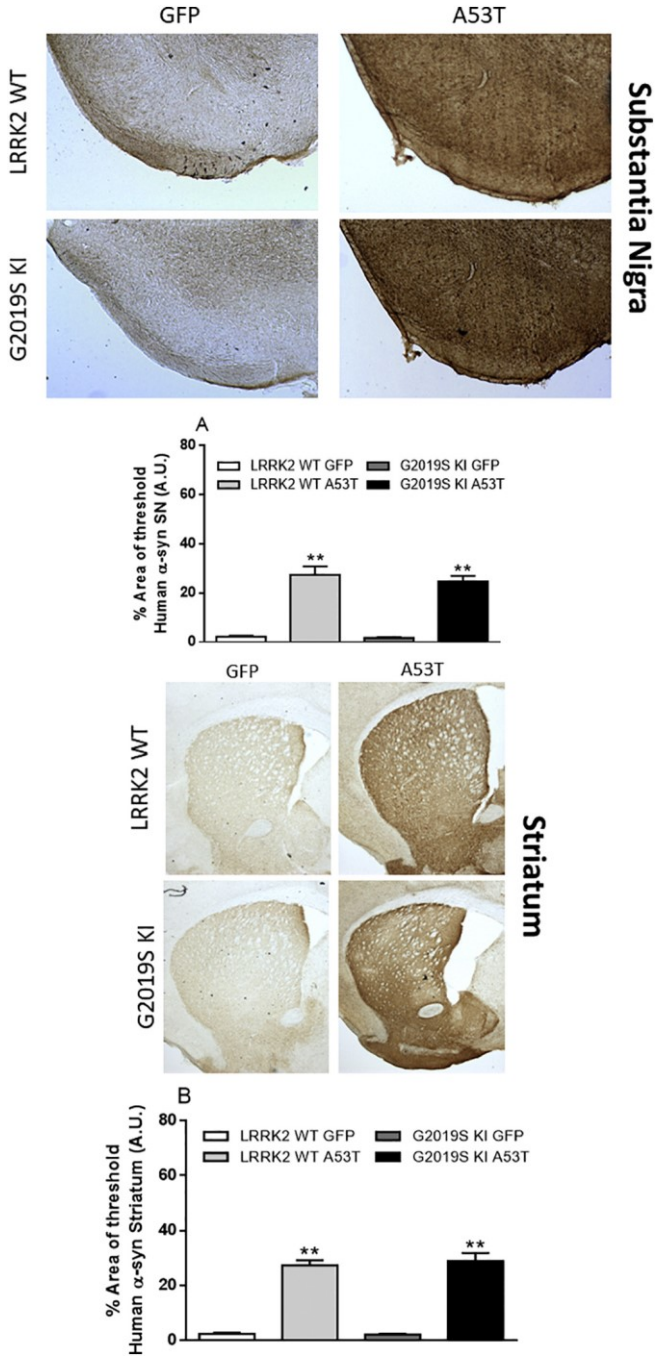

*Fig. 18: Expression of hα-syn in 3-month-old mice. AAV2/9-hα-syn or AAV2/9 GFP (as a control) were injected bilaterally in the SNc of G2019S KI and WT mice and transgene expression evaluated after 20 weeks. Representative images of SNc and striatum, and quantification of the area occupied by hα-syn immunostaining in the SNc (A) or striatum (B). Data are expressed as mean percentage ± SEM of immunopositive surface of the structure of interest of 8 mice per group. Statistical analysis was performed by one-way ANOVA followed by the Bonferroni test for multiple comparisons. **p < 0.01 different from respective GFP controls.*

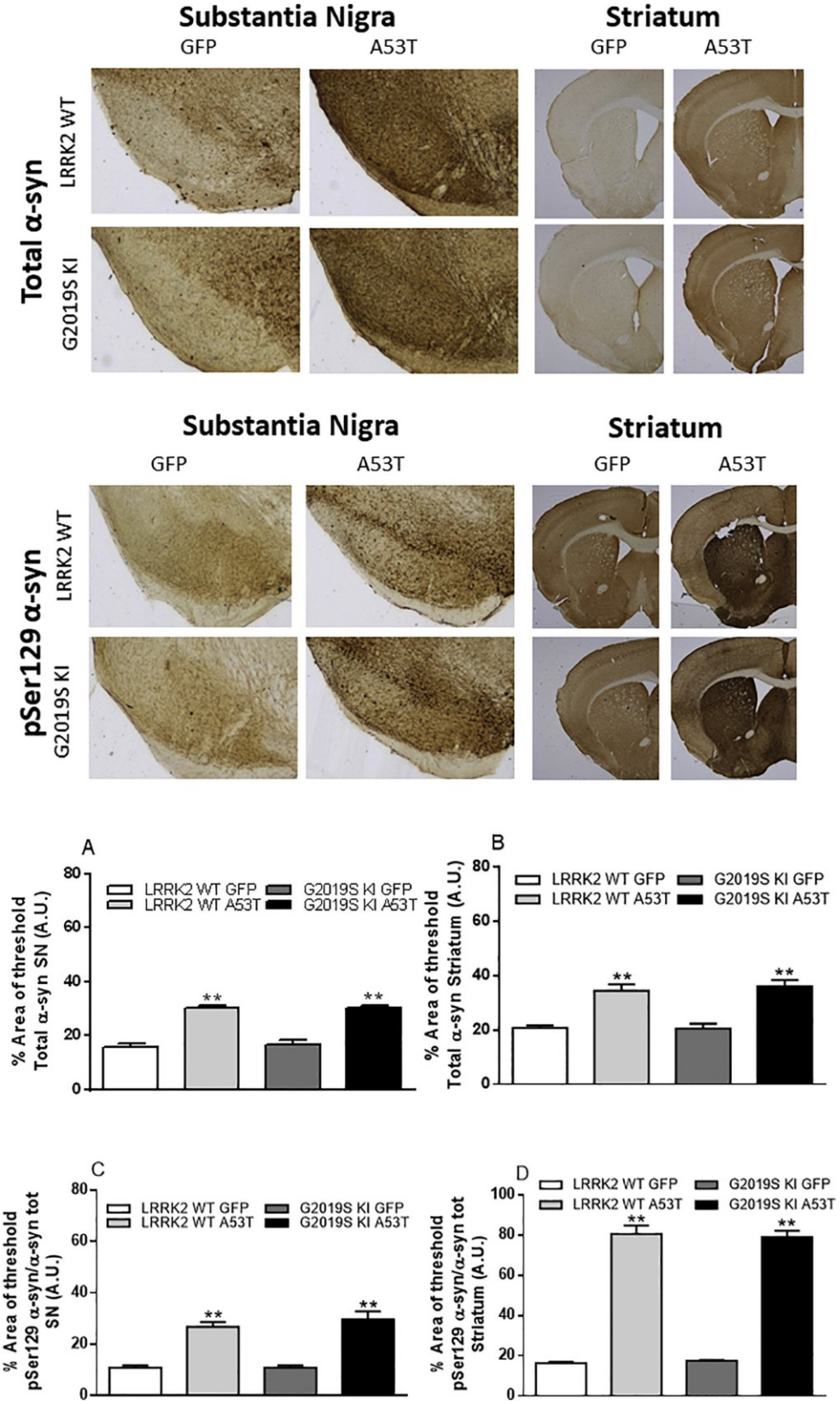

*Fig. 19: Increase of pSer129 α-syn levels following hα-syn overexpression in 3-month-old mice. AAV2/9-hα-syn or AAV2/9 GFP (as a control) were injected bilaterally in the SNc of G2019S KI and WT mice, and pSer129 α-syn or total α-syn levels evaluated after 20 weeks. Representative images of total α-syn signal in SNc and striatum, or pSer129 α-syn signal in SNc and striatum, and relative quantifications (A, B, C, D, respectively). Data are expressed as mean percentage ± SEM of immunopositive surface of the structure of interest of 8 mice per group. Statistical analysis was performed by one-way ANOVA followed by the Bonferroni test for multiple comparisons. **$p < 0.01$ different from respective GFP controls.*

α-synuclein neuropathology in 3-month-old mice

To confirm the occurrence of α-syn pathology, the levels of pSer129 α-syn, i.e. the most prominent form of α-syn present in LB (Fujiwara et al., 2002, Anderson et al., 2006), were measured. As shown in Fig. 19, total α-syn labelling, which encompasses both human and endogenous α-syn due to the lack of antibody selectivity, was 2.5-fold greater in the SNc (Fig. 19A) and 1.5-fold greater in the striatum (Fig. 19B) of AAV2/9-hα-syn injected mice compared to control mice, irrespective of genotype. pSer129 α-syn labelling was also 1.5-fold higher in the SNc (Fig. 19C) and 4-fold higher in the striatum (Fig. 19D) of AAV2/9-hα-syn injected mice compared to AAV GFP mice, again irrespective of genotype. To ascertain whether pSer129 α-syn labelling was constituted by soluble, monomeric or insoluble, oligomeric α-syn forms, slices were treated with proteinase K (Fig. 20). After PK treatment, a significant pSer129 α-syn signal was detected in both the SNc (Fig. 20A) and striatum (Fig. 20B) of AAV2/9-hα-syn injected mice indicating the presence of α-syn aggregates. However, the amount was similar in G2019S KI and WT mice, indicating that the mutation did not facilitate α-syn aggregation in 3-month-old mice. Finally, it was investigated whether α-syn pathology was accompanied by a microglial response (Fig. 21). AAV2/9-hα-syn injection did not change the number and area occupied by iba-1+ cells in SNc (Fig. 21A-B) or striatum (Fig. 21C-D), indicating the absence of sustained microgliosis.

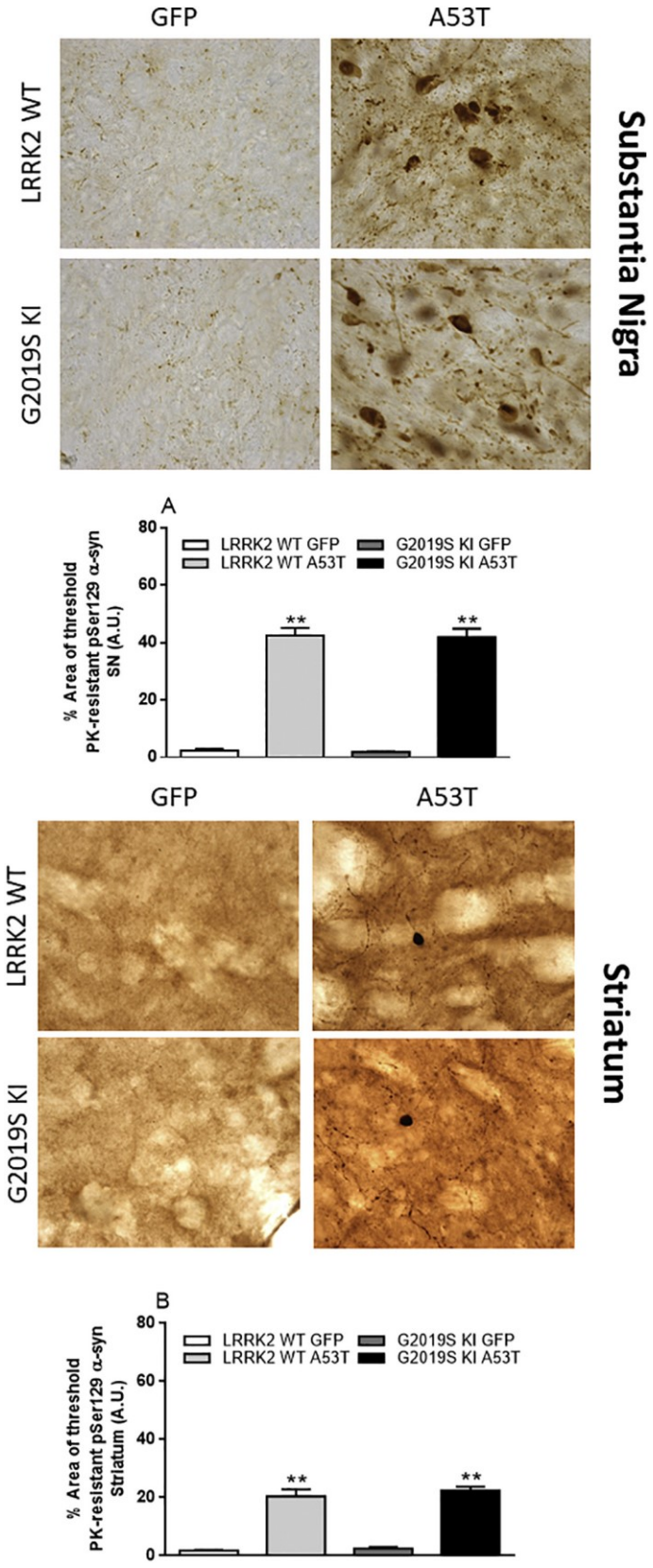

*Fig. 20: pSer129 α-syn aggregates following hα-syn overexpression in 3-month-old mice. AAV2/9-hα-syn or AAV2/9 GFP (as a control) were injected bilaterally in the SNc of G2019S KI and WT mice and pSer129 α-syn signal following Proteinase K (PK) digestion evaluated after 20 weeks. Representative images of SNc and striatum, and relative quantifications of pSer129 α-syn signal (A, B, respectively). Data are expressed as mean percentage ± SEM of immunopositive surface of the structure of interest of 8 mice per group. Statistical analysis was performed by one-way ANOVA followed by the Bonferroni test for multiple comparisons. **p < 0.01 different from respective GFP controls.*

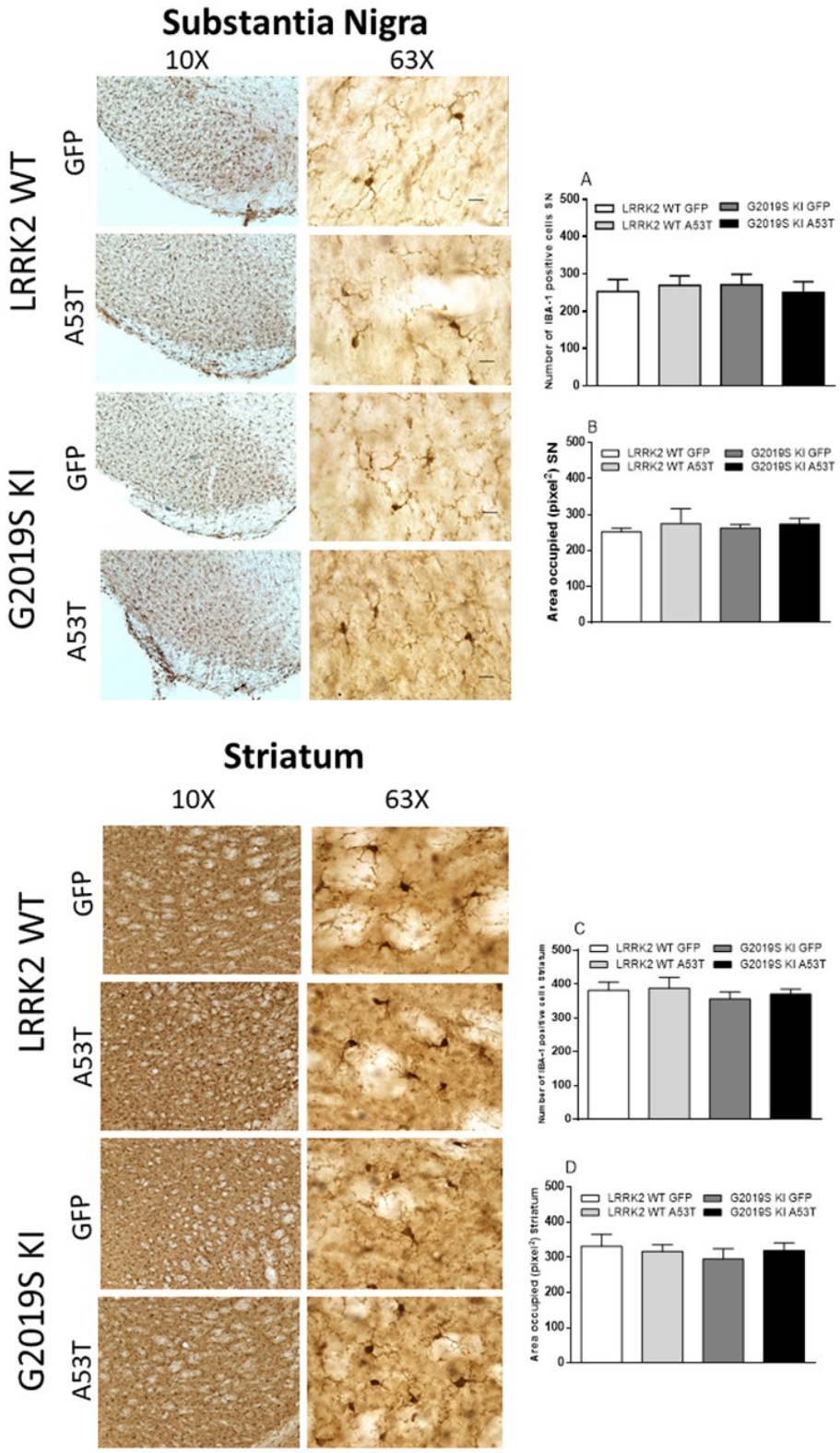

Fig. 21: Lack of microglial activation following hα-syn overexpression in 3-month-old mice. AAV2/9-hα-syn or AAV2/9 GFP (as a control) were injected bilaterally in the SNc of G2019S KI and WT mice and microglia analysed after 20 weeks. Representative images of SNc and striatum at low (10X) and high magnification (63X), and relative quantifications of the number (A, C) and the area occupied (B, D) by iba-1 positive microglial cells. Data are expressed as mean ± SEM of 8 mice per group.

Experiment II: injection of AAV2/9-hα-syn in 12-month-old mice

Data obtained in 3-month-old mice indicate that G2019S does not accelerate α-syn toxicity. We then sought to investigate whether G2019S could play a significant contribution in older animals. As aging is a major risk factor in PD and, in addition, we observed synaptic dysfunction and a pSer129 α-syn overload in the striatum of 12-month-old G2019S KI mice, we used older mice to investigate the contribution of age on pathology in our AAV model. Analysis of motor behavior showed that 12-month-old AAV2/9-hα-syn injected mice displayed motor deficits in the drag test (treatment $F_{3,3} = 24.24$, $p < 0.0001$, time $F_{3,93} = 18.31$, $p < 0.0001$, time x treatment interaction $F_{9,93} = 4.55$, $p < 0.0001$; Fig. 22A). Stepping was similarly impaired in both genotypes (20–30%), a significant effect being observed already at 4 weeks after injection (Fig. 22A). The same pattern was confirmed by analysis of global motor activity in the rotarod test (treatment $F_{3,3} = 8.41$, $p = 0.0003$, time $F_{3,93} = 3.81$, $p = 0.0126$, time × treatment interaction $F_{9,93} = 3.80$, $p = 0.0004$; Fig. 22B). Stereological analysis performed 12 weeks after surgery showed that 12-month-old GFP-injected G2019S KI and WT mice had a similar number of nigral DA neurons (4291 ± 167 and 4429 ± 242, respectively; Fig. 22C). However, G2019S KI mice showed significantly larger ($F_{3,31} = 44.16$, $p < 0.0001$) nigral degeneration compared to WT mice (−55% vs −39%, 1944 ± 168 vs 2729 ± 177 DA cells, respectively; Fig. 22C). Nonetheless, striatal TH density analysis revealed that both groups of animals displayed a significant reduction (28%) of TH+ terminals (Fig. 22D).

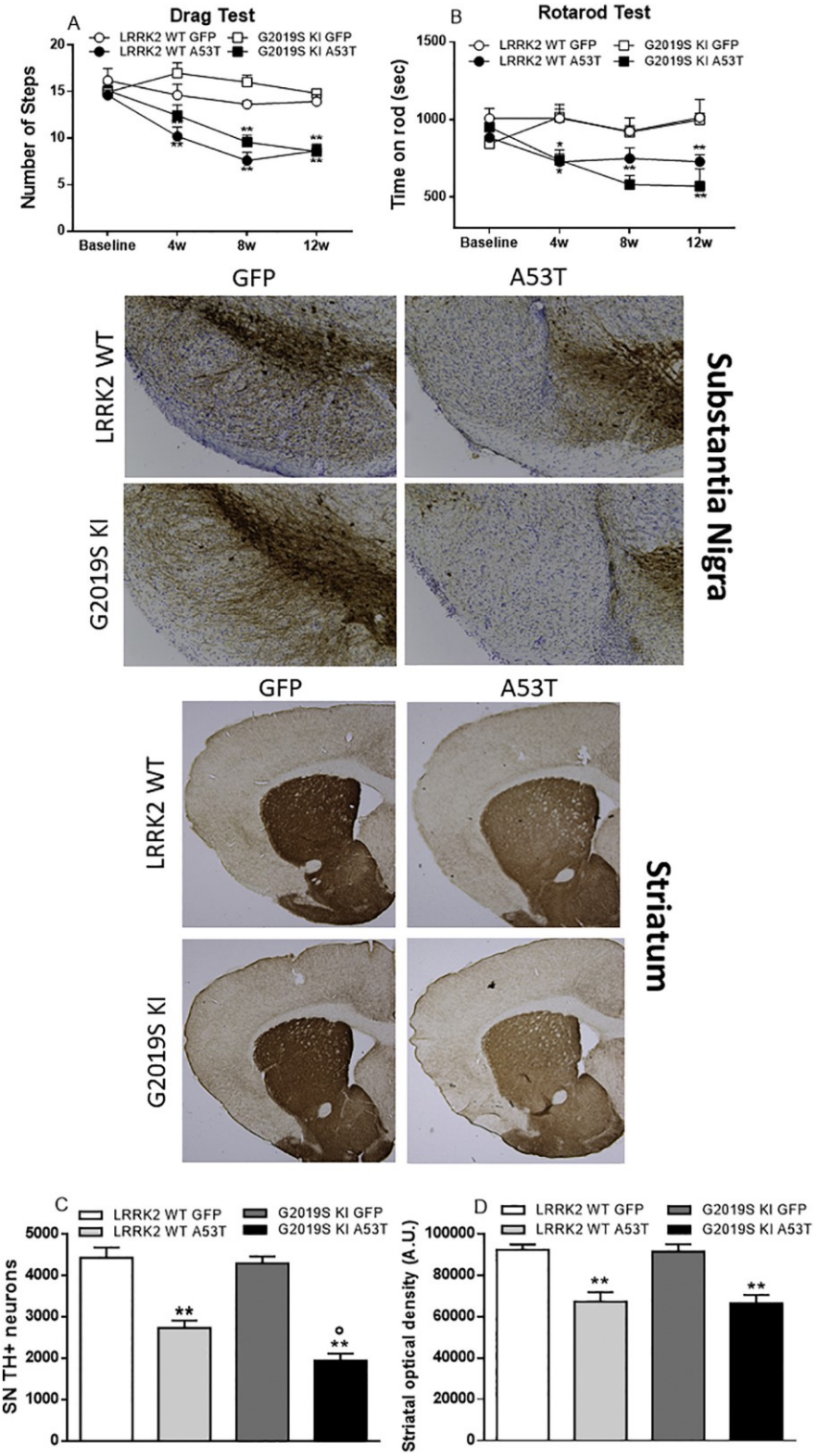

*Fig. 22: Behavioral impairment and nigrostriatal degeneration associated with hα-syn overexpression in 12-month-old mice. AAV2/9-hα-syn or AAV2/9 GFP (as a control) were injected bilaterally in the SNc of G2019S KI and WT mice. Stepping activity was evaluated using the drag test (A) or the rotarod test (B) at baseline and 4, 8, 12 weeks after surgery, and nigrostriatal degeneration was evaluated after 12 weeks. Representative images of SNc and striatum are also given. Data are expressed as number of steps (A), time on rod (in sec; B), number of nigral neurons (C) and optical density (grey scale arbitrary units, B) are means ± SEM of n = 7 (LRRK2 WT GFP), 8 (LRRK2 WT A53T) and 10 (G2019S KI GFP and G2019S KI A53T) mice per group. Statistical analysis was performed by two-way RM ANOVA followed by the Bonferroni test for multiple comparisons (A-B) or one-way ANOVA followed by the Bonferroni test for multiple comparisons (C–D). **p < 0.01 different from respective GFP controls, °p < 0.05 different from LRRK2 WT A53T.*

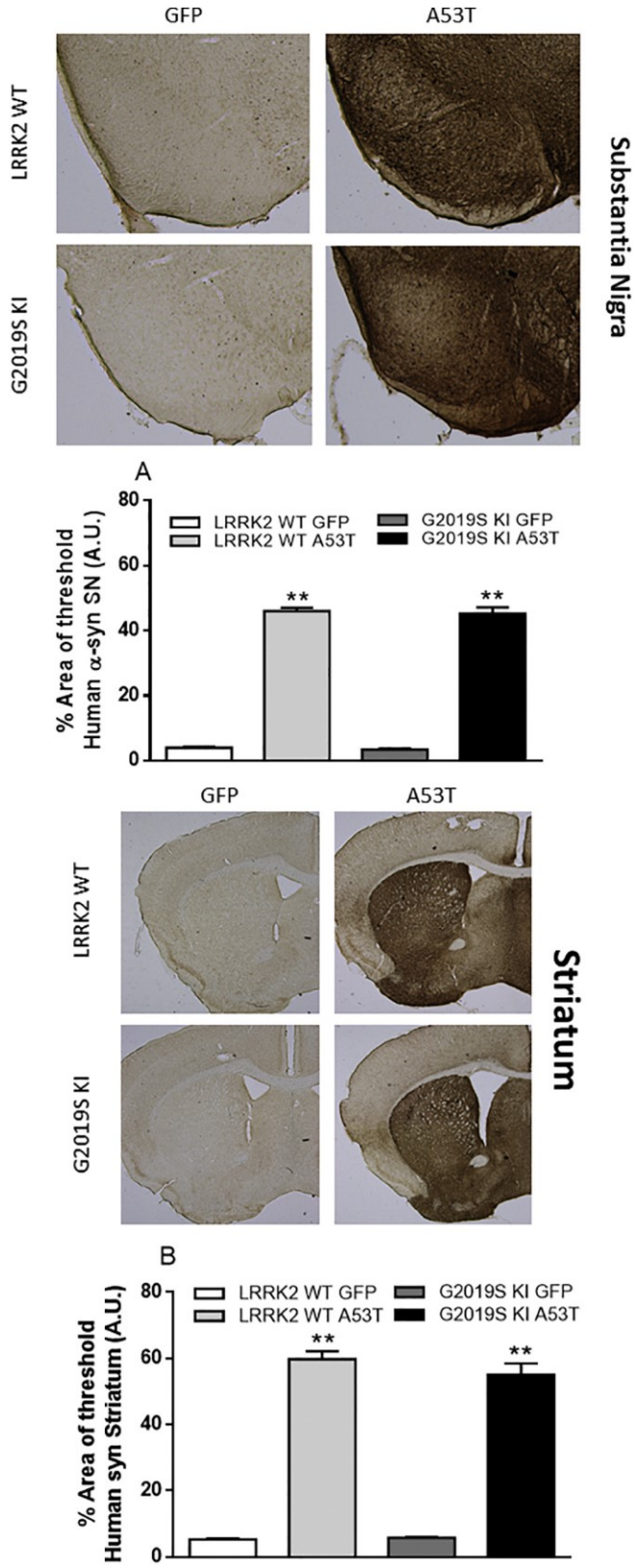

*Fig. 23: Expression of hα-syn in 12-month-old mice. AAV2/9-hα-syn or AAV2/9 GFP (as a control) were injected bilaterally in the SNc of G2019S KI and WT mice and transgene expression evaluated after 12 weeks. Representative images of SNc and striatum, and quantification of the area occupied by hα-syn immunostaining in the SNc (A) or striatum (B). Data are expressed as mean percentage ± SEM of n = 7 (LRRK2 WT GFP), 8 (LRRK2 WT A53T) and 10 (G2019S KI GFP and G2019S KI A53T) mice per group. Statistical analysis was performed by one-way ANOVA followed by the Bonferroni test for multiple comparisons. **p < 0.01 different from respective GFP controls.*

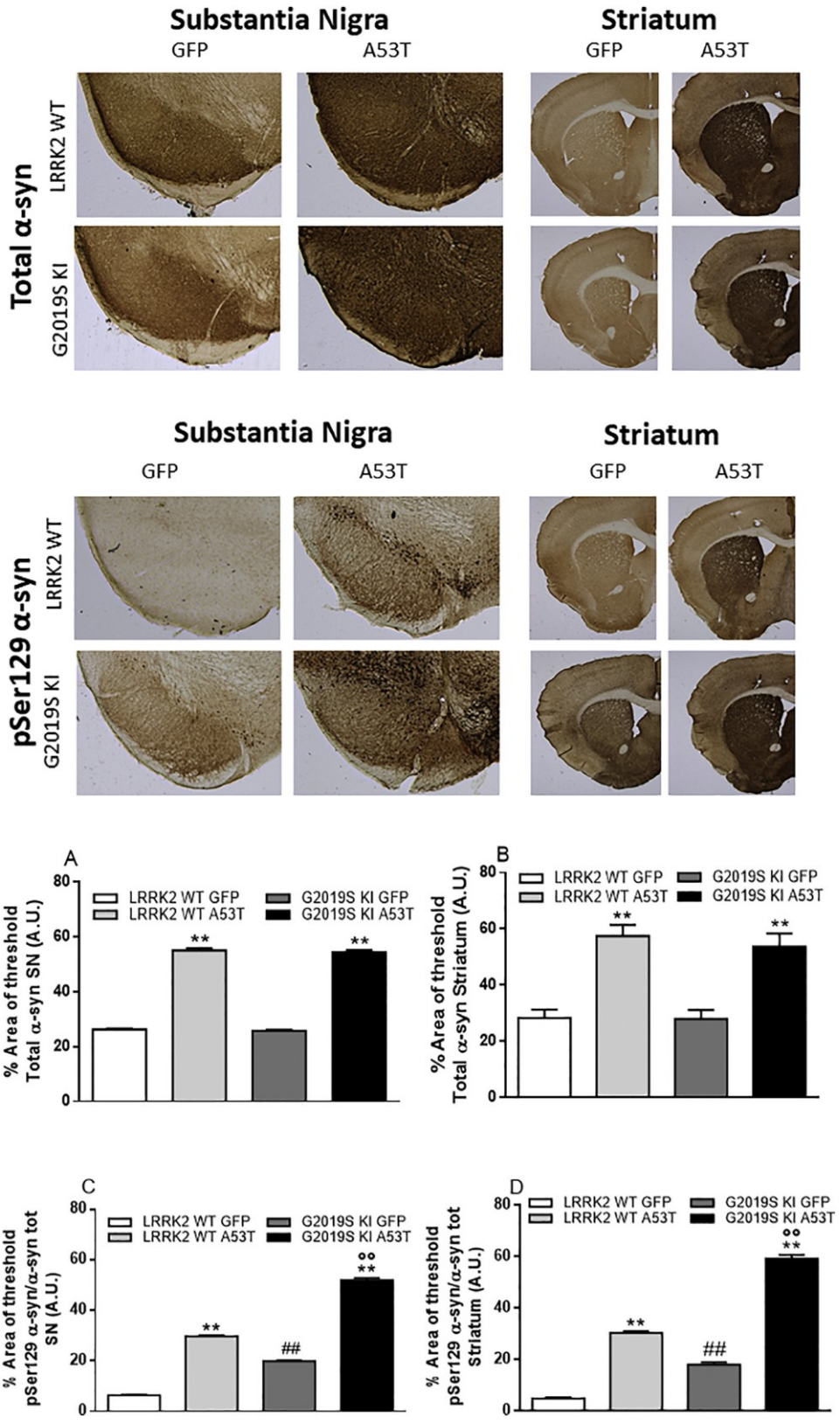

*Figure 24: Increase of pSer129 α-syn levels following hα-syn overexpression in 12-month-old mice. AAV2/9-hα-syn or AAV2/9 GFP (as a control) were injected bilaterally in the SNc of G2019S KI and WT mice, and pSer129 α-syn or total α-syn levels evaluated after 12 weeks. Representative images of total α-syn signal in SNc and striatum, or pSer129 α-syn signal in SNc and striatum, and relative quantifications (A, B, C, D, respectively), data are expressed as mean percentage ± SEM of immunopositive surface of the structure of interest of 9 mice per group. Statistical analysis was performed by one-way ANOVA followed by the Bonferroni test for multiple comparisons. **p < 0.01 different from respective GFP controls; ##p < 0.01 different from LRRK2 WT GFP; °°p < 0.01 different from LRRK2 WT A53T.*

α-synuclein neuropathology in 12-month-old mice

Similar to 3-month-old mice, AAV2/9-hα-syn injection caused comparable expression of hα-syn (Fig. 23) in SNc (Fig. 23A) and striatum (Fig. 23B) of G29019S KI and WT mice, suggesting comparable transduction efficiencies. Likewise, as in the 3-month-old cohort, total α-syn load (Fig. 24) was ~2-fold elevated in the SNc (Fig. 24A) and striatum (Fig. 24B) of AAV2/9-hα-syn injected mice compared to GFP-injected mice. However, different from 3-month-old mice, significant changes in the levels of pSer129 α-syn in SNc (treatment $F_{3,32} = 1393$ $p < 0.0001$) and striatum (treatment $F_{3,32} = 524.8$, $p < 0.0001$) were found. In particular, GFP-treated G2019S KI mice had ~3-fold higher levels of pSer129 α-syn in SNc (Fig. 24C) and striatum (Fig. 24D) compared to GFP-treated WT mice. Moreover, G2019S KI mice injected with AAV2/9-hα-syn showed a ~2-fold larger area of signal in both areas with respect to WT mice injected with the same construct. The area occupied by PK-resistant pSer129 α-syn aggregates was then analyzed (Fig. 25). Interestingly, upon PK treatment no difference in pSer129 α-syn load between G2019S KI and WT could be observed anymore, both in SNc (Fig. 25A) and striatum (Fig. 25B). However, there was still a doubling of pSer129 α-syn levels detectable in G2019S KI versus WT mice injected with AAV2/9-hα-syn. Finally, we investigated the microglial response in this cohort of 12-month-old mice (Fig. 26). No changes in the number and area occupied by Iba-1+ microglial cells in SNc (Fig. 26A–B) or striatum (Fig. 26C–D), were detected between AAV2/9-hα-syn injected and AAV GFP injected mice, again suggesting no active microglial response at 12 weeks after viral injection.

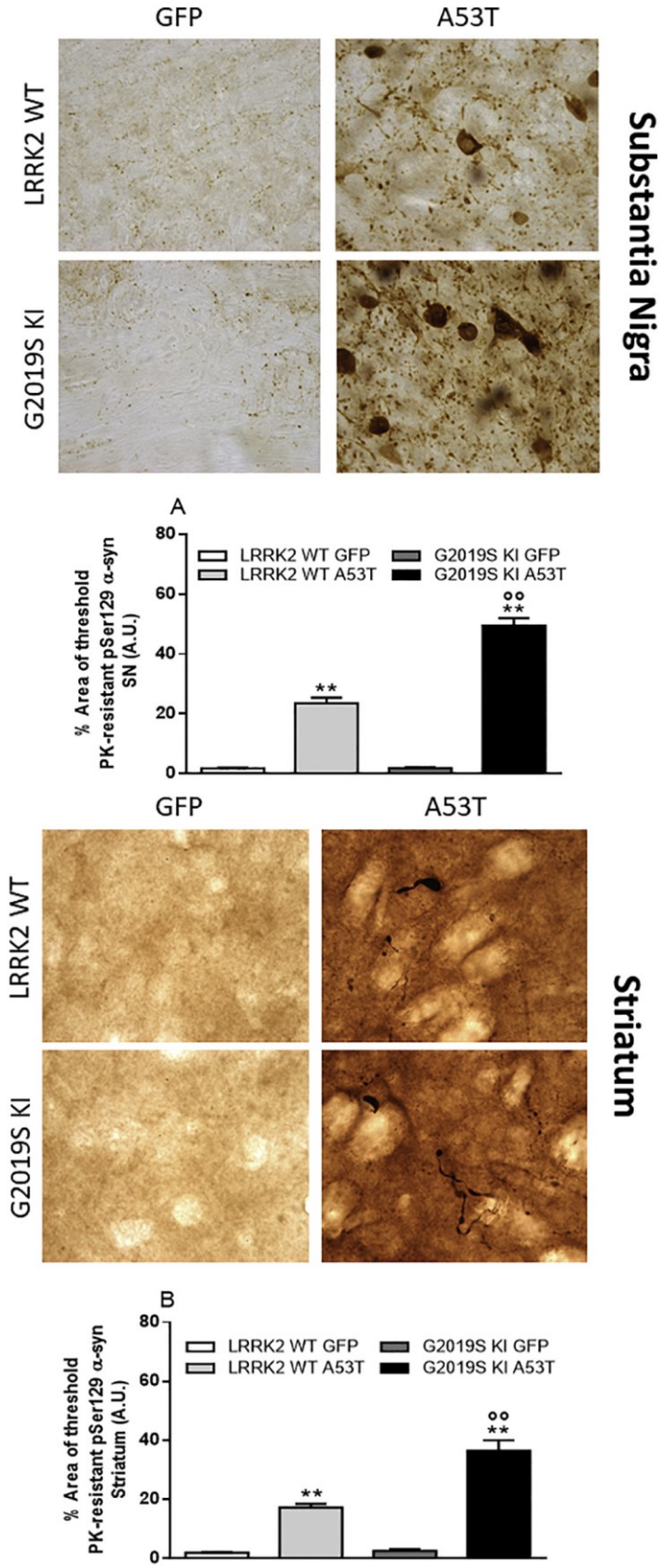

*Fig. 25: pSer129 α-syn aggregates following hα-syn overexpression in 12-month-old mice. AAV2/9-hα-syn or AAV2/9 GFP (as a control) were injected bilaterally in the SNc of G2019S KI and WT mice, and pSer129 α-syn signal following Proteinase K (PK) digestion evaluated after 12 weeks. Representative images of SNc and striatum, and relative quantifications of pSer129 α-syn signal (A, B, respectively). Data are expressed as mean percentage ± SEM of immunopositive surface of the structure of interest of 9 mice per group. Statistical analysis was performed by one-way ANOVA followed by the Bonferroni test for multiple comparisons. **$p < 0.01$ different from respective GFP controls; °°$p < 0.01$ different from LRRK2 WT A53T.*

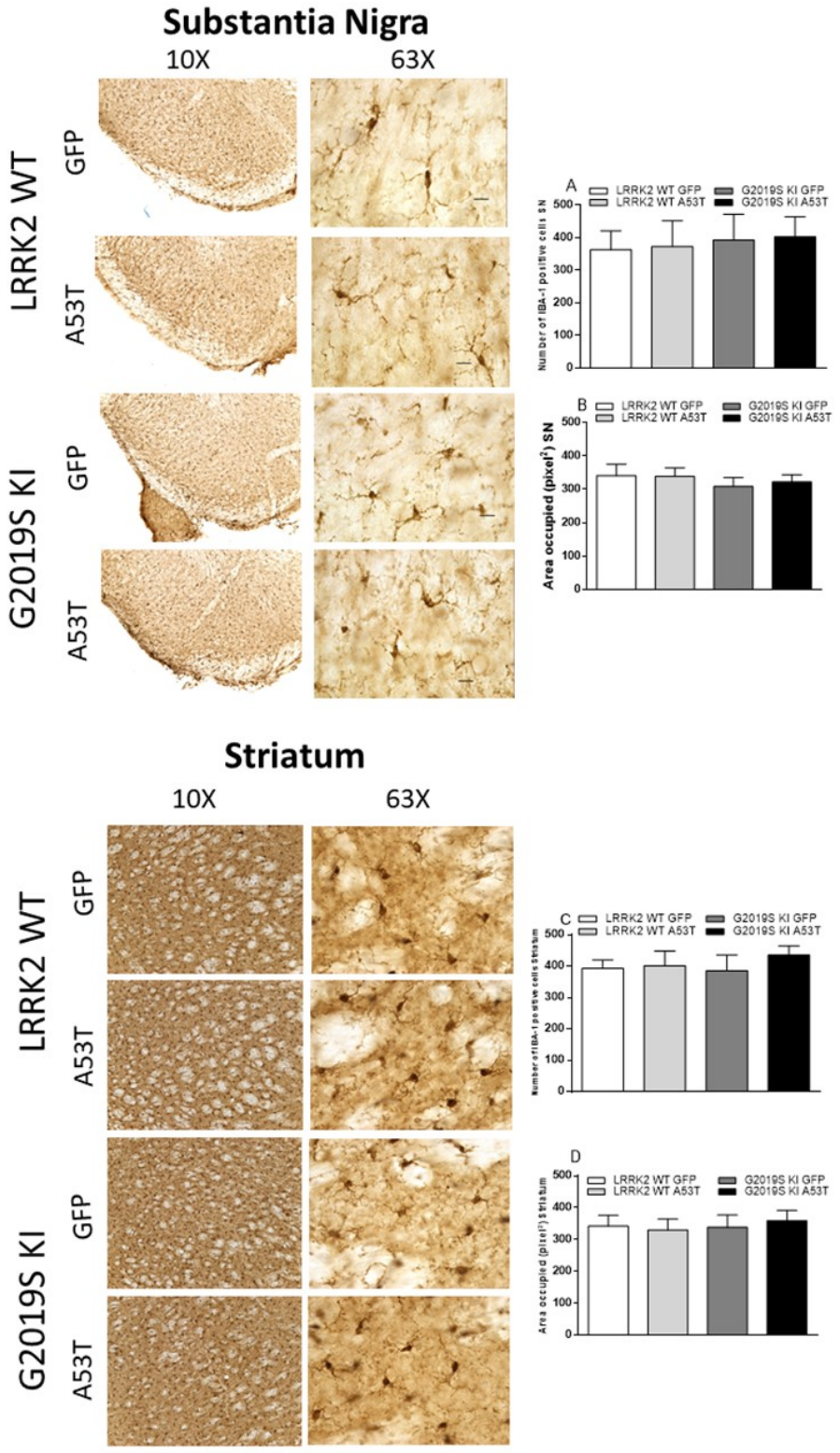

Fig. 26: Lack of microglial activation following hα-syn overexpression in 12-month-old mice. AAV2/9-hα-syn or AAV2/9 GFP (as a control) were injected bilaterally in the SNc of G2019S KI and WT mice and microglia analysed after 12 weeks. Representative images of SNc and striatum at low (10X) and High magnification (63X), and relative quantifications of the number (A, C) and the area occupied (B, D) by iba-1 positive microglial cells. Data are expressed as mean ± SEM of 9 mice per group.

Study III: impact of LRRK2 G2019S mutation on MPTP susceptibility

Experiment I: Comparison between WT, LRRK2, KO and G2019S KI mice

In the attempt to prove the enhanced susceptibility of G2019S KI mice to MPTP, MPTP was administered subacutely to WT, KO, KD and G2019S KI mice, and the integrity of the nigrostriatal pathway was investigated (Fig. 27). These genotypes had similar amount of DA neurons in SNc (5473 ± 315, 5086 ± 256, 5663 ± 354 and 5182 ± 97 respectively; Fig. 27A), and were all sensitive to MPTP ($F_{7,69}$ = 63,99, p<0,0001). The loss of DA neurons was similar in WT, KO and KD mice (50%) but significantly greater in G2019S KI mice (75%). Consistently, MPTP reduced the density of striatal TH+ terminals in all genotypes ($F_{7,52}$=56,43; p<0.0001; Fig. 27B). However, G2019S KI mice showed a larger reduction compared to WT, KO and KD mice.

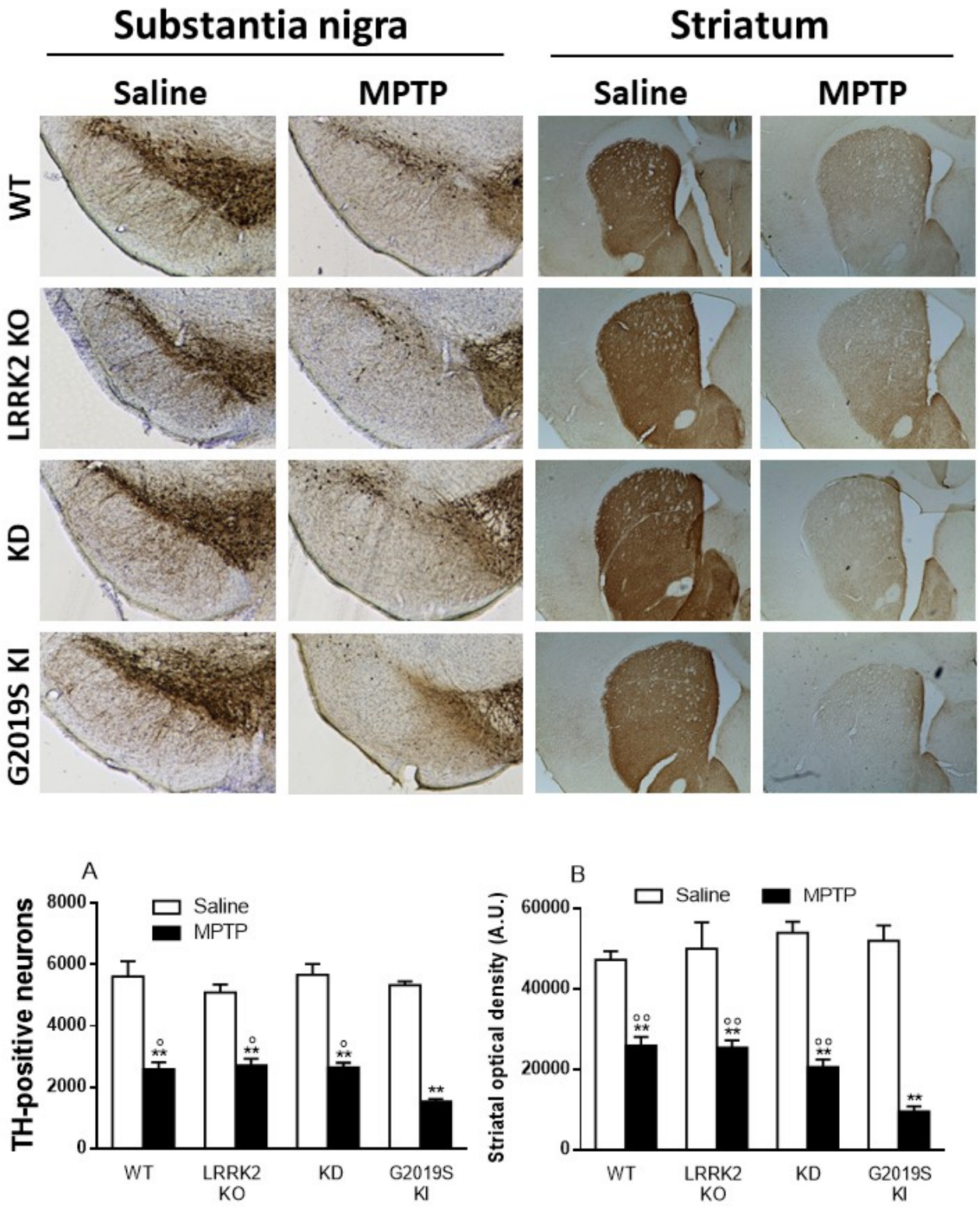

*Fig. 27: MPTP-induced nigrostriatal degeneration in 3-month-old G2019S KI, LRRK2 KO, KD and WT mice. Representative images of SNc and Striatum are also given. Data are expressed as number of TH+ neurons (A) and striatal optical density (grey scale arbitrary units, B) and are mean ± SEM of n = 4 (LRRK2 KO + Saline), 5 (KD + Saline), 8 (LRRK2 KO and KD + MPTP) and 13 (G2019S KI and WT + Saline and G2019S KI and WT + MPTP) mice per group. Statistical analysis was performed by one-way ANOVA followed by the Bonferroni test for multiple comparisons. **p<0.01 different from respective Saline controls; °p<0.05 and °°p < 0.01 different from G2019S KI + MPTP.*

Experiment II: neuroprotective potential of LRRK2 kinase inhibitor

Neuroprotective effect of PF-06447475

We first attempted to demonstrate the neuroprotective potential of PF-06447475 (10 mg/Kg) by pretreating G2019S KI mice with PF-06447475, i.e. by mice. administering the compound 3 days before, and simultaneously with MPTP. Behavioral analysis did not highlight any impact of treatments on motor activity in all tests employed (Fig. 28A-C). Nevertheless, MPTP caused a 72% loss of nigral DA neurons ($F_{3,24}=33.89$ $p<0.0001$; Fig. 28D) and a similar 75% loss of striatal TH terminals ($F_{3,28}=33.24$ $p<0.0001$; Fig. 28E). PF-06447475 prevented the MPTP-induced loss of nigral DA neurons but was unable to attenuate the degeneration of striatal TH+ terminals associated with it.

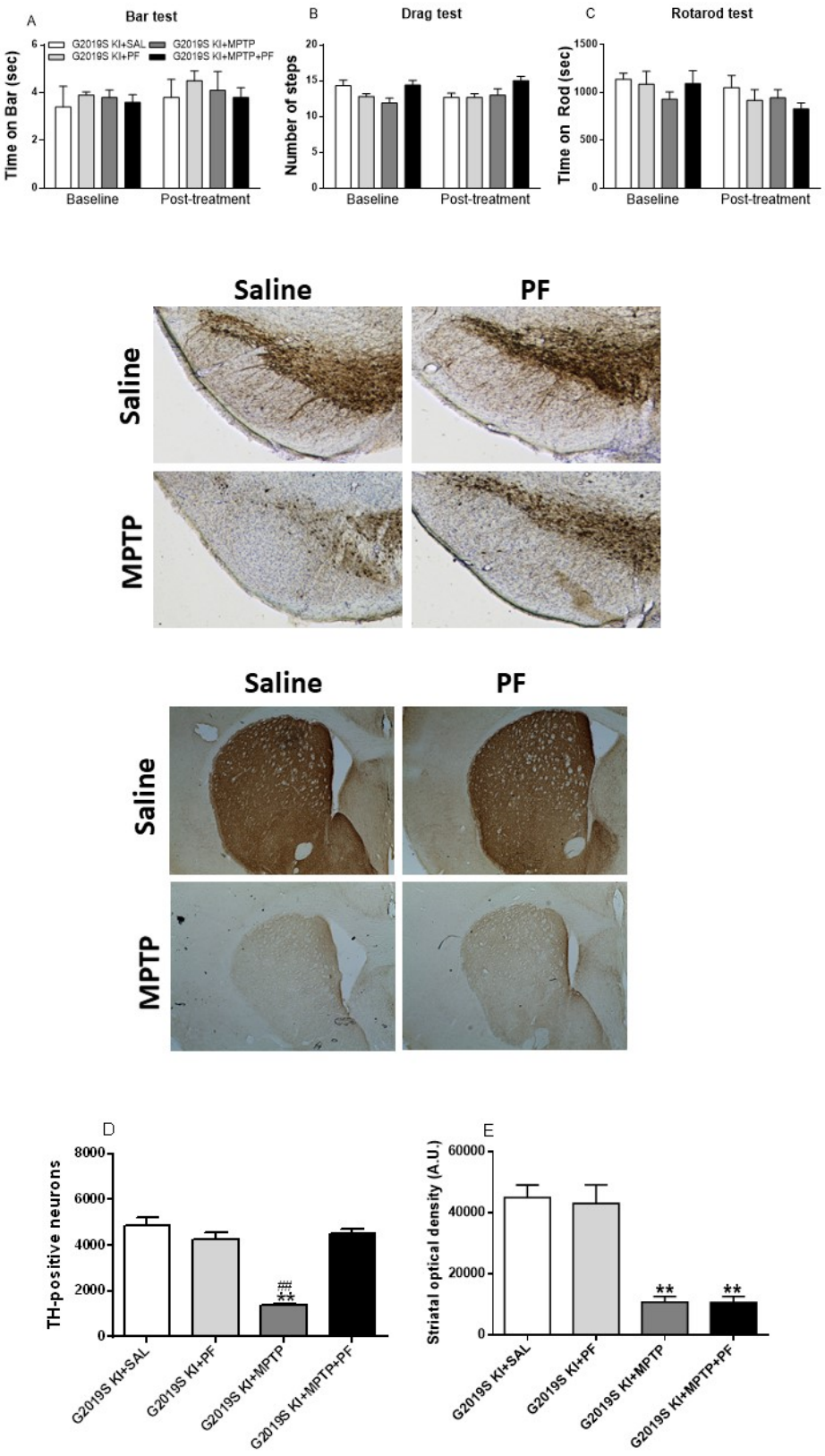

*Fig. 28: motor activity and nigrostriatal degeneration in 3-month-old G2019S KI mice pre-treated with PF-06447475 and then with subacute MPTP. Representative images of SNc and Striatum are also given. Motor activity was assessed using the bar (A), drag (B) and rotarod (C) tests, before (baseline) and after (post-treatment) drug administration. Data are expressed as time on bar (in sec; A), number of steps (B), time on rod (in sec; C), number of TH+ neurons (D) and striatal optical density (grey scale arbitrary units, E) and are mean ± SEM of n=7 mice per group. Statistical analysis was performed by two-way or one-way ANOVA followed by the Bonferroni test for multiple comparisons. **p<0.01 different from G2019S KI+SAL; $^{\#\#}p < 0.01$ different from G2019S KI +MPTP+PF.*

Experiment III: Comparison of LRRK2 kinase inhibitors as disease-modifiers drugs

PF-06447475 protects/rescues from MPTP-induced neurotoxicity

To further prove the neuroprotective/neurorescue potential of PF-06447475, in a second experiment PF-06447475 was given subacutely for 10 days, to both WT and G2019S KI mice treated with MPTP or saline (Fig. 29). In this "clinically driven" protocol, treatment with PF-06447475 was delayed with respect to MPTP, specifically starting the 4th day after the onset of MPTP and ending 6 days after MPTP withdrawal. Once again, behavioral analysis did not show any significant effect after treatments (Fig. 29A-C). Stereology (Fig. 29D) revealed that MPTP caused a larger DA neuron degeneration in G2019S KI mice (70%) than WT mice (43%) (genotype X toxin $F_{1,1}$=7.27 p=0.0100). PF-06447475 did not affect the MPTP-induced loss of nigral DA neurons in WT mice but attenuated that in G2019S KI mice (genotype X treatment $F_{1,1}$=11.86 p=0.0013) bringing the number of spared neurons close to that observed in WT animals. Different from that observed in SNc, PF-06447475 was unable to affect the MPTP-induced striatal TH+ terminal degeneration in both genotypes (Fig. 29E).

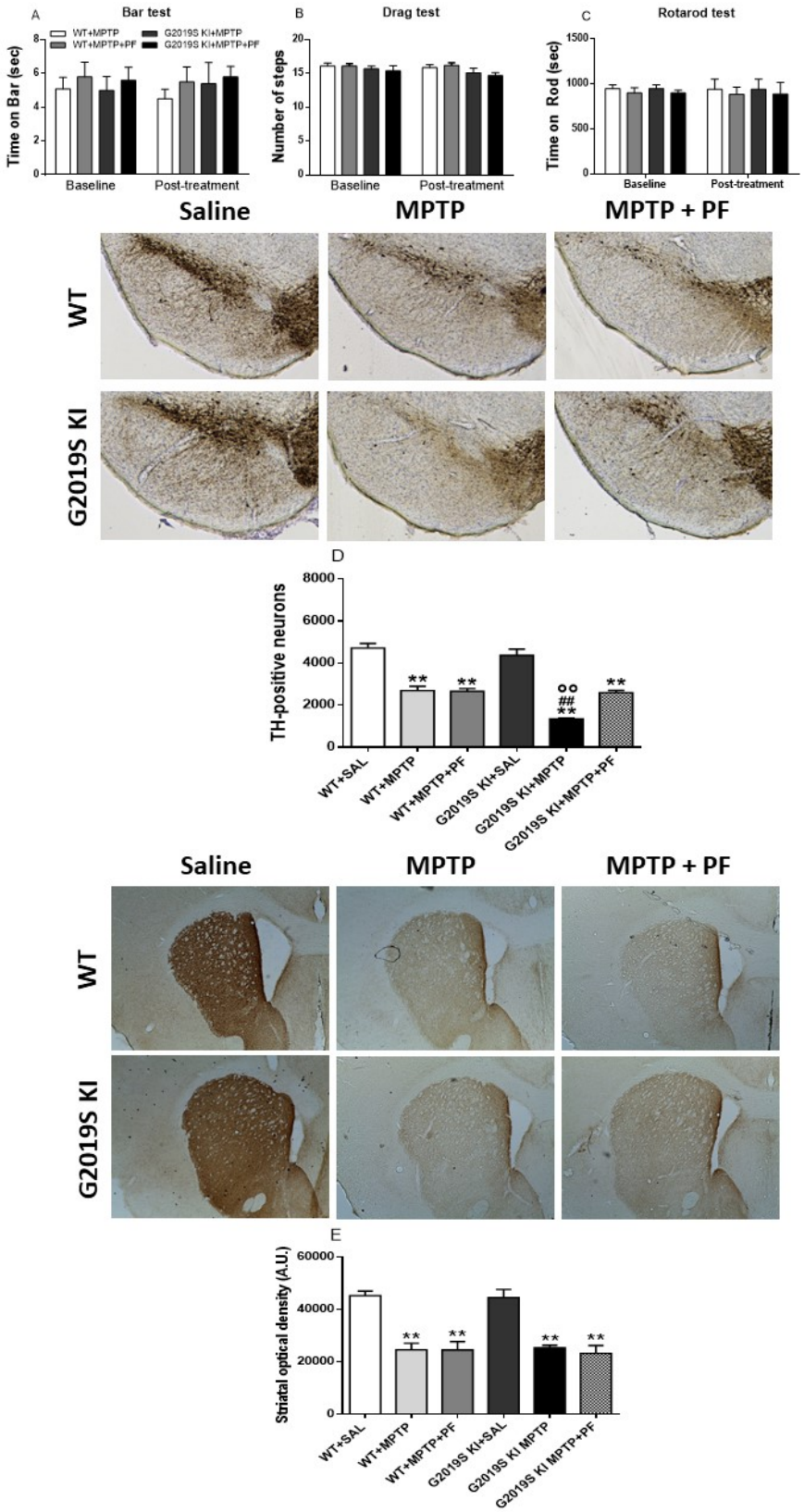

*Fig. 29: motor activity and nigrostriatal degeneration in 3-month-old G2019S KI mice treated subactutely with MPTP and PF-06447475. Representative images of SNc and Striatum are also given. Motor activity was assessed using the bar (A), drag (B) and rotarod (C) tests, before (baseline) and after (post-treatment) drug administration. Data are expressed as time on bar (in sec; A), number of steps (B), time on rod (in sec; C), number of TH+ neurons (D) and striatal optical density (grey scale arbitrary units, E) and are mean ± SEM of n = 8 mice per group. Statistical analysis was performed by two-way or one-way ANOVA followed by the Bonferroni test for multiple comparisons. **p < 0.01 different from Saline controls; ##p < 0.01 different from WT+MPTP; °°p<0.01 different from G2019S KI MPTP+PF.*

MLi-2 protects/rescues from MPTP-induced neurotoxicity

To confirm the neuroprotective potential of LRRK2 inhibitors, MLi-2 was tested under a "clinically-driven" protocol in MPTP-treated WT and G2019S KI mice (Fig. 30). Also in this set of experiments, MPTP caused a larger degeneration of DA neurons (Fig. 30A) in G201S KI mice (66%) than WT mice (35%) (genotype X toxin $F_{1,1}$=6.61 p=0.0124). MLi-2, ineffective on its own, attenuated the loss of DA neurons in G2019S KI but not WT mice (genotype X treatment $F_{1,1}$=7.24 p=0.00911;). Consistent with what found in SNc (Fig. 30B), MPTP caused a more profound loss of TH+ terminals in the striatum of G2019S KI mice with respect to WT controls (genotype X toxin $F_{1,1}$=3.61 p=0.0618). Surprisingly, however, MLi-2 rescued this effect in both genotypes.

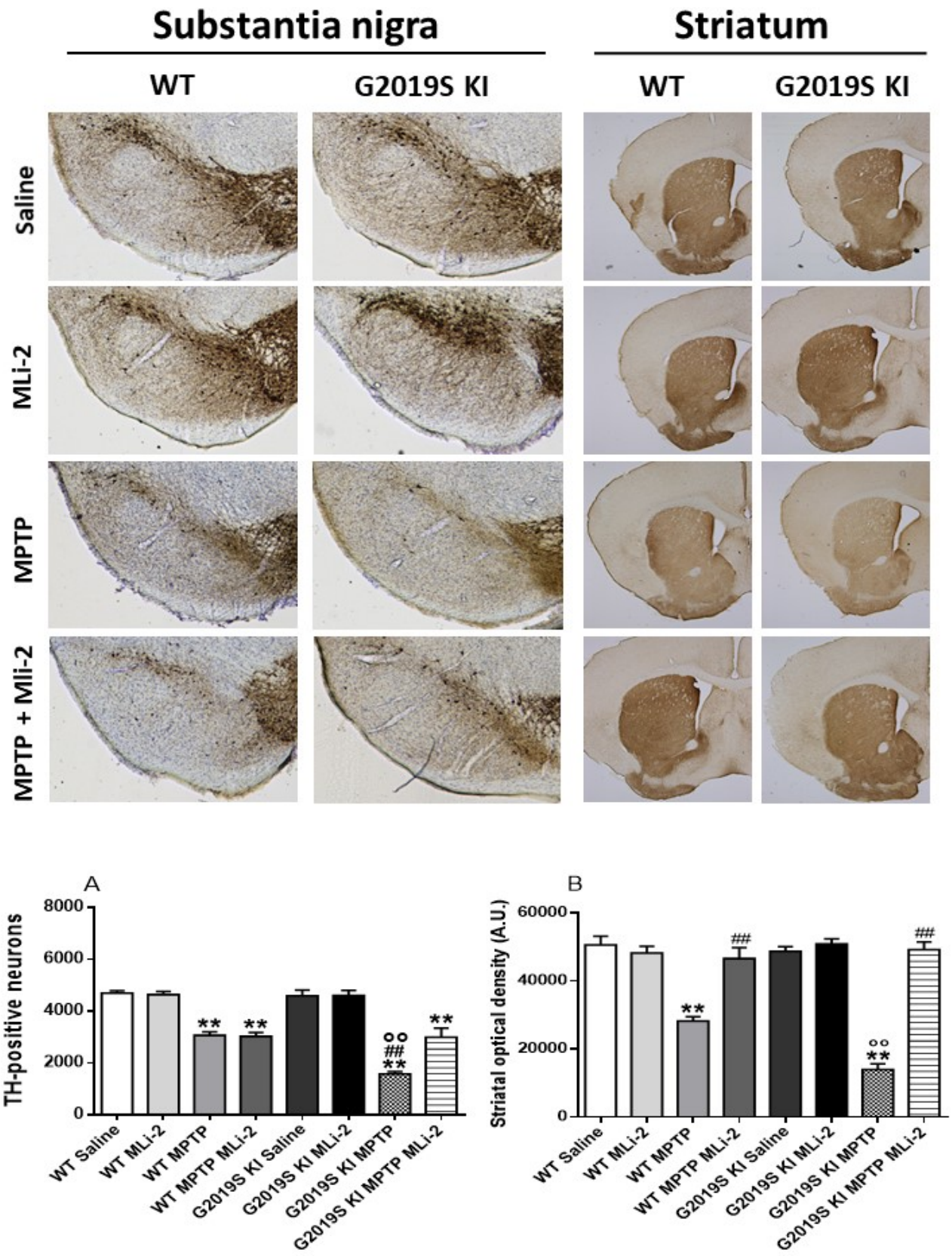

*Figure 30: motor activity and nigrostriatal degeneration in 3-month-old G2019S KI mice treated subactutely with MPTP and MLi-2. Representative images of SNc and Striatum are also given. Data are expressed as number of TH+ neurons (A) and striatal optical density (grey scale arbitrary units, B) and are mean ± SEM of n = 9 mice per group. Statistical analysis was performed by one-way ANOVA followed by the Bonferroni test for multiple comparisons. **p < 0.01 different from Saline controls; ##p < 0.01 different from WT+MPTP; °°p<0.01 different from G2019S KI MPTP+MLi-2.*

LRRK2 targeting in vivo

To confirm that LRRK2 inhibitors were really targeting LRRK2, PF-06447475 and MLi-2 were administered to G29019S KI mice at the single dose of 10 mg/kg and striatal levels of pSer1292 LRRK2, a readout of LRRK2 kinase inhibition, were measured by Western blot (Fig. 31). PF-06447475 reduced pSer1292 levels by 35% (Fig. 31A) whereas the inhibition induced by MLi-2 was two-fold greater (72%; Fig. 31C). Neither antagonist reduced total LRRK2 levels (Fig. 31B, D).

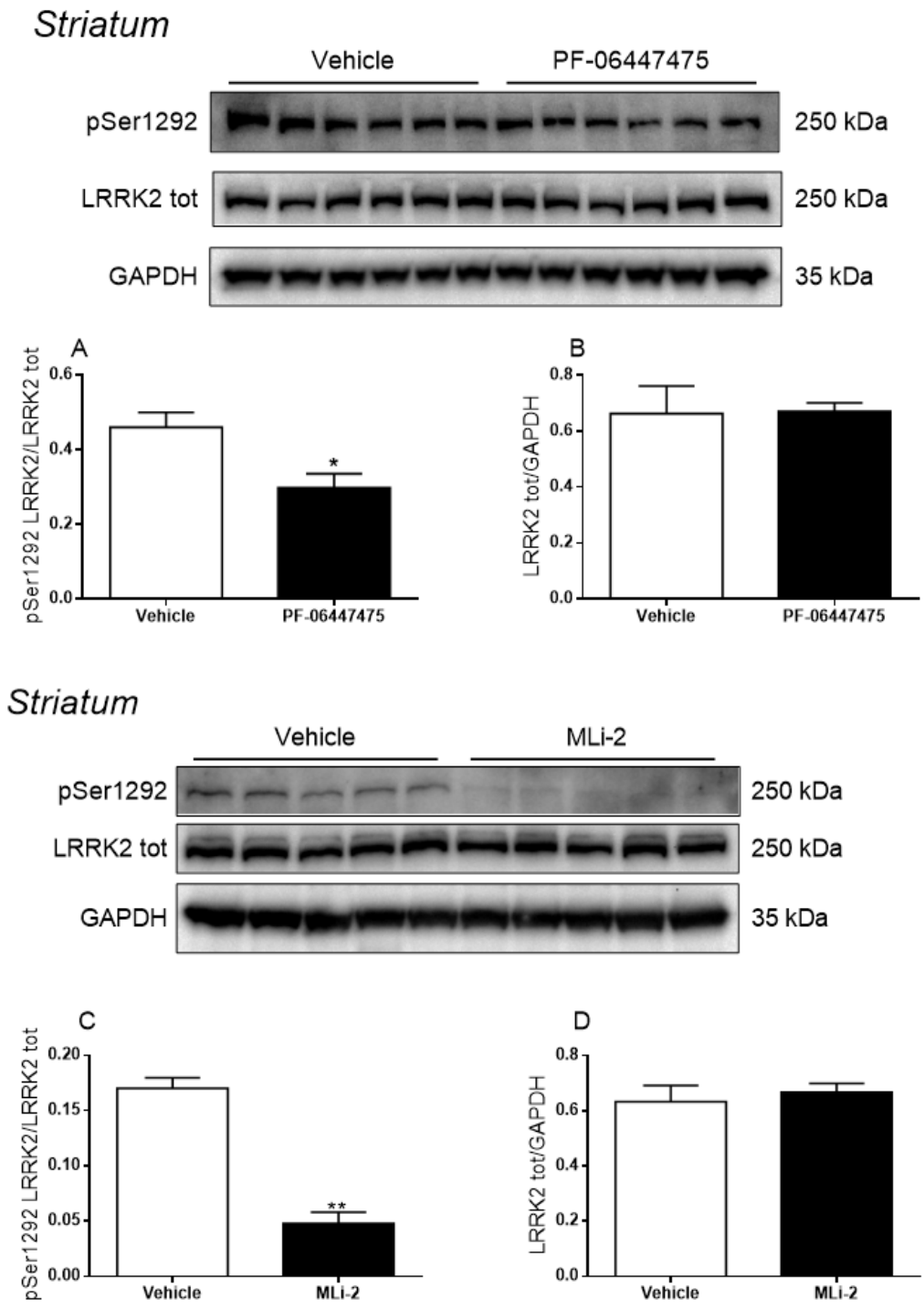

*Fig. 31: Striatal phosphorylation levels of LRRK2 at Ser1292 (pSer1292) and total LRRK2 levels in G2019S KI mice treated with either vehicle, PF-06447475 or MLi-2. Representative blots and quantification are shown. Data are expressed as pSer1292 LRRK2/total LRRK2 and are means ± SEM of 5 mice per group. Statistical analysis was performed with the Student t-test, two tailed for unpaired data. **p < 0.01, different from vehicle.*

PF-06447475 and microglial response

Preliminary investigation on the role of inflammation in the response to MPTP and the LRRK2 inhibitors was made via Iba-1 immunohistochemistry (Fig. 32A-B). Morphological analysis revealed that MPTP induces a profound microglial response in the striatum of WT animals when compared to the control group treated with saline (Fig. 32A), as shown by the 165% increase in the

number of IBA-1+ cells. Microglial recruitment by MPTP was however greater in G2019S KI mice which showed a 484% increase relative to the control group (genotype X MPTP $F_{1,1}$= 32.11, p<0.0001). Treatment with the LRRK2 kinase inhibitor PF-06447475 did not alter the microglial response to MPTP in WT micebut quenched by 39.5% the microglial proliferation in G2019S KI mice (genotype X treatment $F_{1,1}$=15.07 p=0.0004). Similar results were obtained by analyzing the area occupied by IBA-1+ cells (Fig. 32B): no genotype difference was observed in saline-treated animals displaying similar values between the two genotypes (54 ± 8 vs 57 ± 5 pixel^2 for WT and G2019S KI mice respectively) whereas G2019S KI mice showed a more marked (16-fold) response to MPTP compared to WT mice (8-fold; $F_{1,1}$=24.65 p<0.0001). Even in this case, PF-064447475 normalized the response in G2019S KI mice, being ineffective in WT mice ($F_{1,1}$=18.89 p<0.0001).

MLi-2 and microglial response

The degree of microglial activation was also evaluated in MLi-2-treated mice (Fig. 32C, D). Once again, MPTP-treatment induced a more profound increase in number ($F_{1,1}$=38.41 p<0.0001) and area occupied ($F_{1,1}$=34.36 p<0.0001) by IBA-1+ cells in G2019S KI animals compared to WT controls. Different from what observed with PF-06447475, MLi-2 increased the number of IBA-1+ cells in WT mice but did not impact this microglial response in G2019S KI mice. In addition, MLi-2 did not change the area occupied by IBA-1 positive cells in both genotypes.

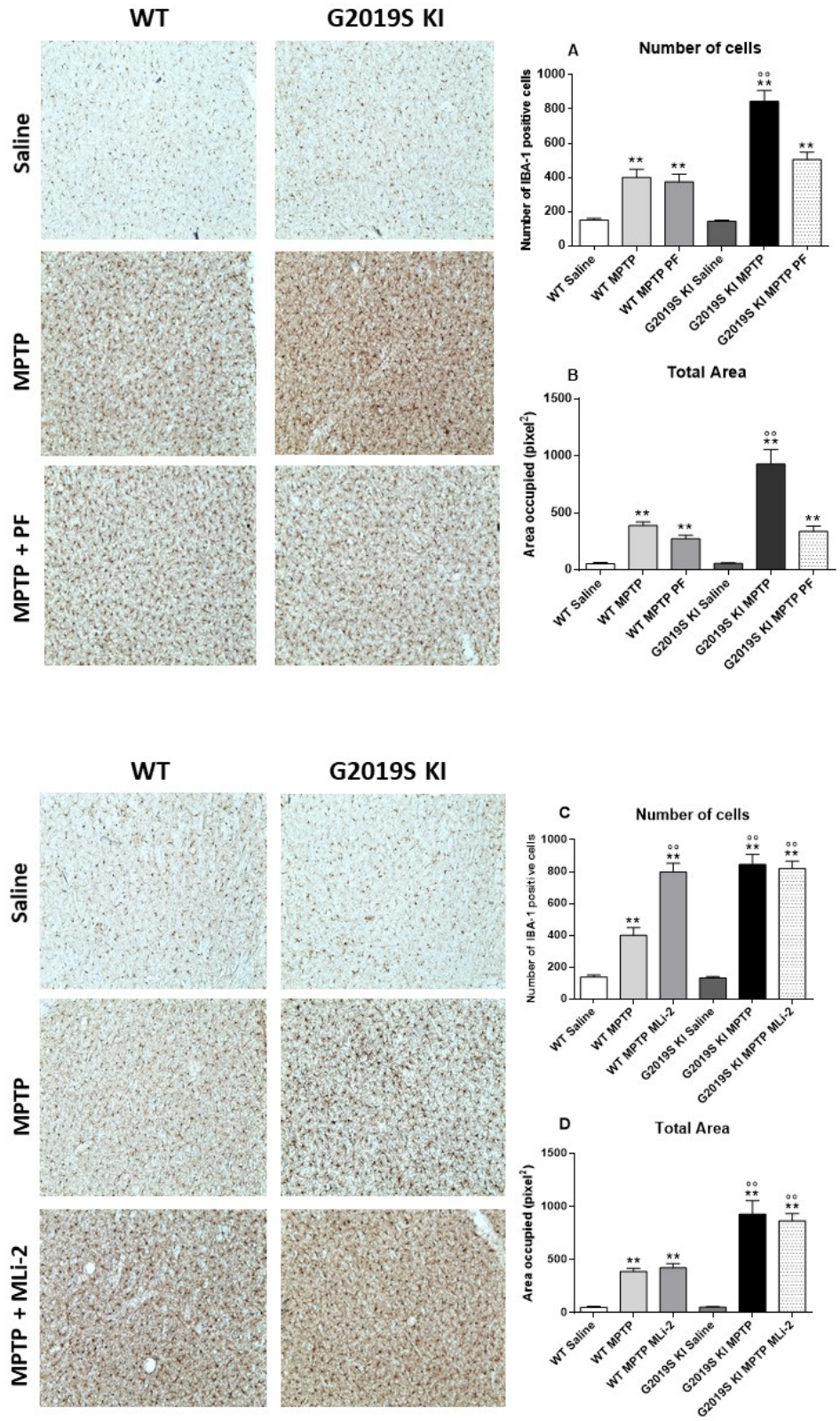

*Fig. 32: Microglial response in MPTP, PF-06447475 and MLi-2-treated WT and G2019S KI animals. Representative images of striatum and relative quantifications of the number (A, C) and the area occupied (B, D) by IBA-1 positive microglial cells. Data are expressed as number of IBA-1 positive cells and area occupied (pixel^2) and are mean ± SEM of 8 (PF-06447475 cohort) or 9 (MLi-2 cohort) mice per group. Statistical analysis was performed by one-way ANOVA followed by the Bonferroni test for multiple comparisons. **$p < 0.01$ different from respective saline controls; °°$p<0.01$ different from WT MPTP.*

DISCUSSION

Study I

We previously reported that G2019S KI mice have a hyperkinetic phenotype relying on elevated kinase activity (Longo et al., 2014). In this follow-up, we show that 12-month-old G2019S KI and WT mice bear similar numbers of nigral DA neurons and striatal DA terminals, in keeping with previous studies in the same genotype (Herzig et al., 2011, Yue et al., 2015) or in BAC G2019S overexpressing mice (Li et al., 2010a, Melrose et al., 2010) and rats (Zhou et al., 2011, Lee et al., 2015, Sloan et al., 2016), as well as similar extracellular DA levels and depolarization-evoked striatal DA release, in line with that found in 22-month old R1441G KI mice (Tong et al., 2009). Since the LRRK2 kinase inhibitor Nov-LRRK2-11 (Longo et al., 2014) also failed to affect striatal DA release in vivo in any genotypes, we conclude that the nigro-striatal DA system is morphologically intact and the exocytotic properties of DA neurons are functionally preserved in G2019S LRRK2 carriers. The lack of changes of striatal DA release is at striking variance with the 60% reduction in basal striatal extracellular DA levels reported, in the absence of motor phenotype change, in 12-month-old G2019S KI mice (Yue et al., 2015). We cannot easily explain this difference since both strains of G2019S KI mice are backcrossed on C57BL and bear similar kinase-enhancing mutations on exon 41 (Herzig et al., 2011, Yue et al., 2015). Indeed, kinase activity appears to be elevated in both strains, as evaluated by in vitro kinase assays on synthetic substrates (Herzig et al., 2011, Yue et al., 2015). We confirmed this finding in vivo, showing that, in good agreement with previous work on brain lysates of BAC G2019S mice (Sheng et al., 2012), pSer1292 levels were ~8-fold higher in the striatum of G2019S KI mice compared to WT controls. pSer1292 appears a more reliable marker of kinase activity with respect to ATP γ-phosphate incorporation measured in in vitro assays. Indeed, Ser1292 LRRK2 is an autophosphorylation site, and pSer1292 levels correlate with in vivo kinase activity (Sheng et al., 2012). pSer1292 levels are a more reliable readout of in vivo LRRK2 kinase activity even compared to pSer935 levels, since LRRK2 is phosphorylated at Ser935 by other kinases (Dzamko et al., 2010, Chia et al., 2014, Reynolds et al., 2014). The discrepancies between these two strains of G2019S KI mice might be explained by quantitative differences in kinase activity along with inter-individual genomic variability, motor tests used, or environmental conditions. Despite the lack of changes of DA release, the levels and functions of proteins involved in DA synaptic load (DAT) and vesicular storage (VMAT2) were altered in 12-month-old G2019S KI mice. Strikingly, these changes were age-dependent, since they were not observed in 3-month-old animals, indicating these changes are elements of an orchestrated, progressive response relying on the interaction between a genetic factor (the G2019S mutation) and aging, i.e. the main risk factor in PD. DAT was upregulated in G2019S KI mice, which might represent a vulnerability factors for DA neurons (Miller et al., 1999b). Indeed, DAT overexpression has been associated with an increase of oxidative stress and neuronal degeneration (Masoud et al., 2015) likely because cytosolic DA accumulation causes the

buildup of reactive oxygen species and quinones, generated by DA autoxidation (Stokes et al., 1999, Sulzer and Zecca, 2000, Goldstein et al., 2012). Moreover, cytosolic DA is metabolized by monoamine oxidase A to DOPAL, which causes synaptic dysfunction and terminal loss acting via different mechanisms, including cross-linking with α-syn (Burke et al., 2008). Finally, environmental toxins causing PD, such as the toxic metabolite of MPTP, MPP^+, are taken up by DA neurons through DAT. In fact, the greater susceptibility of BAC hG2019S overexpressing mice to the parkinsonian toxin MPTP can be explained by DAT upregulation (Karuppagounder et al., 2016). Quite paradoxically, the increase of DAT activity was associated with a blunted neurochemical and behavioral response to GBR-12783. This is consistent with microdialysis works reporting a 35-50% reduction of nomifensine-induced DA release in the striatum of KI mice constitutively expressing R1441G LRRK2 (Li et al., 2009) or temporally expressing G2019S LRRK2 (Zhou et al., 2011). Previous studies in cells have shown that DAT expression levels inversely correlate with the potency of DAT blockers (Chen and Reith, 2007), a phenomenon also observed for the serotonin transporter (Ramsey and DeFelice, 2002). Membrane DAT is in equilibrium between oligomeric and monomeric forms, and it has been hypothesized that higher DAT expression leads to higher DAT oligomerization, and DAT oligomers have lower affinity for DAT blockers with respect to monomers (Li et al., 2010b). In line with that found in G2019S overexpressing mice (Liu et al., 2015), G2019S KI mice showed reduced striatal VMAT2 levels. This reduction was robust and consistent with the two different antibodies, one of which validated in $VMAT2^{+/-}$ mice (Cliburn et al., 2016). Reduction of VMAT2 is observed also in PD patients (Miller et al., 1999a) and is pathogenic in PD. In fact, filling synaptic vesicles via VMAT2 is a way to keep cytosolic DA levels in a nontoxic range; accordingly, VMAT2 deletion induces neurodegeneration (Taylor et al., 2011) whereas VMAT2 overexpression protects DA neurons (Caudle et al., 2007, Lohr et al., 2014). However, despite VMAT2 reduction further enhanced the already higher DAT/VMAT2 ratio in nigro-striatal DA neurons, thus increasing their vulnerability (Miller et al., 1999b), G2019S KI mice did not show overt neurodegeneration (up to 19-months at least) or even significantly enhanced levels of DOPAL-bound α-syn, a marker of DA cytotoxicity. This questions the physiological meaning of the 50% reduction of VMAT2 observed in the striatal homogenate of G2019S KI mice. Indeed, contrary to that expected from the Western blot data, an increase in tetrabenazine-sensitive vesicular DA uptake was measured in G2019S KI mice in vitro. Although we cannot rule out the possibility that such increase is compensatory in nature, the possibility that this discrepancy relies on technical reasons should be considered. In fact, the reduction of VMAT2 levels measured in striatal homogenate might not faithfully reflect a reduction of active VMAT2 expressed on mature, release-prone synaptic vesicles. In fact, VMAT2 levels measured by Western blot encompass also VMAT2 contained in immature secretory vesicles trafficking from the soma to presynaptic vesicle membrane, or recycling from the plasma membrane (Hogan et al., 2000). Interestingly, Sonsalla and collaborators (Hogan et al., 2000)

proved a disparity between tetrabenazine binding measured in striatal homogenate and striatal synaptic vesicles at 24 hrs after MPTP, showing that, under certain conditions, tetrabenazine binding measured in striatal homogenate may not be representative of vesicular VMAT2. On the other hand, the major limitation of a whole-brain preparation of synaptic vesicles is heterogeneity. VMAT2 is present not only in striatal dopaminergic terminals but also in noradrenergic, serotoninergic and histaminergic terminals in striatal and extrastriatal areas. Since there is no possibility to dissect out the contribution of the different populations of VMAT2-positive synaptic vesicles in this whole-brain preparation, we cannot prove that the observed increase of vesicle uptake is really due to VMAT2 expressed on striatal vesicles or is the net result of all changes of VMAT2 activity in different nerve terminals and brain areas. Nonetheless, in favor of the hypothesis that vesicular DA uptake might be increased rather than reduced in G2019S KI mice, G2019S KI mice were relatively more resistant than WT controls to the hypolocomotive action of 1 mg/Kg reserpine in vivo, which is opposite from that expected from DA depleted vesicles. We can speculate that the greater resistance to reserpine might be due to a greater competition for VMAT2 of reserpine and cytosolic DA (the increase in DAT activity and the reduced DA turnover might overwhelm the buffering capacity of VMAT2, thus causing an increase in cytosolic DA). Alternatively, we might speculate that synaptic vesicles in G2019S KI mice are more enriched in DA, although only a trend to an increase in extracellular DA levels or in the K^+-induced DA release was observed in the G2019S LRRK2 carriers. It is therefore plausible that VMAT2 uptake elevation compensates for the loss of VMAT2 protein and protects from cytosolic DA toxicity, even in the presence of upregulated DAT. Whether this adaptive change will be effective throughout the life-span of G2019S KI mice is unknown, since we have investigated G2019S KI mice up to 19 months. However, it is also possible that other compensatory mechanisms will come into play to preserve DA homeostasis and DA neuron integrity. In this respect, one important finding of the present study is that pSer129 α-syn levels are elevated in the striatum of G2019S KI mice. Since this was not paralleled by an elevation of total α-syn levels, we concluded that G2019S LRRK2 facilitates this posttranslational modification of α-syn. This is in line with a recent study showing that the formation of pSer129 α-syn-positive inclusions in nigral DA neurons in response to intranigral α-syn fibrils injection is accelerated in BAC hG2019S rats (Volpicelli-Daley et al., 2016). pSer129 α-syn (Fujiwara et al., 2002) is the predominant form of syn in Lewy bodies (Anderson et al., 2006), and for this reason it has been hypothesized to favor α-syn aggregation, thus contributing to PD (Oueslati, 2016). However, the role of pSer129 α-syn phosphorylation in α-syn toxicity in vivo is still under debate (Tenreiro et al., 2014a, Oueslati, 2016). In fact, from the published literature it appears that depending on which kinase is involved in Ser129 α-syn phosphorylation, either neurotoxicity (G protein receptor kinases) (Chen and Feany, 2005, Sato et al., 2011) or neuroprotection (Polo-like kinase 2) (Oueslati et al., 2013) can ensue. Moreover, LRRK2, and more intensely G2019S LRRK2, can directly Ser129-phosphorylate α-syn in vitro

(Qing et al., 2009). Pinning down the pathway underlying Ser129 α-syn phosphorylation might help understand whether this modification is protective or pathogenic for DA neurons.

Study II

Major finding of the present study is that G2019S KI mice are more susceptible than WT controls to develop nigral DA neuron degeneration and synucleinopathy after injection of hα-syn delivered via AAV2/9 vector. The G2019S effect emerges at 12-months of age, further strengthening the role of aging in G2019S-induced synucleinopathy. Viral vectors are an efficient way to allow overexpression of native or mutant α-syn in nigral DA neurons of rats, mice and nonhuman primates (for reviews see (Ulusoy et al., 2010, Low and Aebischer, 2012, Van der Perren et al., 2015). Consistent with previous studies (Lauwers et al., 2003, Bourdenx et al., 2015, Song et al., 2015, Thome et al., 2015, Svarcbahs et al., 2016, Ip et al., 2017), AAV2/9-hα-syn injection resulted in efficient expression of the human transgene in SN and, after diffusion, in striatum. Accordingly, degeneration of nigral DA neurons (Lauwers et al., 2003, Bourdenx et al., 2015, Song et al., 2015, Thome et al., 2015, Svarcbahs et al., 2016, Ip et al., 2017) and α-syn pathology (increased pSer129 α-syn levels and PK-resistant α-syn aggregates) appeared. Different from studies where unilateral injection was performed (Lauwers et al., 2003, Bourdenx et al., 2015, Thome et al., 2015, Svarcbahs et al., 2016, Ip et al., 2017), the bilateral AAV2/9 injection caused a larger reduction of nigral DA neurons (50% vs 20-30%) (also see (Song et al., 2015). Consistent with such higher levels of neurodegeneration, deficits in stepping (drag test) and global motor (rotarod test) activity were observed both in 3-month-old and 12-month-old mice, with the difference that in older mice motor deficits appeared earlier, i.e. already at 4 weeks after intranigral AAV2/9 injection, perhaps suggesting an acceleration of the neurotoxic process associated with aging. The finding that 12-month-old G2019S KI mice were more prone to α-syn toxicity cannot be attributed to different efficiencies of transgene expression (or other surgery variables) since hα-syn expression and diffusion were similar among the different cohorts of mice. Thus, the neuropathological changes between 12-month-old G2019S KI and WT mice are likely due to LRRK2 mutation. This corroborates previous reports that WT LRRK2/A53T α-syn and G2019S LRRK2/A53T α-syn double TG mice (Lin et al., 2009) or BAC G2019S KI rats injected with a AAV2 α-syn (Daher et al., 2015) display greater loss of nigral DA neurons compared to controls. Greater nigral degeneration in 12-month-old G2019S KI mice was associated with greater load of PK-resistant, insoluble pSer129 α-syn aggregates. This is in line with the finding that α-syn fibrils injection in BAC G2019S overexpressors favours pSer129 α-syn inclusions in DA neurons (Volpicelli-Daley et al., 2016), although in this model of synucleinopathy no overt nigro-striatal degeneration was observed (at 4 weeks after injection). Therefore, since the AAV hα-syn model is a model for α-syn aggregation but not fibrillization, our study would suggest that in aged G2019S KI mice,

excessive deposition of pSer129 α-syn aggregates in SNc accelerates DA neuron loss. In fact, expression of G2019S LRRK2 in *C. elegans* caused age-dependent accumulation of α-syn and degeneration of DA neurons (Saha et al., 2015). α-syn aggregates per se can disrupt cellular homeostasis, altering cellular trafficking (Giasson and Lee, 2003, Stefanis, 2012). Among the possible mechanisms through which G2019S LRRK2 accelerates α-syn synucleinopathy, we investigated microglial activation. In fact, it is established that LRRK2 promotes microglial activation and the release of pro-inflammatory cytokines (Gillardon et al., 2012, Moehle et al., 2012, Russo et al., 2015) and that G2019S mutation amplifies this response (Kim et al., 2012, Moehle et al., 2015). Another mechanisms has been recently proposed by a study showing that G2019S LRRK2 increases phagocytic activity of microglia and macrophages through stabilization of WAVE2 complex, which is directly linked to DA cell death (Kim et al., 2018). Consistent with those reports, microgliosis was associated with the greater loss of DA neurons observed in G2019S LRRK2/A53T α-syn double TG mice (Lin et al., 2009) or BAC G2019S rats injected with AAV α-syn (Daher et al., 2015). Different from these reports, however, we failed to detect an increased number of Iba-1+ cells in both the SN and striatum of WT and G2019S KI mice injected with AAV-hα-syn, regardless of the age examined. Lack of microglial activation (Litteljohn et al., 2018) or even inhibition of microglial motility (Choi et al., 2015) have been reported in G2019S LRRK2 models. However, we should consider that in the AAV model of synucleinopathy, the number of microglia cells appears to be transiently elevated only at 4-8 weeks after injection (Chung et al., 2009, Sanchez-Guajardo et al., 2010, Daher et al., 2015), consistent with a role of microglia in early stages of AAV α-syn toxicity. Since we performed the microglia analysis at 12 or 20 weeks after AAV injection, we might have missed the initial microglial response. We should also consider that in previous studies a sustained microglial activation was observed in the presence of elevated levels of G2019S LRRK2 (either genetically- or virus-induced) which might have further amplified such response. The lack of a sustained microglial response and the age-dependence of the G2019S KI pattern of response would suggest other mechanisms underlying the G2019S effect. In particular, G2019S LRRK2 can potently regulate cellular proteostasis through autophagy pathways. In fact, α-syn is degraded mainly via chaperone-mediated autophagy (Cuervo et al., 2004, Lee et al., 2004) and G2019S LRRK2 impairs α-syn clearance (Orenstein et al., 2013, Saha et al., 2015) by promoting α-syn oligomerization at the lysosomal membrane (Orenstein et al., 2013). Indeed, G2019S LRRK2 has been shown to impair lysosomal α-syn degradation and cause endogenous α-syn accumulation, an effect reversed by LRRK2 kinase inhibitors, in primary cortical neurons (Schapansky et al., 2018). Interestingly, aging is accompanied by impairment of chaperone-mediated autophagy and proteasome clearance (Mattson and Magnus, 2006, Xilouri and Stefanis, 2016), which leads to the accumulation of α-syn aggregates, at least in primates (Chu and Kordower, 2007). Thus, the increased deposition of α-syn aggregates in aged G2019S KI

mice might be due to a detrimental effect of G2019S LRRK2 combined with the reduced brain capability to handle α-syn overload of the aged brain. The fact that we did not observe a genotype effect in young G2019S KI mice, might thus depend on a greater capability of young mice to cope with changes of α-syn overload. In support of the role of aging in G2019S LRRK2 pathology, a recent study reported nigral DA loss and prolonged microgliosis in 19-month-old but not 2-3-month-old WT mice intrastriatally-injected with an adenoviral vector carrying human G2019S LRRK2 (Kritzinger et al., 2018). G2019S KI mice, therefore, might represent a model recapitulating the effect of aging (the major risk factor in PD) over the interaction between a pathogenic genetic component (the G2019S mutation) and a PD-relevant trigger (hα-syn). Nonetheless, there seems to be a dissociation between neurodegeneration and synucleinopathy in striatum where, different from SNc, no greater loss of DA terminals was detected in G2019S KI mice compared to controls. It is possible that, consistent with the anterograde nature of the AAV2/9-hα-syn toxicity process, the greater loss of nigral DA cell bodies in G2019S KI mice needs more time to translate into a significant change at the striatal terminal level. Alternatively, we could speculate that the toxic effect exerted by G2019S LRRK2 at the terminal levels is compensated.

Study III

The present study shows that G2019S KI mice are more susceptible to MPTP-induced nigrostriatal neurodegeneration than WT mice, mice lacking LRRK2 or carrying a LRRK2 kinase-dead mutation. This suggests that an increase in LRRK2 kinase activity makes G2019S KI mice more susceptible to MPTP-induced parkinsonism, confirming that LRRK2 kinase activity is instrumental for LRRK2 G2019S-mediated toxicity (West et al., 2005, Greggio et al., 2006, Yao et al., 2010). This finding corroborates the results of a study showing greater susceptibility of hG2019S overexpressing mice to acute MPTP in comparison with WT mice (Karuppagounder et al., 2016). Remarkable similarities in the degrees of MPTP-induced nigral dopamine neurodegeneration were observed between the two studies (75% in transgenic mice vs 50% in WT mice), despite the different protocol of MPTP administration (acute vs subacute). The higher sensitivity of G2019S KI mice to MPTP is also consistent with the larger reduction of field potential amplitude, an index of deranged neurotransmission, in striatal slices of G2019S KI mice exposed to the complex I inhibitor rotenone in comparison with striatal slices from LRRK2 KO or KD mice (Tozzi et al., 2018). This higher sensitivity to mitochondrial complex I inhibition likely relies on the evident mitochondrial dysfunctions observed in G2019S KI mice (Yue et al., 2015), fibroblasts (Mortiboys et al., 2010) or iPSC (Cooper et al., 2012, Sanders et al., 2014) from LRRK2 G2019S patients, and even cells overexpressing G2019S (Tozzi et al., 2018). The role of LRRK2 kinase activity in MPTP-induced toxicity is further strengthened by the fact that pharmacological inhibition of LRRK2 rescues the enhanced sensitivity of G2019S KI mice to MPTP. Indeed, in the presence of

either PF-06447475 or MLi-2 the number of DA neurons spared in the SNc of G2019S KI mice approximated that observed in WT mice. This adds to the neuroprotective effect of PF-06447475 in a rat model of α-syn-induced toxicity (Daher et al., 2015), and is the first in vivo evidence that MLi-2 can counteract nigrostriatal neurodegeneration in vivo, since this compound failed to alter PD-like neurochemical and functional changes the in MitoPark mouse model of PD (Fell et al., 2015). Despite their consistent neuroprotective effects in SNc, PF-06447475 and MLi-2 exerted different effects on striatal DA terminal density: PF-06447474 did not attenuate the nerve terminal loss induced by MPTP whereas MLi-2 prevented it. PF-06447475 and MLi-2 are structurally-unrelated, brain penetrant, LRRK2 inhibitors showing high LRRK2 selectivity and different potencies in inhibiting LRRK2 in vitro. In fact, MLi-2 is ~4-fold more potent than PF-06447475 in inhibiting purified LRRK2 (IC_{50} 0.76 nM and 3 nM, respectively) and ~18-fold more potent than PF-06447475 in inhibiting pSer935 (IC_{50} 1.4 nM and 24 nM, respectively) (Fell et al., 2015, Henderson et al., 2015). This difference in potency (along with a different brain penetrability) might ensue in a different degree of LRRK2 inhibition in vivo, thus explaining the different neuroprotective profiles in striatum. In fact, MLi-2 induced a twice greater inhibition of striatal pSer1292 levels than PF-06447475 (72% vs 36% respectively). The fact that both inhibitors were equally effective in SN is in line with the lower levels of endogenous LRRK2 in this region. Thus, full neuroprotection in SN can be achieved also with the less potent inhibitor. It is also relevant that neither LRRK2 inhibitor reduced total LRRK2 levels, in agreement with the original characterization studies of the inhibitors (Fell et al., 2015, Henderson et al., 2015). One intriguing finding is that MLi-2 prevented MPTP-induced toxicity not only in G2019S KI mice but also in WT controls. The specificity of this effect awaits further confirmation in LRRK2 KO mice. Nonetheless, MLi-2 is reported to be highly selective for LRRK2 (Fell et al., 2015), possibly ruling out any off target effects. Consistent with this view, also a LRRK2 inhibitor structurally unrelated to MLi-2, PF-06447475, prevented a-syn-induced neurodegeneration in both LRRK2 G2019S transgenic and WT rats (Daher et al., 2015), overall suggesting that LRRK2 kinase activity contributes to MPTP-induced parkinsonism in WT animals. This is quite is puzzling because we confirm that LRRK2 KO mice are not resistant to MPTP (Andres-Mateos et al., 2009). The discrepancy might be explained taking into account a developmental compensation phenomenon. In particular, the LRRK2 homologue, LRRK1 might compensate for the loss of LRRK2, since their tissue expression, particularly during development, is coordinated (Biskup et al., 2007). Consistently, it has been shown that mice lacking both LRRK2 and LRRK1, but not mice lacking either protein, show early parkinsonian phenotype and loss of nigral DA neurons (Giaime et al., 2017). In adult mice, however, only LRRK2 is expressed in nigrostriatal neurons, thus acute blockade of LRRK2 might leave cellular function regulated by LRRK2 uncompensated. Modulation of microgliosis might be a possible mechanism underlying the neuroprotection exerted by LRRK2 inhibitors in the MPTP model of PD. MPTP caused an increase of the number of iba-1

positive cells in striatum as well as of the area occupied by these cells in both WT and G2019S KI mice, suggesting a correlation between MPTP toxicity and microglial activation. In fact, the increases of both parameters were significantly higher in G2019S KI mice than in WT mice, which positively correlated with the larger neurodegeneration associated with LRRK2 G2019S. Although the role played by microglia in MPTP-induced toxicity is complex (Smeyne et al., 2005, Barnum and Tansey, 2010, Joers et al., 2017), acute MPTP is known to upregulate inducible nitric oxide synthase (iNOS) in microglial cells, which is responsible for nigral DA cell death (Liberatore et al., 1999), through the release of radical species (NO, superoxide radicals) and oxidative stress. Thus, acute MPTP-activated microglia has a dominant proinflammatory phenotype, releasing cytokines that harm DA neurons (Teismann et al., 2003). It is not clear however whether the same microglia phenotype is also replicated in a subacute MPTP model. In fact, a dissociation between microglial activation and neuroprotection of striatal dopaminergic terminals was observed. PF-06447475 prevented the MPTP-induced increase in microglia recruitment whereas MLi-2 did not. Conversely, PF-06447475 did not prevent the MPTP-induced striatal terminals degeneration whereas MLi-2 prevented it. Moreover, MLi-2 further enhanced the MPTP-induced microglia number in WT mice, simultaneously preventing the MPTP-induced striatal terminal loss. These data would be rather in favor of a recruitment of antinflammatory microglia in WT mice. This paradox might rely on the different protocol of MPTP administration and the time the morphological analysis was conducted, i.e. 6 days after MPTP withdrawal. Microglia analysis at earlier time-points should address this discrepancy with the acute MPTP model. Anyway, morphological analysis alone cannot clarify the pro- or antinflammatory profile of microglia, and functional analysis (cytokine release, membrane receptor or inflammatory gene expression) should be conducted in parallel. In conclusion, this study shows that LRRK2 G2019S confers greater susceptibility to the parkinsonian neurotoxin, complex I inhibitor, MPTP. This relies on LRRK2 kinase activity since both kinase dead mutation or pharmacological inhibitors of LRRK2 kinase activity prevent or attenuate the enhanced sensitivity of nigral DA neurons to the toxin. Since different environmental toxins (e.g. pesticides) are inhibitors of the mitochondrial electron transport chain, this study might offer a mechanistic basis to explain why LRRK2 G2019S carriers are more susceptible to develop PD.

Concluding remarks

The present thesis provides novel information on the role of G2019S LRRK2 in experimental parkinsonism and possibly, PD etiopathogenesis, in particular replicating in a genetic model of PD out the positive interaction of LRRK2 G2019S mutation with genetic (α-syn), physiological (aging) or environmental (MPTP) risk factors in PD. This study confirms the neuroprotective potential of LRRK2 inhibitors, strengthening the view that the increased kinase activity associated with the LRRK2 G2019S mutation is instrumental for LRRK2 toxicity. Finally, the present work supports

the view that G2019S KI mice represent a model for presymptomatic/premotor PD, useful to study the interaction between genetic, intrinsic and environmental factors, or in other words, between "triggers, facilitators and aggravators" in the pathogenesis of PD (Johnson et al., 2018)

BIBLIOGRAPHY

Abeliovich A, Schmitz Y, Farinas I, Choi-Lundberg D, Ho WH, Castillo PE, Shinsky N, Verdugo JM, Armanini M, Ryan A, Hynes M, Phillips H, Sulzer D, Rosenthal A (2000) Mice lacking alpha-synuclein display functional deficits in the nigrostriatal dopamine system. Neuron 25:239-252.

Alcalay RN, Mirelman A, Saunders-Pullman R, Tang MX, Mejia Santana H, Raymond D, Roos E, Orbe-Reilly M, Gurevich T, Bar Shira A, Gana Weisz M, Yasinovsky K, Zalis M, Thaler A, Deik A, Barrett MJ, Cabassa J, Groves M, Hunt AL, Lubarr N, San Luciano M, Miravite J, Palmese C, Sachdev R, Sarva H, Severt L, Shanker V, Swan MC, Soto-Valencia J, Johannes B, Ortega R, Fahn S, Cote L, Waters C, Mazzoni P, Ford B, Louis E, Levy O, Rosado L, Ruiz D, Dorovski T, Pauciulo M, Nichols W, Orr-Urtreger A, Ozelius L, Clark L, Giladi N, Bressman S, Marder KS (2013) Parkinson disease phenotype in Ashkenazi Jews with and without LRRK2 G2019S mutations. Movement disorders : official journal of the Movement Disorder Society 28:1966-1971.

Alegre-Abarrategui J, Christian H, Lufino MM, Mutihac R, Venda LL, Ansorge O, Wade-Martins R (2009) LRRK2 regulates autophagic activity and localizes to specific membrane microdomains in a novel human genomic reporter cellular model. Human molecular genetics 18:4022-4034.

Anderson JP, Walker DE, Goldstein JM, de Laat R, Banducci K, Caccavello RJ, Barbour R, Huang J, Kling K, Lee M, Diep L, Keim PS, Shen X, Chataway T, Schlossmacher MG, Seubert P, Schenk D, Sinha S, Gai WP, Chilcote TJ (2006) Phosphorylation of Ser-129 is the dominant pathological modification of alpha-synuclein in familial and sporadic Lewy body disease. The Journal of biological chemistry 281:29739-29752.

Andres-Mateos E, Mejias R, Sasaki M, Li X, Lin BM, Biskup S, Zhang L, Banerjee R, Thomas B, Yang L, Liu G, Beal MF, Huso DL, Dawson TM, Dawson VL (2009) Unexpected lack of hypersensitivity in LRRK2 knock-out mice to MPTP (1-methyl-4-phenyl-1,2,3,6-tetrahydropyridine). The Journal of neuroscience : the official journal of the Society for Neuroscience 29:15846-15850.

Arcuri L, Viaro R, Bido S, Longo F, Calcagno M, Fernagut PO, Zaveri NT, Calo G, Bezard E, Morari M (2016) Genetic and pharmacological evidence that endogenous nociceptin/orphanin FQ contributes to dopamine cell loss in Parkinson's disease. Neurobiology of disease 89:55-64.

Asai H, Ikezu S, Tsunoda S, Medalla M, Luebke J, Haydar T, Wolozin B, Butovsky O, Kugler S, Ikezu T (2015) Depletion of microglia and inhibition of exosome synthesis halt tau propagation. Nature neuroscience 18:1584-1593.

Azeredo da Silveira S, Schneider BL, Cifuentes-Diaz C, Sage D, Abbas-Terki T, Iwatsubo T, Unser M, Aebischer P (2009) Phosphorylation does not prompt, nor prevent, the formation of alpha-synuclein toxic species in a rat model of Parkinson's disease. Human molecular genetics 18:872-887.

Barnum CJ, Tansey MG (2010) Modeling neuroinflammatory pathogenesis of Parkinson's disease. Progress in brain research 184:113-132.

Barrett JC, Hansoul S, Nicolae DL, Cho JH, Duerr RH, Rioux JD, Brant SR, Silverberg MS, Taylor KD, Barmada MM, Bitton A, Dassopoulos T, Datta LW, Green T, Griffiths AM, Kistner EO, Murtha MT, Regueiro MD, Rotter JI, Schumm LP, Steinhart AH, Targan SR, Xavier RJ, Consortium NIG, Libioulle C, Sandor C, Lathrop M, Belaiche J, Dewit O, Gut I, Heath S, Laukens D, Mni M, Rutgeerts P, Van Gossum A, Zelenika D, Franchimont D, Hugot JP, de Vos M, Vermeire S, Louis E, Belgian-French IBDC, Wellcome Trust Case Control C, Cardon LR, Anderson CA, Drummond H, Nimmo E, Ahmad T, Prescott NJ, Onnie CM, Fisher SA, Marchini J, Ghori J, Bumpstead S, Gwilliam R, Tremelling M, Deloukas P, Mansfield J, Jewell D, Satsangi J, Mathew CG, Parkes M, Georges M, Daly MJ (2008) Genome-wide

association defines more than 30 distinct susceptibility loci for Crohn's disease. Nature genetics 40:955-962.
Berg D, Riess O, Bornemann A (2003) Specification of 14-3-3 proteins in Lewy bodies. Annals of neurology 54:135.
Bergeron M, Motter R, Tanaka P, Fauss D, Babcock M, Chiou SS, Nelson S, San Pablo F, Anderson JP (2014) In vivo modulation of polo-like kinases supports a key role for PLK2 in Ser129 alpha-synuclein phosphorylation in mouse brain. Neuroscience 256:72-82.
Bido S, Marti M, Morari M (2011) Amantadine attenuates levodopa-induced dyskinesia in mice and rats preventing the accompanying rise in nigral GABA levels. Journal of neurochemistry 118:1043-1055.
Biosa A, Trancikova A, Civiero L, Glauser L, Bubacco L, Greggio E, Moore DJ (2013) GTPase activity regulates kinase activity and cellular phenotypes of Parkinson's disease-associated LRRK2. Human molecular genetics 22:1140-1156.
Bisaglia M, Tessari I, Mammi S, Bubacco L (2009) Interaction between alpha-synuclein and metal ions, still looking for a role in the pathogenesis of Parkinson's disease. Neuromolecular medicine 11:239-251.
Biskup S, Moore DJ, Celsi F, Higashi S, West AB, Andrabi SA, Kurkinen K, Yu SW, Savitt JM, Waldvogel HJ, Faull RL, Emson PC, Torp R, Ottersen OP, Dawson TM, Dawson VL (2006) Localization of LRRK2 to membranous and vesicular structures in mammalian brain. Ann Neurol 60:557-569.
Biskup S, Moore DJ, Rea A, Lorenz-Deperieux B, Coombes CE, Dawson VL, Dawson TM, West AB (2007) Dynamic and redundant regulation of LRRK2 and LRRK1 expression. BMC neuroscience 8:102.
Bonifati DM, Scaravilli T, Leone M, De Biasia F, Naccarato M, Ottina M, Triggiani L, Mancuso M (2003) Quality of neurology residency programmes: an Italian survey. European journal of neurology 10:301-306.
Bosgraaf L, Van Haastert PJ (2003) Roc, a Ras/GTPase domain in complex proteins. Biochimica et biophysica acta 1643:5-10.
Botta-Orfila T, Ezquerra M, Pastor P, Fernandez-Santiago R, Pont-Sunyer C, Compta Y, Lorenzo-Betancor O, Samaranch L, Marti MJ, Valldeoriola F, Calopa M, Fernandez M, Aguilar M, de Fabregas O, Hernandez-Vara J, Tolosa E (2012) Age at onset in LRRK2-associated PD is modified by SNCA variants. Journal of molecular neuroscience : MN 48:245-247.
Bourdenx M, Dovero S, Engeln M, Bido S, Bastide MF, Dutheil N, Vollenweider I, Baud L, Piron C, Grouthier V, Boraud T, Porras G, Li Q, Baekelandt V, Scheller D, Michel A, Fernagut PO, Georges F, Courtine G, Bezard E, Dehay B (2015) Lack of additive role of ageing in nigrostriatal neurodegeneration triggered by alpha-synuclein overexpression. Acta neuropathologica communications 3:46.
Braak H, Del Tredici K, Rub U, de Vos RA, Jansen Steur EN, Braak E (2003a) Staging of brain pathology related to sporadic Parkinson's disease. Neurobiology of aging 24:197-211.
Braak H, Rub U, Gai WP, Del Tredici K (2003b) Idiopathic Parkinson's disease: possible routes by which vulnerable neuronal types may be subject to neuroinvasion by an unknown pathogen. Journal of neural transmission 110:517-536.
Breid S, Bernis ME, Babila JT, Garza MC, Wille H, Tamguney G (2016) Neuroinvasion of alpha-Synuclein Prionoids after Intraperitoneal and Intraglossal Inoculation. Journal of virology 90:9182-9193.
Brundin P, Melki R, Kopito R (2010) Prion-like transmission of protein aggregates in neurodegenerative diseases. Nature reviews Molecular cell biology 11:301-307.
Burke WJ (2003) 3,4-dihydroxyphenylacetaldehyde: a potential target for neuroprotective therapy in Parkinson's disease. Current drug targets CNS and neurological disorders 2:143-148.
Burke WJ, Kumar VB, Pandey N, Panneton WM, Gan Q, Franko MW, O'Dell M, Li SW, Pan Y, Chung HD, Galvin JE (2008) Aggregation of alpha-synuclein by DOPAL, the monoamine oxidase metabolite of dopamine. Acta Neuropathol 115:193-203.

Burre J (2015) The Synaptic Function of alpha-Synuclein. Journal of Parkinson's disease 5:699-713.
Burre J, Sharma M, Sudhof TC (2014) alpha-Synuclein assembles into higher-order multimers upon membrane binding to promote SNARE complex formation. Proceedings of the National Academy of Sciences of the United States of America 111:E4274-4283.
Burre J, Sharma M, Sudhof TC (2015) Definition of a molecular pathway mediating alpha-synuclein neurotoxicity. The Journal of neuroscience : the official journal of the Society for Neuroscience 35:5221-5232.
Burre J, Sharma M, Tsetsenis T, Buchman V, Etherton MR, Sudhof TC (2010) Alpha-synuclein promotes SNARE-complex assembly in vivo and in vitro. Science 329:1663-1667.
Cali T, Ottolini D, Negro A, Brini M (2012) alpha-Synuclein controls mitochondrial calcium homeostasis by enhancing endoplasmic reticulum-mitochondria interactions. The Journal of biological chemistry 287:17914-17929.
Cardona F, Tormos-Perez M, Perez-Tur J (2014) Structural and functional in silico analysis of LRRK2 missense substitutions. Molecular biology reports 41:2529-2542.
Caudle WM, Richardson JR, Wang MZ, Taylor TN, Guillot TS, McCormack AL, Colebrooke RE, Di Monte DA, Emson PC, Miller GW (2007) Reduced vesicular storage of dopamine causes progressive nigrostriatal neurodegeneration. J Neurosci 27:8138-8148.
Chau KY, Ching HL, Schapira AH, Cooper JM (2009) Relationship between alpha synuclein phosphorylation, proteasomal inhibition and cell death: relevance to Parkinson's disease pathogenesis. Journal of neurochemistry 110:1005-1013.
Chen L, Feany MB (2005) Alpha-synuclein phosphorylation controls neurotoxicity and inclusion formation in a Drosophila model of Parkinson disease. Nat Neurosci 8:657-663.
Chen L, Xie Z, Turkson S, Zhuang X (2015) A53T human alpha-synuclein overexpression in transgenic mice induces pervasive mitochondria macroautophagy defects preceding dopamine neuron degeneration. The Journal of neuroscience : the official journal of the Society for Neuroscience 35:890-905.
Chen N, Reith ME (2007) Substrates and inhibitors display different sensitivity to expression level of the dopamine transporter in heterologously expressing cells. J Neurochem 101:377-388.
Chen X, de Silva HA, Pettenati MJ, Rao PN, St George-Hyslop P, Roses AD, Xia Y, Horsburgh K, Ueda K, Saitoh T (1995) The human NACP/alpha-synuclein gene: chromosome assignment to 4q21.3-q22 and TaqI RFLP analysis. Genomics 26:425-427.
Chia R, Haddock S, Beilina A, Rudenko IN, Mamais A, Kaganovich A, Li Y, Kumaran R, Nalls MA, Cookson MR (2014) Phosphorylation of LRRK2 by casein kinase 1alpha regulates trans-Golgi clustering via differential interaction with ARHGEF7. Nature communications 5:5827.
Chinta SJ, Mallajosyula JK, Rane A, Andersen JK (2010) Mitochondrial alpha-synuclein accumulation impairs complex I function in dopaminergic neurons and results in increased mitophagy in vivo. Neuroscience letters 486:235-239.
Choi BK, Choi MG, Kim JY, Yang Y, Lai Y, Kweon DH, Lee NK, Shin YK (2013) Large alpha-synuclein oligomers inhibit neuronal SNARE-mediated vesicle docking. Proceedings of the National Academy of Sciences of the United States of America 110:4087-4092.
Choi I, Kim B, Byun JW, Baik SH, Huh YH, Kim JH, Mook-Jung I, Song WK, Shin JH, Seo H, Suh YH, Jou I, Park SM, Kang HC, Joe EH (2015) LRRK2 G2019S mutation attenuates microglial motility by inhibiting focal adhesion kinase. Nature communications 6:8255.
Choubey V, Safiulina D, Vaarmann A, Cagalinec M, Wareski P, Kuum M, Zharkovsky A, Kaasik A (2011) Mutant A53T alpha-synuclein induces neuronal death by increasing mitochondrial autophagy. The Journal of biological chemistry 286:10814-10824.
Chu Y, Kordower JH (2007) Age-associated increases of alpha-synuclein in monkeys and humans are associated with nigrostriatal dopamine depletion: Is this the target for Parkinson's disease? Neurobiol Dis 25:134-149.

Chung CY, Koprich JB, Siddiqi H, Isacson O (2009) Dynamic changes in presynaptic and axonal transport proteins combined with striatal neuroinflammation precede dopaminergic neuronal loss in a rat model of AAV alpha-synucleinopathy. J Neurosci 29:3365-3373.

Cliburn RA, Dunn AR, Stout KA, Hoffman CA, Lohr KM, Bernstein AI, Winokur EJ, Burkett J, Shmitz Y, Caudle WM, Miller GW (2016) Immunochemical localization of vesicular monoamine transporter 2 (VMAT2) in mouse brain. J Chem Neuroanat.

Conway KA, Harper JD, Lansbury PT (1998) Accelerated in vitro fibril formation by a mutant alpha-synuclein linked to early-onset Parkinson disease. Nature medicine 4:1318-1320.

Cookson MR (2010) The role of leucine-rich repeat kinase 2 (LRRK2) in Parkinson's disease. Nature reviews Neuroscience 11:791-797.

Cookson MR, Bandmann O (2010) Parkinson's disease: insights from pathways. Human molecular genetics 19:R21-27.

Cooper AA, Gitler AD, Cashikar A, Haynes CM, Hill KJ, Bhullar B, Liu K, Xu K, Strathearn KE, Liu F, Cao S, Caldwell KA, Caldwell GA, Marsischky G, Kolodner RD, Labaer J, Rochet JC, Bonini NM, Lindquist S (2006) Alpha-synuclein blocks ER-Golgi traffic and Rab1 rescues neuron loss in Parkinson's models. Science 313:324-328.

Cooper O, Seo H, Andrabi S, Guardia-Laguarta C, Graziotto J, Sundberg M, McLean JR, Carrillo-Reid L, Xie Z, Osborn T, Hargus G, Deleidi M, Lawson T, Bogetofte H, Perez-Torres E, Clark L, Moskowitz C, Mazzulli J, Chen L, Volpicelli-Daley L, Romero N, Jiang H, Uitti RJ, Huang Z, Opala G, Scarffe LA, Dawson VL, Klein C, Feng J, Ross OA, Trojanowski JQ, Lee VM, Marder K, Surmeier DJ, Wszolek ZK, Przedborski S, Krainc D, Dawson TM, Isacson O (2012) Pharmacological rescue of mitochondrial deficits in iPSC-derived neural cells from patients with familial Parkinson's disease. Sci Transl Med 4:141ra190.

Coskuner O, Wise-Scira O (2013) Structures and free energy landscapes of the A53T mutant-type alpha-synuclein protein and impact of A53T mutation on the structures of the wild-type alpha-synuclein protein with dynamics. ACS chemical neuroscience 4:1101-1113.

Cremades N, Cohen SI, Deas E, Abramov AY, Chen AY, Orte A, Sandal M, Clarke RW, Dunne P, Aprile FA, Bertoncini CW, Wood NW, Knowles TP, Dobson CM, Klenerman D (2012) Direct observation of the interconversion of normal and toxic forms of alpha-synuclein. Cell 149:1048-1059.

Cuervo AM, Stefanis L, Fredenburg R, Lansbury PT, Sulzer D (2004) Impaired degradation of mutant alpha-synuclein by chaperone-mediated autophagy. Science 305:1292-1295.

Daher JP, Abdelmotilib HA, Hu X, Volpicelli-Daley LA, Moehle MS, Fraser KB, Needle E, Chen Y, Steyn SJ, Galatsis P, Hirst WD, West AB (2015) Leucine-rich Repeat Kinase 2 (LRRK2) Pharmacological Inhibition Abates alpha-Synuclein Gene-induced Neurodegeneration. The Journal of biological chemistry 290:19433-19444.

Daniele SG, Beraud D, Davenport C, Cheng K, Yin H, Maguire-Zeiss KA (2015) Activation of MyD88-dependent TLR1/2 signaling by misfolded alpha-synuclein, a protein linked to neurodegenerative disorders. Science signaling 8:ra45.

Deng H, Wang P, Jankovic J (2018) The genetics of Parkinson disease. Ageing Res Rev 42:72-85.

Deng J, Lewis PA, Greggio E, Sluch E, Beilina A, Cookson MR (2008) Structure of the ROC domain from the Parkinson's disease-associated leucine-rich repeat kinase 2 reveals a dimeric GTPase. Proceedings of the National Academy of Sciences of the United States of America 105:1499-1504.

Deng X, Choi HG, Buhrlage SJ, Gray NS (2012) Leucine-rich repeat kinase 2 inhibitors: a patent review (2006 - 2011). Expert Opin Ther Pat 22:1415-1426.

Deng X, Dzamko N, Prescott A, Davies P, Liu Q, Yang Q, Lee JD, Patricelli MP, Nomanbhoy TK, Alessi DR, Gray NS (2011) Characterization of a selective inhibitor of the Parkinson's disease kinase LRRK2. Nature chemical biology 7:203-205.

Deng X, Elkins JM, Zhang J, Yang Q, Erazo T, Gomez N, Choi HG, Wang J, Dzamko N, Lee JD, Sim T, Kim N, Alessi DR, Lizcano JM, Knapp S, Gray NS (2013) Structural determinants for ERK5

(MAPK7) and leucine rich repeat kinase 2 activities of benzo[e]pyrimido-[5,4-b]diazepine-6(11H)-ones. Eur J Med Chem 70:758-767.

Devi L, Raghavendran V, Prabhu BM, Avadhani NG, Anandatheerthavarada HK (2008) Mitochondrial import and accumulation of alpha-synuclein impair complex I in human dopaminergic neuronal cultures and Parkinson disease brain. The Journal of biological chemistry 283:9089-9100.

Di Maio R, Barrett PJ, Hoffman EK, Barrett CW, Zharikov A, Borah A, Hu X, McCoy J, Chu CT, Burton EA, Hastings TG, Greenamyre JT (2016) alpha-Synuclein binds to TOM20 and inhibits mitochondrial protein import in Parkinson's disease. Science translational medicine 8:342ra378.

Dinter E, Saridaki T, Nippold M, Plum S, Diederichs L, Komnig D, Fensky L, May C, Marcus K, Voigt A, Schulz JB, Falkenburger BH (2016) Rab7 induces clearance of alpha-synuclein aggregates. Journal of neurochemistry 138:758-774.

Dodson MW, Zhang T, Jiang C, Chen S, Guo M (2012) Roles of the Drosophila LRRK2 homolog in Rab7-dependent lysosomal positioning. Human molecular genetics 21:1350-1363.

Dufty BM, Warner LR, Hou ST, Jiang SX, Gomez-Isla T, Leenhouts KM, Oxford JT, Feany MB, Masliah E, Rohn TT (2007) Calpain-cleavage of alpha-synuclein: connecting proteolytic processing to disease-linked aggregation. The American journal of pathology 170:1725-1738.

Dzamko N, Deak M, Hentati F, Reith AD, Prescott AR, Alessi DR, Nichols RJ (2010) Inhibition of LRRK2 kinase activity leads to dephosphorylation of Ser(910)/Ser(935), disruption of 14-3-3 binding and altered cytoplasmic localization. Biochem J 430:405-413.

Dzamko N, Halliday GM (2012) An emerging role for LRRK2 in the immune system. Biochemical Society transactions 40:1134-1139.

Endicott JA, Noble ME, Johnson LN (2012) The structural basis for control of eukaryotic protein kinases. Annual review of biochemistry 81:587-613.

Esteves AR, Swerdlow RH, Cardoso SM (2014) LRRK2, a puzzling protein: insights into Parkinson's disease pathogenesis. Experimental neurology 261:206-216.

Fares MB, Ait-Bouziad N, Dikiy I, Mbefo MK, Jovicic A, Kiely A, Holton JL, Lee SJ, Gitler AD, Eliezer D, Lashuel HA (2014) The novel Parkinson's disease linked mutation G51D attenuates in vitro aggregation and membrane binding of alpha-synuclein, and enhances its secretion and nuclear localization in cells. Human molecular genetics 23:4491-4509.

Fava VM, Manry J, Cobat A, Orlova M, Van Thuc N, Ba NN, Thai VH, Abel L, Alcais A, Schurr E, Canadian Lrrk2 in Inflammation T (2016) A Missense LRRK2 Variant Is a Risk Factor for Excessive Inflammatory Responses in Leprosy. PLoS neglected tropical diseases 10:e0004412.

Fell MJ, Mirescu C, Basu K, Cheewatrakoolpong B, DeMong DE, Ellis JM, Hyde LA, Lin Y, Markgraf CG, Mei H, Miller M, Poulet FM, Scott JD, Smith MD, Yin Z, Zhou X, Parker EM, Kennedy ME, Morrow JA (2015) MLi-2, a Potent, Selective, and Centrally Active Compound for Exploring the Therapeutic Potential and Safety of LRRK2 Kinase Inhibition. J Pharmacol Exp Ther 355:397-409.

Flagmeier P, Meisl G, Vendruscolo M, Knowles TP, Dobson CM, Buell AK, Galvagnion C (2016) Mutations associated with familial Parkinson's disease alter the initiation and amplification steps of alpha-synuclein aggregation. Proceedings of the National Academy of Sciences of the United States of America 113:10328-10333.

Follmer C, Coelho-Cerqueira E, Yatabe-Franco DY, Araujo GD, Pinheiro AS, Domont GB, Eliezer D (2015) Oligomerization and Membrane-binding Properties of Covalent Adducts Formed by the Interaction of alpha-Synuclein with the Toxic Dopamine Metabolite 3,4-Dihydroxyphenylacetaldehyde (DOPAL). J Biol Chem 290:27660-27679.

Fountaine TM, Wade-Martins R (2007) RNA interference-mediated knockdown of alpha-synuclein protects human dopaminergic neuroblastoma cells from MPP(+) toxicity and reduces dopamine transport. Journal of neuroscience research 85:351-363.

Friedman LG, Lachenmayer ML, Wang J, He L, Poulose SM, Komatsu M, Holstein GR, Yue Z (2012) Disrupted autophagy leads to dopaminergic axon and dendrite degeneration and promotes presynaptic accumulation of alpha-synuclein and LRRK2 in the brain. The Journal of neuroscience : the official journal of the Society for Neuroscience 32:7585-7593.

Fu H, Subramanian RR, Masters SC (2000) 14-3-3 proteins: structure, function, and regulation. Annu Rev Pharmacol Toxicol 40:617-647.

Fuji RN, Flagella M, Baca M, Baptista MA, Brodbeck J, Chan BK, Fiske BK, Honigberg L, Jubb AM, Katavolos P, Lee DW, Lewin-Koh SC, Lin T, Liu X, Liu S, Lyssikatos JP, O'Mahony J, Reichelt M, Roose-Girma M, Sheng Z, Sherer T, Smith A, Solon M, Sweeney ZK, Tarrant J, Urkowitz A, Warming S, Yaylaoglu M, Zhang S, Zhu H, Estrada AA, Watts RJ (2015) Effect of selective LRRK2 kinase inhibition on nonhuman primate lung. Science translational medicine 7:273ra215.

Fujiwara H, Hasegawa M, Dohmae N, Kawashima A, Masliah E, Goldberg MS, Shen J, Takio K, Iwatsubo T (2002) alpha-Synuclein is phosphorylated in synucleinopathy lesions. Nature cell biology 4:160-164.

Funayama M, Hasegawa K, Kowa H, Saito M, Tsuji S, Obata F (2002) A new locus for Parkinson's disease (PARK8) maps to chromosome 12p11.2-q13.1. Annals of neurology 51:296-301.

Funayama M, Hasegawa K, Ohta E, Kawashima N, Komiyama M, Kowa H, Tsuji S, Obata F (2005) An LRRK2 mutation as a cause for the parkinsonism in the original PARK8 family. Annals of neurology 57:918-921.

Gardet A, Benita Y, Li C, Sands BE, Ballester I, Stevens C, Korzenik JR, Rioux JD, Daly MJ, Xavier RJ, Podolsky DK (2010) LRRK2 is involved in the IFN-gamma response and host response to pathogens. Journal of immunology 185:5577-5585.

Gasser T (2009) Molecular pathogenesis of Parkinson disease: insights from genetic studies. Expert reviews in molecular medicine 11:e22.

Ghosh D, Sahay S, Ranjan P, Salot S, Mohite GM, Singh PK, Dwivedi S, Carvalho E, Banerjee R, Kumar A, Maji SK (2014) The newly discovered Parkinson's disease associated Finnish mutation (A53E) attenuates alpha-synuclein aggregation and membrane binding. Biochemistry 53:6419-6421.

Giaime E, Tong Y, Wagner LK, Yuan Y, Huang G, Shen J (2017) Age-Dependent Dopaminergic Neurodegeneration and Impairment of the Autophagy-Lysosomal Pathway in LRRK-Deficient Mice. Neuron 96:796-807 e796.

Giasson BI, Lee VM (2003) Are ubiquitination pathways central to Parkinson's disease? Cell 114:1-8.

Gillardon F (2009) Leucine-rich repeat kinase 2 phosphorylates brain tubulin-beta isoforms and modulates microtubule stability--a point of convergence in parkinsonian neurodegeneration? Journal of neurochemistry 110:1514-1522.

Gillardon F, Schmid R, Draheim H (2012) Parkinson's disease-linked leucine-rich repeat kinase 2(R1441G) mutation increases proinflammatory cytokine release from activated primary microglial cells and resultant neurotoxicity. Neuroscience 208:41-48.

Gilsbach BK, Ho FY, Vetter IR, van Haastert PJ, Wittinghofer A, Kortholt A (2012) Roco kinase structures give insights into the mechanism of Parkinson disease-related leucine-rich-repeat kinase 2 mutations. Proceedings of the National Academy of Sciences of the United States of America 109:10322-10327.

Golbe LI, Di Iorio G, Bonavita V, Miller DC, Duvoisin RC (1990) A large kindred with autosomal dominant Parkinson's disease. Annals of neurology 27:276-282.

Goldstein DS, Sullivan P, Cooney A, Jinsmaa Y, Sullivan R, Gross DJ, Holmes C, Kopin IJ, Sharabi Y (2012) Vesicular uptake blockade generates the toxic dopamine metabolite 3,4-dihydroxyphenylacetaldehyde in PC12 cells: relevance to the pathogenesis of Parkinson's disease. J Neurochem 123:932-943.

Gomez-Suaga P, Luzon-Toro B, Churamani D, Zhang L, Bloor-Young D, Patel S, Woodman PG, Churchill GC, Hilfiker S (2012) Leucine-rich repeat kinase 2 regulates autophagy through a calcium-dependent pathway involving NAADP. Human molecular genetics 21:511-525.

Gotthardt K, Weyand M, Kortholt A, Van Haastert PJ, Wittinghofer A (2008) Structure of the Roc-COR domain tandem of C. tepidum, a prokaryotic homologue of the human LRRK2 Parkinson kinase. The EMBO journal 27:2239-2249.

Greggio E, Jain S, Kingsbury A, Bandopadhyay R, Lewis P, Kaganovich A, van der Brug MP, Beilina A, Blackinton J, Thomas KJ, Ahmad R, Miller DW, Kesavapany S, Singleton A, Lees A, Harvey RJ, Harvey K, Cookson MR (2006) Kinase activity is required for the toxic effects of mutant LRRK2/dardarin. Neurobiology of disease 23:329-341.

Greggio E, Zambrano I, Kaganovich A, Beilina A, Taymans JM, Daniels V, Lewis P, Jain S, Ding J, Syed A, Thomas KJ, Baekelandt V, Cookson MR (2008) The Parkinson disease-associated leucine-rich repeat kinase 2 (LRRK2) is a dimer that undergoes intramolecular autophosphorylation. The Journal of biological chemistry 283:16906-16914.

Guardia-Laguarta C, Area-Gomez E, Rub C, Liu Y, Magrane J, Becker D, Voos W, Schon EA, Przedborski S (2014) alpha-Synuclein is localized to mitochondria-associated ER membranes. The Journal of neuroscience : the official journal of the Society for Neuroscience 34:249-259.

Gustot A, Gallea JI, Sarroukh R, Celej MS, Ruysschaert JM, Raussens V (2015) Amyloid fibrils are the molecular trigger of inflammation in Parkinson's disease. The Biochemical journal 471:323-333.

Habig K, Gellhaar S, Heim B, Djuric V, Giesert F, Wurst W, Walter C, Hentrich T, Riess O, Bonin M (2013) LRRK2 guides the actin cytoskeleton at growth cones together with ARHGEF7 and Tropomyosin 4. Biochimica et biophysica acta 1832:2352-2367.

Hara S, Arawaka S, Sato H, Machiya Y, Cui C, Sasaki A, Koyama S, Kato T (2013) Serine 129 phosphorylation of membrane-associated alpha-synuclein modulates dopamine transporter function in a G protein-coupled receptor kinase-dependent manner. Molecular biology of the cell 24:1649-1660, S1641-1643.

Hatcher JM, Choi HG, Alessi DR, Gray NS (2017) Small-Molecule Inhibitors of LRRK2. Advances in neurobiology 14:241-264.

Healy DG, Falchi M, O'Sullivan SS, Bonifati V, Durr A, Bressman S, Brice A, Aasly J, Zabetian CP, Goldwurm S, Ferreira JJ, Tolosa E, Kay DM, Klein C, Williams DR, Marras C, Lang AE, Wszolek ZK, Berciano J, Schapira AH, Lynch T, Bhatia KP, Gasser T, Lees AJ, Wood NW, International LC (2008) Phenotype, genotype, and worldwide genetic penetrance of LRRK2-associated Parkinson's disease: a case-control study. Lancet Neurol 7:583-590.

Henderson JL, Kormos BL, Hayward MM, Coffman KJ, Jasti J, Kurumbail RG, Wager TT, Verhoest PR, Noell GS, Chen Y, Needle E, Berger Z, Steyn SJ, Houle C, Hirst WD, Galatsis P (2015) Discovery and preclinical profiling of 3-[4-(morpholin-4-yl)-7H-pyrrolo[2,3-d]pyrimidin-5-yl]benzonitrile (PF-06447475), a highly potent, selective, brain penetrant, and in vivo active LRRK2 kinase inhibitor. Journal of medicinal chemistry 58:419-432.

Henry AG, Aghamohammadzadeh S, Samaroo H, Chen Y, Mou K, Needle E, Hirst WD (2015) Pathogenic LRRK2 mutations, through increased kinase activity, produce enlarged lysosomes with reduced degradative capacity and increase ATP13A2 expression. Human molecular genetics 24:6013-6028.

Herzig MC, Kolly C, Persohn E, Theil D, Schweizer T, Hafner T, Stemmelen C, Troxler TJ, Schmid P, Danner S, Schnell CR, Mueller M, Kinzel B, Grevot A, Bolognani F, Stirn M, Kuhn RR, Kaupmann K, van der Putten PH, Rovelli G, Shimshek DR (2011) LRRK2 protein levels are determined by kinase function and are crucial for kidney and lung homeostasis in mice. Hum Mol Genet 20:4209-4223.

Hirai Y, Fujita SC, Iwatsubo T, Hasegawa M (2004) Phosphorylated alpha-synuclein in normal mouse brain. FEBS letters 572:227-232.

Ho CC, Rideout HJ, Ribe E, Troy CM, Dauer WT (2009) The Parkinson disease protein leucine-rich repeat kinase 2 transduces death signals via Fas-associated protein with death domain and caspase-8 in a cellular model of neurodegeneration. The Journal of neuroscience : the official journal of the Society for Neuroscience 29:1011-1016.

Hoenen C, Gustin A, Birck C, Kirchmeyer M, Beaume N, Felten P, Grandbarbe L, Heuschling P, Heurtaux T (2016) Alpha-Synuclein Proteins Promote Pro-Inflammatory Cascades in Microglia: Stronger Effects of the A53T Mutant. PloS one 11:e0162717.

Hogan KA, Staal RG, Sonsalla PK (2000) Analysis of VMAT2 binding after methamphetamine or MPTP treatment: disparity between homogenates and vesicle preparations. J Neurochem 74:2217-2220.

Hunot S, Dugas N, Faucheux B, Hartmann A, Tardieu M, Debre P, Agid Y, Dugas B, Hirsch EC (1999) FcepsilonRII/CD23 is expressed in Parkinson's disease and induces, in vitro, production of nitric oxide and tumor necrosis factor-alpha in glial cells. The Journal of neuroscience : the official journal of the Society for Neuroscience 19:3440-3447.

Hyun CH, Yoon CY, Lee HJ, Lee SJ (2013) LRRK2 as a Potential Genetic Modifier of Synucleinopathies: Interlacing the Two Major Genetic Factors of Parkinson's Disease. Experimental neurobiology 22:249-257.

Iaccarino C, Crosio C, Vitale C, Sanna G, Carri MT, Barone P (2007) Apoptotic mechanisms in mutant LRRK2-mediated cell death. Human molecular genetics 16:1319-1326.

Imai Y, Gehrke S, Wang HQ, Takahashi R, Hasegawa K, Oota E, Lu B (2008) Phosphorylation of 4E-BP by LRRK2 affects the maintenance of dopaminergic neurons in Drosophila. The EMBO journal 27:2432-2443.

Inoshita T, Arano T, Hosaka Y, Meng H, Umezaki Y, Kosugi S, Morimoto T, Koike M, Chang HY, Imai Y, Hattori N (2017) Vps35 in cooperation with LRRK2 regulates synaptic vesicle endocytosis through the endosomal pathway in Drosophila. Human molecular genetics 26:2933-2948.

Ip CW, Klaus LC, Karikari AA, Visanji NP, Brotchie JM, Lang AE, Volkmann J, Koprich JB (2017) AAV1/2-induced overexpression of A53T-alpha-synuclein in the substantia nigra results in degeneration of the nigrostriatal system with Lewy-like pathology and motor impairment: a new mouse model for Parkinson's disease. Acta neuropathologica communications 5:11.

Iwata A, Maruyama M, Akagi T, Hashikawa T, Kanazawa I, Tsuji S, Nukina N (2003) Alpha-synuclein degradation by serine protease neurosin: implication for pathogenesis of synucleinopathies. Human molecular genetics 12:2625-2635.

Jaleel M, Nichols RJ, Deak M, Campbell DG, Gillardon F, Knebel A, Alessi DR (2007) LRRK2 phosphorylates moesin at threonine-558: characterization of how Parkinson's disease mutants affect kinase activity. The Biochemical journal 405:307-317.

Joers V, Tansey MG, Mulas G, Carta AR (2017) Microglial phenotypes in Parkinson's disease and animal models of the disease. Progress in neurobiology 155:57-75.

Johnson ME, Stecher B, Labrie V, Brundin L, Brundin P (2018) Triggers, Facilitators, and Aggravators: Redefining Parkinson's Disease Pathogenesis. Trends in neurosciences.

Johnson SJ, Wade-Martins R (2011) A BACwards glance at neurodegeneration: molecular insights into disease from LRRK2, SNCA and MAPT BAC-transgenic mice. Biochemical Society transactions 39:862-867.

Jones DH, Ley S, Aitken A (1995) Isoforms of 14-3-3 protein can form homo- and heterodimers in vivo and in vitro: implications for function as adapter proteins. FEBS letters 368:55-58.

Jorgensen ND, Peng Y, Ho CC, Rideout HJ, Petrey D, Liu P, Dauer WT (2009) The WD40 domain is required for LRRK2 neurotoxicity. PloS one 4:e8463.

Kanao T, Venderova K, Park DS, Unterman T, Lu B, Imai Y (2010) Activation of FoxO by LRRK2 induces expression of proapoptotic proteins and alters survival of postmitotic dopaminergic neuron in Drosophila. Human molecular genetics 19:3747-3758.

Karuppagounder SS, Xiong Y, Lee Y, Lawless MC, Kim D, Nordquist E, Martin I, Ge P, Brahmachari S, Jhaldiyal A, Kumar M, Andrabi SA, Dawson TM, Dawson VL (2016) LRRK2 G2019S

transgenic mice display increased susceptibility to 1-methyl-4-phenyl-1,2,3,6-tetrahydropyridine (MPTP)-mediated neurotoxicity. J Chem Neuroanat.
Kawai T, Akira S (2011) Toll-like receptors and their crosstalk with other innate receptors in infection and immunity. Immunity 34:637-650.
Kestenbaum M, Alcalay RN (2017) Clinical Features of LRRK2 Carriers with Parkinson's Disease. Advances in neurobiology 14:31-48.
Kett LR, Dauer WT (2012) Leucine-rich repeat kinase 2 for beginners: six key questions. Cold Spring Harbor perspectives in medicine 2:a009407.
Kim B, Yang MS, Choi D, Kim JH, Kim HS, Seol W, Choi S, Jou I, Kim EY, Joe EH (2012) Impaired inflammatory responses in murine Lrrk2-knockdown brain microglia. PLoS One 7:e34693.
Kim KS, Marcogliese PC, Yang J, Callaghan SM, Resende V, Abdel-Messih E, Marras C, Visanji NP, Huang J, Schlossmacher MG, Trinkle-Mulcahy L, Slack RS, Lang AE, Canadian Lrrk2 in Inflammation T, Park DS (2018) Regulation of myeloid cell phagocytosis by LRRK2 via WAVE2 complex stabilization is altered in Parkinson's disease. Proc Natl Acad Sci U S A 115:E5164-E5173.
Kim TD, Choi E, Rhim H, Paik SR, Yang CH (2004) Alpha-synuclein has structural and functional similarities to small heat shock proteins. Biochemical and biophysical research communications 324:1352-1359.
Kitada T, Asakawa S, Hattori N, Matsumine H, Yamamura Y, Minoshima S, Yokochi M, Mizuno Y, Shimizu N (1998) Mutations in the parkin gene cause autosomal recessive juvenile parkinsonism. Nature 392:605-608.
Kondo K, Obitsu S, Teshima R (2011) alpha-Synuclein aggregation and transmission are enhanced by leucine-rich repeat kinase 2 in human neuroblastoma SH-SY5Y cells. Biological & pharmaceutical bulletin 34:1078-1083.
Kordower JH, Chu Y, Hauser RA, Freeman TB, Olanow CW (2008) Lewy body-like pathology in long-term embryonic nigral transplants in Parkinson's disease. Nature medicine 14:504-506.
Kornev AP, Haste NM, Taylor SS, Eyck LF (2006) Surface comparison of active and inactive protein kinases identifies a conserved activation mechanism. Proceedings of the National Academy of Sciences of the United States of America 103:17783-17788.
Kozina E, Sadasivan S, Jiao Y, Dou Y, Ma Z, Tan H, Kodali K, Shaw T, Peng J, Smeyne RJ (2018) Mutant LRRK2 mediates peripheral and central immune responses leading to neurodegeneration in vivo. Brain : a journal of neurology 141:1753-1769.
Kritzinger A, Ferger B, Gillardon F, Stierstorfer B, Birk G, Kochanek S, Ciossek T (2018) Age-related pathology after adenoviral overexpression of the leucine-rich repeat kinase 2 in the mouse striatum. Neurobiol Aging 66:97-111.
Kruger R, Kuhn W, Muller T, Woitalla D, Graeber M, Kosel S, Przuntek H, Epplen JT, Schols L, Riess O (1998) Ala30Pro mutation in the gene encoding alpha-synuclein in Parkinson's disease. Nature genetics 18:106-108.
Kumar A, Cookson MR (2011) Role of LRRK2 kinase dysfunction in Parkinson disease. Expert reviews in molecular medicine 13:e20.
Lai Y, Kim S, Varkey J, Lou X, Song JK, Diao J, Langen R, Shin YK (2014) Nonaggregated alpha-synuclein influences SNARE-dependent vesicle docking via membrane binding. Biochemistry 53:3889-3896.
Larsen JO, Gundersen HJ, Nielsen J (1998) Global spatial sampling with isotropic virtual planes: estimators of length density and total length in thick, arbitrarily orientated sections. Journal of microscopy 191:238-248.
Larsen KE, Schmitz Y, Troyer MD, Mosharov E, Dietrich P, Quazi AZ, Savalle M, Nemani V, Chaudhry FA, Edwards RH, Stefanis L, Sulzer D (2006) Alpha-synuclein overexpression in PC12 and chromaffin cells impairs catecholamine release by interfering with a late step in exocytosis. The Journal of neuroscience : the official journal of the Society for Neuroscience 26:11915-11922.

Lashuel HA, Petre BM, Wall J, Simon M, Nowak RJ, Walz T, Lansbury PT, Jr. (2002) Alpha-synuclein, especially the Parkinson's disease-associated mutants, forms pore-like annular and tubular protofibrils. Journal of molecular biology 322:1089-1102.

Lauwers E, Debyser Z, Van Dorpe J, De Strooper B, Nuttin B, Baekelandt V (2003) Neuropathology and neurodegeneration in rodent brain induced by lentiviral vector-mediated overexpression of alpha-synuclein. Brain Pathol 13:364-372.

Lee FJ, Liu F, Pristupa ZB, Niznik HB (2001) Direct binding and functional coupling of alpha-synuclein to the dopamine transporters accelerate dopamine-induced apoptosis. FASEB journal : official publication of the Federation of American Societies for Experimental Biology 15:916-926.

Lee HJ, Khoshaghideh F, Patel S, Lee SJ (2004) Clearance of alpha-synuclein oligomeric intermediates via the lysosomal degradation pathway. J Neurosci 24:1888-1896.

Lee HJ, Suk JE, Bae EJ, Lee SJ (2008) Clearance and deposition of extracellular alpha-synuclein aggregates in microglia. Biochemical and biophysical research communications 372:423-428.

Lee HJ, Suk JE, Patrick C, Bae EJ, Cho JH, Rho S, Hwang D, Masliah E, Lee SJ (2010a) Direct transfer of alpha-synuclein from neuron to astroglia causes inflammatory responses in synucleinopathies. The Journal of biological chemistry 285:9262-9272.

Lee JW, Tapias V, Di Maio R, Greenamyre JT, Cannon JR (2015) Behavioral, neurochemical, and pathologic alterations in bacterial artificial chromosome transgenic G2019S leucine-rich repeated kinase 2 rats. Neurobiol Aging 36:505-518.

Lee S, Liu HP, Lin WY, Guo H, Lu B (2010b) LRRK2 kinase regulates synaptic morphology through distinct substrates at the presynaptic and postsynaptic compartments of the Drosophila neuromuscular junction. The Journal of neuroscience : the official journal of the Society for Neuroscience 30:16959-16969.

Lesage S, Anheim M, Letournel F, Bousset L, Honore A, Rozas N, Pieri L, Madiona K, Durr A, Melki R, Verny C, Brice A, French Parkinson's Disease Genetics Study G (2013) G51D alpha-synuclein mutation causes a novel parkinsonian-pyramidal syndrome. Annals of neurology 73:459-471.

Levin J, Giese A, Boetzel K, Israel L, Hogen T, Nubling G, Kretzschmar H, Lorenzl S (2009) Increased alpha-synuclein aggregation following limited cleavage by certain matrix metalloproteinases. Experimental neurology 215:201-208.

Li J, Uversky VN, Fink AL (2001) Effect of familial Parkinson's disease point mutations A30P and A53T on the structural properties, aggregation, and fibrillation of human alpha-synuclein. Biochemistry 40:11604-11613.

Li W, West N, Colla E, Pletnikova O, Troncoso JC, Marsh L, Dawson TM, Jakala P, Hartmann T, Price DL, Lee MK (2005) Aggregation promoting C-terminal truncation of alpha-synuclein is a normal cellular process and is enhanced by the familial Parkinson's disease-linked mutations. Proceedings of the National Academy of Sciences of the United States of America 102:2162-2167.

Li X, Patel JC, Wang J, Avshalumov MV, Nicholson C, Buxbaum JD, Elder GA, Rice ME, Yue Z (2010a) Enhanced striatal dopamine transmission and motor performance with LRRK2 overexpression in mice is eliminated by familial Parkinson's disease mutation G2019S. J Neurosci 30:1788-1797.

Li X, Wang QJ, Pan N, Lee S, Zhao Y, Chait BT, Yue Z (2011) Phosphorylation-dependent 14-3-3 binding to LRRK2 is impaired by common mutations of familial Parkinson's disease. PloS one 6:e17153.

Li Y, Cheng SY, Chen N, Reith ME (2010b) Interrelation of dopamine transporter oligomerization and surface presence as studied with mutant transporter proteins and amphetamine. J Neurochem 114:873-885.

Li Y, Liu W, Oo TF, Wang L, Tang Y, Jackson-Lewis V, Zhou C, Geghman K, Bogdanov M, Przedborski S, Beal MF, Burke RE, Li C (2009) Mutant LRRK2(R1441G) BAC transgenic mice recapitulate cardinal features of Parkinson's disease. Nat Neurosci 12:826-828.

Liao J, Wu CX, Burlak C, Zhang S, Sahm H, Wang M, Zhang ZY, Vogel KW, Federici M, Riddle SM, Nichols RJ, Liu D, Cookson MR, Stone TA, Hoang QQ (2014) Parkinson disease-associated mutation R1441H in LRRK2 prolongs the "active state" of its GTPase domain. Proceedings of the National Academy of Sciences of the United States of America 111:4055-4060.

Liberatore GT, Jackson-Lewis V, Vukosavic S, Mandir AS, Vila M, McAuliffe WG, Dawson VL, Dawson TM, Przedborski S (1999) Inducible nitric oxide synthase stimulates dopaminergic neurodegeneration in the MPTP model of Parkinson disease. Nature medicine 5:1403-1409.

Lin X, Parisiadou L, Gu XL, Wang L, Shim H, Sun L, Xie C, Long CX, Yang WJ, Ding J, Chen ZZ, Gallant PE, Tao-Cheng JH, Rudow G, Troncoso JC, Liu Z, Li Z, Cai H (2009) Leucine-rich repeat kinase 2 regulates the progression of neuropathology induced by Parkinson's-disease-related mutant alpha-synuclein. Neuron 64:807-827.

Linhart R, Wong SA, Cao J, Tran M, Huynh A, Ardrey C, Park JM, Hsu C, Taha S, Peterson R, Shea S, Kurian J, Venderova K (2014) Vacuolar protein sorting 35 (Vps35) rescues locomotor deficits and shortened lifespan in Drosophila expressing a Parkinson's disease mutant of Leucine-Rich Repeat Kinase 2 (LRRK2). Molecular neurodegeneration 9:23.

Litteljohn D, Rudyk C, Dwyer Z, Farmer K, Fortin T, Hayley S, Canadian Lrrk2 in Inflammation T (2018) The impact of murine LRRK2 G2019S transgene overexpression on acute responses to inflammatory challenge. Brain, behavior, and immunity 67:246-256.

Liu G, Sgobio C, Gu X, Sun L, Lin X, Yu J, Parisiadou L, Xie C, Sastry N, Ding J, Lohr KM, Miller GW, Mateo Y, Lovinger DM, Cai H (2015) Selective expression of Parkinson's disease-related Leucine-rich repeat kinase 2 G2019S missense mutation in midbrain dopaminergic neurons impairs dopamine release and dopaminergic gene expression. Hum Mol Genet 24:5299-5312.

Liu LL, Franz KJ (2007) Phosphorylation-dependent metal binding by alpha-synuclein peptide fragments. Journal of biological inorganic chemistry : JBIC : a publication of the Society of Biological Inorganic Chemistry 12:234-247.

Lobbestael E, Baekelandt V, Taymans JM (2012) Phosphorylation of LRRK2: from kinase to substrate. Biochemical Society transactions 40:1102-1110.

Lohr KM, Bernstein AI, Stout KA, Dunn AR, Lazo CR, Alter SP, Wang M, Li Y, Fan X, Hess EJ, Yi H, Vecchio LM, Goldstein DS, Guillot TS, Salahpour A, Miller GW (2014) Increased vesicular monoamine transporter enhances dopamine release and opposes Parkinson disease-related neurodegeneration in vivo. Proc Natl Acad Sci U S A 111:9977-9982.

Longo F, Russo I, Shimshek DR, Greggio E, Morari M (2014) Genetic and pharmacological evidence that G2019S LRRK2 confers a hyperkinetic phenotype, resistant to motor decline associated with aging. Neurobiol Dis 71:62-73.

Low K, Aebischer P (2012) Use of viral vectors to create animal models for Parkinson's disease. Neurobiol Dis 48:189-201.

Luk KC, Kehm VM, Zhang B, O'Brien P, Trojanowski JQ, Lee VM (2012) Intracerebral inoculation of pathological alpha-synuclein initiates a rapidly progressive neurodegenerative alpha-synucleinopathy in mice. The Journal of experimental medicine 209:975-986.

Luk KC, Song C, O'Brien P, Stieber A, Branch JR, Brunden KR, Trojanowski JQ, Lee VM (2009) Exogenous alpha-synuclein fibrils seed the formation of Lewy body-like intracellular inclusions in cultured cells. Proceedings of the National Academy of Sciences of the United States of America 106:20051-20056.

Lundblad M, Decressac M, Mattsson B, Bjorklund A (2012) Impaired neurotransmission caused by overexpression of alpha-synuclein in nigral dopamine neurons. Proceedings of the National Academy of Sciences of the United States of America 109:3213-3219.

Mabrouk OS, Marti M, Morari M (2010) Endogenous nociceptin/orphanin FQ (N/OFQ) contributes to haloperidol-induced changes of nigral amino acid transmission and parkinsonism: a combined microdialysis and behavioral study in naive and nociceptin/orphanin FQ receptor knockout mice. Neuroscience 166:40-48.

Machiya Y, Hara S, Arawaka S, Fukushima S, Sato H, Sakamoto M, Koyama S, Kato T (2010) Phosphorylated alpha-synuclein at Ser-129 is targeted to the proteasome pathway in a ubiquitin-independent manner. The Journal of biological chemistry 285:40732-40744.

Mackintosh C (2004) Dynamic interactions between 14-3-3 proteins and phosphoproteins regulate diverse cellular processes. The Biochemical journal 381:329-342.

MacLeod D, Dowman J, Hammond R, Leete T, Inoue K, Abeliovich A (2006) The familial Parkinsonism gene LRRK2 regulates neurite process morphology. Neuron 52:587-593.

MacLeod DA, Rhinn H, Kuwahara T, Zolin A, Di Paolo G, McCabe BD, Marder KS, Honig LS, Clark LN, Small SA, Abeliovich A (2013) RAB7L1 interacts with LRRK2 to modify intraneuronal protein sorting and Parkinson's disease risk. Neuron 77:425-439.

Mamais A, Chia R, Beilina A, Hauser DN, Hall C, Lewis PA, Cookson MR, Bandopadhyay R (2014) Arsenite stress down-regulates phosphorylation and 14-3-3 binding of leucine-rich repeat kinase 2 (LRRK2), promoting self-association and cellular redistribution. The Journal of biological chemistry 289:21386-21400.

Mao X, Ou MT, Karuppagounder SS, Kam TI, Yin X, Xiong Y, Ge P, Umanah GE, Brahmachari S, Shin JH, Kang HC, Zhang J, Xu J, Chen R, Park H, Andrabi SA, Kang SU, Goncalves RA, Liang Y, Zhang S, Qi C, Lam S, Keiler JA, Tyson J, Kim D, Panicker N, Yun SP, Workman CJ, Vignali DA, Dawson VL, Ko HS, Dawson TM (2016) Pathological alpha-synuclein transmission initiated by binding lymphocyte-activation gene 3. Science 353.

Maroteaux L, Campanelli JT, Scheller RH (1988) Synuclein: a neuron-specific protein localized to the nucleus and presynaptic nerve terminal. The Journal of neuroscience : the official journal of the Society for Neuroscience 8:2804-2815.

Marras C, Schule B, Munhoz RP, Rogaeva E, Langston JW, Kasten M, Meaney C, Klein C, Wadia PM, Lim SY, Chuang RS, Zadikof C, Steeves T, Prakash KM, de Bie RM, Adeli G, Thomsen T, Johansen KK, Teive HA, Asante A, Reginold W, Lang AE (2011) Phenotype in parkinsonian and nonparkinsonian LRRK2 G2019S mutation carriers. Neurology 77:325-333.

Marti M, Mela F, Fantin M, Zucchini S, Brown JM, Witta J, Di Benedetto M, Buzas B, Reinscheid RK, Salvadori S, Guerrini R, Romualdi P, Candeletti S, Simonato M, Cox BM, Morari M (2005) Blockade of nociceptin/orphanin FQ transmission attenuates symptoms and neurodegeneration associated with Parkinson's disease. The Journal of neuroscience : the official journal of the Society for Neuroscience 25:9591-9601.

Marti M, Mela F, Ulazzi L, Hanau S, Stocchi S, Paganini F, Beani L, Bianchi C, Morari M (2003) Differential responsiveness of rat striatal nerve endings to the mitochondrial toxin 3-nitropropionic acid: implications for Huntington's disease. The European journal of neuroscience 18:759-767.

Martinez-Vicente M, Talloczy Z, Kaushik S, Massey AC, Mazzulli J, Mosharov EV, Hodara R, Fredenburg R, Wu DC, Follenzi A, Dauer W, Przedborski S, Ischiropoulos H, Lansbury PT, Sulzer D, Cuervo AM (2008) Dopamine-modified alpha-synuclein blocks chaperone-mediated autophagy. The Journal of clinical investigation 118:777-788.

Masoud ST, Vecchio LM, Bergeron Y, Hossain MM, Nguyen LT, Bermejo MK, Kile B, Sotnikova TD, Siesser WB, Gainetdinov RR, Wightman RM, Caron MG, Richardson JR, Miller GW, Ramsey AJ, Cyr M, Salahpour A (2015) Increased expression of the dopamine transporter leads to loss of dopamine neurons, oxidative stress and l-DOPA reversible motor deficits. Neurobiol Dis 74:66-75.

Matsumoto T, Wang PY, Ma W, Sung HJ, Matoba S, Hwang PM (2009) Polo-like kinases mediate cell survival in mitochondrial dysfunction. Proceedings of the National Academy of Sciences of the United States of America 106:14542-14546.

Matta S, Van Kolen K, da Cunha R, van den Bogaart G, Mandemakers W, Miskiewicz K, De Bock PJ, Morais VA, Vilain S, Haddad D, Delbroek L, Swerts J, Chavez-Gutierrez L, Esposito G, Daneels G, Karran E, Holt M, Gevaert K, Moechars DW, De Strooper B, Verstreken P (2012) LRRK2 controls an EndoA phosphorylation cycle in synaptic endocytosis. Neuron 75:1008-1021.

Mattammal MB, Haring JH, Chung HD, Raghu G, Strong R (1995) An endogenous dopaminergic neurotoxin: implication for Parkinson's disease. Neurodegeneration : a journal for neurodegenerative disorders, neuroprotection, and neuroregeneration 4:271-281.

Mattson MP, Magnus T (2006) Ageing and neuronal vulnerability. Nat Rev Neurosci 7:278-294.

Mazzulli JR, Xu YH, Sun Y, Knight AL, McLean PJ, Caldwell GA, Sidransky E, Grabowski GA, Krainc D (2011) Gaucher disease glucocerebrosidase and alpha-synuclein form a bidirectional pathogenic loop in synucleinopathies. Cell 146:37-52.

Mazzulli JR, Zunke F, Isacson O, Studer L, Krainc D (2016) alpha-Synuclein-induced lysosomal dysfunction occurs through disruptions in protein trafficking in human midbrain synucleinopathy models. Proceedings of the National Academy of Sciences of the United States of America 113:1931-1936.

McFarland MA, Ellis CE, Markey SP, Nussbaum RL (2008) Proteomics analysis identifies phosphorylation-dependent alpha-synuclein protein interactions. Molecular & cellular proteomics : MCP 7:2123-2137.

Melrose HL, Dachsel JC, Behrouz B, Lincoln SJ, Yue M, Hinkle KM, Kent CB, Korvatska E, Taylor JP, Witten L, Liang YQ, Beevers JE, Boules M, Dugger BN, Serna VA, Gaukhman A, Yu X, Castanedes-Casey M, Braithwaite AT, Ogholikhan S, Yu N, Bass D, Tyndall G, Schellenberg GD, Dickson DW, Janus C, Farrer MJ (2010) Impaired dopaminergic neurotransmission and microtubule-associated protein tau alterations in human LRRK2 transgenic mice. Neurobiol Dis 40:503-517.

Miklossy J, Arai T, Guo JP, Klegeris A, Yu S, McGeer EG, McGeer PL (2006) LRRK2 expression in normal and pathologic human brain and in human cell lines. Journal of neuropathology and experimental neurology 65:953-963.

Miller GW, Erickson JD, Perez JT, Penland SN, Mash DC, Rye DB, Levey AI (1999a) Immunochemical analysis of vesicular monoamine transporter (VMAT2) protein in Parkinson's disease. Exp Neurol 156:138-148.

Miller GW, Gainetdinov RR, Levey AI, Caron MG (1999b) Dopamine transporters and neuronal injury. Trends Pharmacol Sci 20:424-429.

Mills RD, Mulhern TD, Liu F, Culvenor JG, Cheng HC (2014) Prediction of the repeat domain structures and impact of parkinsonism-associated variations on structure and function of all functional domains of leucine-rich repeat kinase 2 (LRRK2). Human mutation 35:395-412.

Mir R, Tonelli F, Lis P, Macartney T, Polinski NK, Martinez TN, Chou MY, Howden AJM, Konig T, Hotzy C, Milenkovic I, Brucke T, Zimprich A, Sammler E, Alessi DR (2018) The Parkinson's disease VPS35[D620N] mutation enhances LRRK2-mediated Rab protein phosphorylation in mouse and human. The Biochemical journal 475:1861-1883.

Mishizen-Eberz AJ, Norris EH, Giasson BI, Hodara R, Ischiropoulos H, Lee VM, Trojanowski JQ, Lynch DR (2005) Cleavage of alpha-synuclein by calpain: potential role in degradation of fibrillized and nitrated species of alpha-synuclein. Biochemistry 44:7818-7829.

Moehle MS, Daher JP, Hull TD, Boddu R, Abdelmotilib HA, Mobley J, Kannarkat GT, Tansey MG, West AB (2015) The G2019S LRRK2 mutation increases myeloid cell chemotactic responses and enhances LRRK2 binding to actin-regulatory proteins. Human molecular genetics 24:4250-4267.

Moehle MS, Webber PJ, Tse T, Sukar N, Standaert DG, DeSilva TM, Cowell RM, West AB (2012) LRRK2 inhibition attenuates microglial inflammatory responses. J Neurosci 32:1602-1611.

Mogi M, Harada M, Narabayashi H, Inagaki H, Minami M, Nagatsu T (1996) Interleukin (IL)-1 beta, IL-2, IL-4, IL-6 and transforming growth factor-alpha levels are elevated in ventricular

cerebrospinal fluid in juvenile parkinsonism and Parkinson's disease. Neuroscience letters 211:13-16.

Moran JM, Castellanos-Pinedo F, Casado-Naranjo I, Duran-Herrera C, Ramirez-Moreno JM, Gomez M, Zurdo-Hernandez JM, Fuentes E, Ortiz-Ortiz MA, Moreno AD, Gonzalez-Polo RA, Niso-Santano M, Bravo-Sanpedro JM, Perez-Tur J, Ruiz-Mesa LM, Fuentes JM (2010) [Genetic screening for the LRRK2, G2019S and R1441 codon mutations in Parkinson's disease patients from Extremadura, Spain]. Revista de neurologia 50:591-594.

Mortiboys H, Johansen KK, Aasly JO, Bandmann O (2010) Mitochondrial impairment in patients with Parkinson disease with the G2019S mutation in LRRK2. Neurology 75:2017-2020.

Mosavi LK, Cammett TJ, Desrosiers DC, Peng ZY (2004) The ankyrin repeat as molecular architecture for protein recognition. Protein science : a publication of the Protein Society 13:1435-1448.

Nabli F, Ben Sassi S, Amouri R, Duda JE, Farrer MJ, Hentati F (2015) Motor phenotype of LRRK2-associated Parkinson's disease: a Tunisian longitudinal study. Movement disorders : official journal of the Movement Disorder Society 30:253-258.

Nakamura K, Nemani VM, Azarbal F, Skibinski G, Levy JM, Egami K, Munishkina L, Zhang J, Gardner B, Wakabayashi J, Sesaki H, Cheng Y, Finkbeiner S, Nussbaum RL, Masliah E, Edwards RH (2011) Direct membrane association drives mitochondrial fission by the Parkinson disease-associated protein alpha-synuclein. The Journal of biological chemistry 286:20710-20726.

Nalls MA, Pankratz N, Lill CM, Do CB, Hernandez DG, Saad M, DeStefano AL, Kara E, Bras J, Sharma M, Schulte C, Keller MF, Arepalli S, Letson C, Edsall C, Stefansson H, Liu X, Pliner H, Lee JH, Cheng R, International Parkinson's Disease Genomics C, Parkinson's Study Group Parkinson's Research: The Organized GI, andMe, GenePd, NeuroGenetics Research C, Hussman Institute of Human G, Ashkenazi Jewish Dataset I, Cohorts for H, Aging Research in Genetic E, North American Brain Expression C, United Kingdom Brain Expression C, Greek Parkinson's Disease C, Alzheimer Genetic Analysis G, Ikram MA, Ioannidis JP, Hadjigeorgiou GM, Bis JC, Martinez M, Perlmutter JS, Goate A, Marder K, Fiske B, Sutherland M, Xiromerisiou G, Myers RH, Clark LN, Stefansson K, Hardy JA, Heutink P, Chen H, Wood NW, Houlden H, Payami H, Brice A, Scott WK, Gasser T, Bertram L, Eriksson N, Foroud T, Singleton AB (2014) Large-scale meta-analysis of genome-wide association data identifies six new risk loci for Parkinson's disease. Nature genetics 46:989-993.

Narhi L, Wood SJ, Steavenson S, Jiang Y, Wu GM, Anafi D, Kaufman SA, Martin F, Sitney K, Denis P, Louis JC, Wypych J, Biere AL, Citron M (1999) Both familial Parkinson's disease mutations accelerate alpha-synuclein aggregation. The Journal of biological chemistry 274:9843-9846.

Nemani VM, Lu W, Berge V, Nakamura K, Onoa B, Lee MK, Chaudhry FA, Nicoll RA, Edwards RH (2010) Increased expression of alpha-synuclein reduces neurotransmitter release by inhibiting synaptic vesicle reclustering after endocytosis. Neuron 65:66-79.

Neumann M, Kahle PJ, Giasson BI, Ozmen L, Borroni E, Spooren W, Muller V, Odoy S, Fujiwara H, Hasegawa M, Iwatsubo T, Trojanowski JQ, Kretzschmar HA, Haass C (2002) Misfolded proteinase K-resistant hyperphosphorylated alpha-synuclein in aged transgenic mice with locomotor deterioration and in human alpha-synucleinopathies. The Journal of clinical investigation 110:1429-1439.

Nichols RJ, Dzamko N, Hutti JE, Cantley LC, Deak M, Moran J, Bamborough P, Reith AD, Alessi DR (2009) Substrate specificity and inhibitors of LRRK2, a protein kinase mutated in Parkinson's disease. The Biochemical journal 424:47-60.

Nichols RJ, Dzamko N, Morrice NA, Campbell DG, Deak M, Ordureau A, Macartney T, Tong Y, Shen J, Prescott AR, Alessi DR (2010) 14-3-3 binding to LRRK2 is disrupted by multiple Parkinson's disease-associated mutations and regulates cytoplasmic localization. The Biochemical journal 430:393-404.

Niu J, Yu M, Wang C, Xu Z (2012) Leucine-rich repeat kinase 2 disturbs mitochondrial dynamics via Dynamin-like protein. Journal of neurochemistry 122:650-658.
Nubling GS, Levin J, Bader B, Lorenzl S, Hillmer A, Hogen T, Kamp F, Giese A (2014) Modelling Ser129 phosphorylation inhibits membrane binding of pore-forming alpha-synuclein oligomers. PloS one 9:e98906.
Ohta E, Kubo M, Obata F (2010) Prevention of intracellular degradation of I2020T mutant LRRK2 restores its protectivity against apoptosis. Biochemical and biophysical research communications 391:242-247.
Orenstein SJ, Kuo SH, Tasset I, Arias E, Koga H, Fernandez-Carasa I, Cortes E, Honig LS, Dauer W, Consiglio A, Raya A, Sulzer D, Cuervo AM (2013) Interplay of LRRK2 with chaperone-mediated autophagy. Nat Neurosci 16:394-406.
Oueslati A (2016) Implication of Alpha-Synuclein Phosphorylation at S129 in Synucleinopathies: What Have We Learned in the Last Decade? Journal of Parkinson's disease 6:39-51.
Oueslati A, Fournier M, Lashuel HA (2010) Role of post-translational modifications in modulating the structure, function and toxicity of alpha-synuclein: implications for Parkinson's disease pathogenesis and therapies. Progress in brain research 183:115-145.
Oueslati A, Schneider BL, Aebischer P, Lashuel HA (2013) Polo-like kinase 2 regulates selective autophagic alpha-synuclein clearance and suppresses its toxicity in vivo. Proceedings of the National Academy of Sciences of the United States of America 110:E3945-3954.
Oueslati A, Ximerakis M, Vekrellis K (2014) Protein Transmission, Seeding and Degradation: Key Steps for alpha-Synuclein Prion-Like Propagation. Experimental neurobiology 23:324-336.
Paillusson S, Gomez-Suaga P, Stoica R, Little D, Gissen P, Devine MJ, Noble W, Hanger DP, Miller CCJ (2017) alpha-Synuclein binds to the ER-mitochondria tethering protein VAPB to disrupt Ca(2+) homeostasis and mitochondrial ATP production. Acta neuropathologica 134:129-149.
Paisan-Ruiz C, Jain S, Evans EW, Gilks WP, Simon J, van der Brug M, Lopez de Munain A, Aparicio S, Gil AM, Khan N, Johnson J, Martinez JR, Nicholl D, Carrera IM, Pena AS, de Silva R, Lees A, Marti-Masso JF, Perez-Tur J, Wood NW, Singleton AB (2004) Cloning of the gene containing mutations that cause PARK8-linked Parkinson's disease. Neuron 44:595-600.
Paleologou KE, Schmid AW, Rospigliosi CC, Kim HY, Lamberto GR, Fredenburg RA, Lansbury PT, Jr., Fernandez CO, Eliezer D, Zweckstetter M, Lashuel HA (2008) Phosphorylation at Ser-129 but not the phosphomimics S129E/D inhibits the fibrillation of alpha-synuclein. The Journal of biological chemistry 283:16895-16905.
Panneton WM, Kumar VB, Gan Q, Burke WJ, Galvin JE (2010) The neurotoxicity of DOPAL: behavioral and stereological evidence for its role in Parkinson disease pathogenesis. PLoS One 5:e15251.
Papkovskaia TD, Chau KY, Inesta-Vaquera F, Papkovsky DB, Healy DG, Nishio K, Staddon J, Duchen MR, Hardy J, Schapira AH, Cooper JM (2012) G2019S leucine-rich repeat kinase 2 causes uncoupling protein-mediated mitochondrial depolarization. Human molecular genetics 21:4201-4213.
Parisiadou L, Cai H (2010) LRRK2 function on actin and microtubule dynamics in Parkinson disease. Commun Integr Biol 3:396-400.
Paumier KL, Luk KC, Manfredsson FP, Kanaan NM, Lipton JW, Collier TJ, Steece-Collier K, Kemp CJ, Celano S, Schulz E, Sandoval IM, Fleming S, Dirr E, Polinski NK, Trojanowski JQ, Lee VM, Sortwell CE (2015) Intrastriatal injection of pre-formed mouse alpha-synuclein fibrils into rats triggers alpha-synuclein pathology and bilateral nigrostriatal degeneration. Neurobiology of disease 82:185-199.
Paxinos G, Franklin KBJ (2004) The mouse brain in stereotaxic coordinates. Amsterdam ; Boston: Elsevier Academic Press.
Peelaerts W, Bousset L, Van der Perren A, Moskalyuk A, Pulizzi R, Giugliano M, Van den Haute C, Melki R, Baekelandt V (2015) alpha-Synuclein strains cause distinct synucleinopathies after local and systemic administration. Nature 522:340-344.

Pfefferkorn CM, Jiang Z, Lee JC (2012) Biophysics of alpha-synuclein membrane interactions. Biochimica et biophysica acta 1818:162-171.
Pieri L, Chafey P, Le Gall M, Clary G, Melki R, Redeker V (2016) Cellular response of human neuroblastoma cells to alpha-synuclein fibrils, the main constituent of Lewy bodies. Biochimica et biophysica acta 1860:8-19.
Plowey ED, Cherra SJ, 3rd, Liu YJ, Chu CT (2008) Role of autophagy in G2019S-LRRK2-associated neurite shortening in differentiated SH-SY5Y cells. Journal of neurochemistry 105:1048-1056.
Polymeropoulos MH, Higgins JJ, Golbe LI, Johnson WG, Ide SE, Di Iorio G, Sanges G, Stenroos ES, Pho LT, Schaffer AA, Lazzarini AM, Nussbaum RL, Duvoisin RC (1996) Mapping of a gene for Parkinson's disease to chromosome 4q21-q23. Science 274:1197-1199.
Polymeropoulos MH, Lavedan C, Leroy E, Ide SE, Dehejia A, Dutra A, Pike B, Root H, Rubenstein J, Boyer R, Stenroos ES, Chandrasekharappa S, Athanassiadou A, Papapetropoulos T, Johnson WG, Lazzarini AM, Duvoisin RC, Di Iorio G, Golbe LI, Nussbaum RL (1997) Mutation in the alpha-synuclein gene identified in families with Parkinson's disease. Science 276:2045-2047.
Pozo Devoto VM, Dimopoulos N, Alloatti M, Pardi MB, Saez TM, Otero MG, Cromberg LE, Marin-Burgin A, Scassa ME, Stokin GB, Schinder AF, Sevlever G, Falzone TL (2017) alphaSynuclein control of mitochondrial homeostasis in human-derived neurons is disrupted by mutations associated with Parkinson's disease. Sci Rep 7:5042.
Pronin AN, Morris AJ, Surguchov A, Benovic JL (2000) Synucleins are a novel class of substrates for G protein-coupled receptor kinases. The Journal of biological chemistry 275:26515-26522.
Proukakis C, Dudzik CG, Brier T, MacKay DS, Cooper JM, Millhauser GL, Houlden H, Schapira AH (2013) A novel alpha-synuclein missense mutation in Parkinson disease. Neurology 80:1062-1064.
Qing H, Wong W, McGeer EG, McGeer PL (2009) Lrrk2 phosphorylates alpha synuclein at serine 129: Parkinson disease implications. Biochem Biophys Res Commun 387:149-152.
Ramsey IS, DeFelice LJ (2002) Serotonin transporter function and pharmacology are sensitive to expression level: evidence for an endogenous regulatory factor. J Biol Chem 277:14475-14482.
Ray S, Bender S, Kang S, Lin R, Glicksman MA, Liu M (2014) The Parkinson disease-linked LRRK2 protein mutation I2020T stabilizes an active state conformation leading to increased kinase activity. The Journal of biological chemistry 289:13042-13053.
Reith AD, Bamborough P, Jandu K, Andreotti D, Mensah L, Dossang P, Choi HG, Deng X, Zhang J, Alessi DR, Gray NS (2012) GSK2578215A; a potent and highly selective 2-arylmethyloxy-5-substitutent-N-arylbenzamide LRRK2 kinase inhibitor. Bioorganic & medicinal chemistry letters 22:5625-5629.
Reyes JF, Olsson TT, Lamberts JT, Devine MJ, Kunath T, Brundin P (2015) A cell culture model for monitoring alpha-synuclein cell-to-cell transfer. Neurobiology of disease 77:266-275.
Reynolds A, Doggett EA, Riddle SM, Lebakken CS, Nichols RJ (2014) LRRK2 kinase activity and biology are not uniformly predicted by its autophosphorylation and cellular phosphorylation site status. Frontiers in molecular neuroscience 7:54.
Rozas G, Guerra MJ, Labandeira-Garcia JL (1997) An automated rotarod method for quantitative drug-free evaluation of overall motor deficits in rat models of parkinsonism. Brain research Brain research protocols 2:75-84.
Rudenko IN, Cookson MR (2010) 14-3-3 proteins are promising LRRK2 interactors. The Biochemical journal 430:e5-6.
Rudenko IN, Kaganovich A, Hauser DN, Beylina A, Chia R, Ding J, Maric D, Jaffe H, Cookson MR (2012) The G2385R variant of leucine-rich repeat kinase 2 associated with Parkinson's disease is a partial loss-of-function mutation. The Biochemical journal 446:99-111.
Rueden CT, Schindelin J, Hiner MC, DeZonia BE, Walter AE, Arena ET, Eliceiri KW (2017) ImageJ2: ImageJ for the next generation of scientific image data. BMC bioinformatics 18:529.

Russo I, Berti G, Plotegher N, Bernardo G, Filograna R, Bubacco L, Greggio E (2015) Leucine-rich repeat kinase 2 positively regulates inflammation and down-regulates NF-kappaB p50 signaling in cultured microglia cells. J Neuroinflammation 12:230.

Ryan T, Bamm VV, Stykel MG, Coackley CL, Humphries KM, Jamieson-Williams R, Ambasudhan R, Mosser DD, Lipton SA, Harauz G, Ryan SD (2018) Cardiolipin exposure on the outer mitochondrial membrane modulates alpha-synuclein. Nature communications 9:817.

Sacino AN, Brooks M, Thomas MA, McKinney AB, McGarvey NH, Rutherford NJ, Ceballos-Diaz C, Robertson J, Golde TE, Giasson BI (2014) Amyloidogenic alpha-synuclein seeds do not invariably induce rapid, widespread pathology in mice. Acta neuropathologica 127:645-665.

Saha S, Ash PE, Gowda V, Liu L, Shirihai O, Wolozin B (2015) Mutations in LRRK2 potentiate age-related impairment of autophagic flux. Mol Neurodegener 10:26.

Saito Y, Kawashima A, Ruberu NN, Fujiwara H, Koyama S, Sawabe M, Arai T, Nagura H, Yamanouchi H, Hasegawa M, Iwatsubo T, Murayama S (2003) Accumulation of phosphorylated alpha-synuclein in aging human brain. J Neuropathol Exp Neurol 62:644-654.

Salvi M, Trashi E, Marin O, Negro A, Sarno S, Pinna LA (2012) Superiority of PLK-2 as alpha-synuclein phosphorylating agent relies on unique specificity determinants. Biochemical and biophysical research communications 418:156-160.

Sanberg PR, Bunsey MD, Giordano M, Norman AB (1988) The catalepsy test: its ups and downs. Behavioral neuroscience 102:748-759.

Sanchez-Guajardo V, Febbraro F, Kirik D, Romero-Ramos M (2010) Microglia acquire distinct activation profiles depending on the degree of alpha-synuclein neuropathology in a rAAV based model of Parkinson's disease. PLoS One 5:e8784.

Sanders LH, Laganiere J, Cooper O, Mak SK, Vu BJ, Huang YA, Paschon DE, Vangipuram M, Sundararajan R, Urnov FD, Langston JW, Gregory PD, Zhang HS, Greenamyre JT, Isacson O, Schule B (2014) LRRK2 mutations cause mitochondrial DNA damage in iPSC-derived neural cells from Parkinson's disease patients: reversal by gene correction. Neurobiol Dis 62:381-386.

Santpere G, Ferrer I (2009) LRRK2 and neurodegeneration. Acta neuropathologica 117:227-246.

Sato H, Arawaka S, Hara S, Fukushima S, Koga K, Koyama S, Kato T (2011) Authentically phosphorylated alpha-synuclein at Ser129 accelerates neurodegeneration in a rat model of familial Parkinson's disease. The Journal of neuroscience : the official journal of the Society for Neuroscience 31:16884-16894.

Schallert T, De Ryck M, Whishaw IQ, Ramirez VD, Teitelbaum P (1979) Excessive bracing reactions and their control by atropine and L-DOPA in an animal analog of Parkinsonism. Experimental neurology 64:33-43.

Schapansky J, Khasnavis S, DeAndrade MP, Nardozzi JD, Falkson SR, Boyd JD, Sanderson JB, Bartels T, Melrose HL, LaVoie MJ (2018) Familial knockin mutation of LRRK2 causes lysosomal dysfunction and accumulation of endogenous insoluble alpha-synuclein in neurons. Neurobiology of disease 111:26-35.

Schulte C, Gasser T (2011) Genetic basis of Parkinson's disease: inheritance, penetrance, and expression. The application of clinical genetics 4:67-80.

Sevlever D, Jiang P, Yen SH (2008) Cathepsin D is the main lysosomal enzyme involved in the degradation of alpha-synuclein and generation of its carboxy-terminally truncated species. Biochemistry 47:9678-9687.

Sheng Z, Zhang S, Bustos D, Kleinheinz T, Le Pichon CE, Dominguez SL, Solanoy HO, Drummond J, Zhang X, Ding X, Cai F, Song Q, Li X, Yue Z, van der Brug MP, Burdick DJ, Gunzner-Toste J, Chen H, Liu X, Estrada AA, Sweeney ZK, Scearce-Levie K, Moffat JG, Kirkpatrick DS, Zhu H (2012) Ser1292 autophosphorylation is an indicator of LRRK2 kinase activity and contributes to the cellular effects of PD mutations. Sci Transl Med 4:164ra161.

Shrivastava AN, Redeker V, Fritz N, Pieri L, Almeida LG, Spolidoro M, Liebmann T, Bousset L, Renner M, Lena C, Aperia A, Melki R, Triller A (2015) alpha-synuclein assemblies sequester neuronal alpha3-Na+/K+-ATPase and impair Na+ gradient. The EMBO journal 34:2408-2423.

Skibinski G, Nakamura K, Cookson MR, Finkbeiner S (2014) Mutant LRRK2 toxicity in neurons depends on LRRK2 levels and synuclein but not kinase activity or inclusion bodies. The Journal of neuroscience : the official journal of the Society for Neuroscience 34:418-433.

Sloan M, Alegre-Abarrategui J, Potgieter D, Kaufmann AK, Exley R, Deltheil T, Threlfell S, Connor-Robson N, Brimblecombe K, Wallings R, Cioroch M, Bannerman DM, Bolam JP, Magill PJ, Cragg SJ, Dodson PD, Wade-Martins R (2016) LRRK2 BAC transgenic rats develop progressive, L-DOPA-responsive motor impairment, and deficits in dopamine circuit function. Hum Mol Genet 25:951-963.

Slone SR, Lavalley N, McFerrin M, Wang B, Yacoubian TA (2015) Increased 14-3-3 phosphorylation observed in Parkinson's disease reduces neuroprotective potential of 14-3-3 proteins. Neurobiology of disease 79:1-13.

Smeyne M, Jiao Y, Shepherd KR, Smeyne RJ (2005) Glia cell number modulates sensitivity to MPTP in mice. Glia 52:144-152.

Smith WW, Pei Z, Jiang H, Moore DJ, Liang Y, West AB, Dawson VL, Dawson TM, Ross CA (2005) Leucine-rich repeat kinase 2 (LRRK2) interacts with parkin, and mutant LRRK2 induces neuronal degeneration. Proceedings of the National Academy of Sciences of the United States of America 102:18676-18681.

Snead D, Eliezer D (2014) Alpha-synuclein function and dysfunction on cellular membranes. Experimental neurobiology 23:292-313.

Song LK, Ma KL, Yuan YH, Mu Z, Song XY, Niu F, Han N, Chen NH (2015) Targeted Overexpression of alpha-Synuclein by rAAV2/1 Vectors Induces Progressive Nigrostriatal Degeneration and Increases Vulnerability to MPTP in Mouse. PLoS One 10:e0131281.

Song P, Mabrouk OS, Hershey ND, Kennedy RT (2012) In vivo neurochemical monitoring using benzoyl chloride derivatization and liquid chromatography-mass spectrometry. Analytical chemistry 84:412-419.

Spillantini MG, Schmidt ML, Lee VM, Trojanowski JQ, Jakes R, Goedert M (1997) Alpha-synuclein in Lewy bodies. Nature 388:839-840.

Stefanis L (2012) alpha-Synuclein in Parkinson's disease. Cold Spring Harb Perspect Med 2:a009399.

Stokes AH, Hastings TG, Vrana KE (1999) Cytotoxic and genotoxic potential of dopamine. J Neurosci Res 55:659-665.

Su YC, Guo X, Qi X (2015) Threonine 56 phosphorylation of Bcl-2 is required for LRRK2 G2019S-induced mitochondrial depolarization and autophagy. Biochimica et biophysica acta 1852:12-21.

Su YC, Qi X (2013) Inhibition of excessive mitochondrial fission reduced aberrant autophagy and neuronal damage caused by LRRK2 G2019S mutation. Human molecular genetics 22:4545-4561.

Subramaniam SR, Vergnes L, Franich NR, Reue K, Chesselet MF (2014) Region specific mitochondrial impairment in mice with widespread overexpression of alpha-synuclein. Neurobiology of disease 70:204-213.

Sulzer D, Zecca L (2000) Intraneuronal dopamine-quinone synthesis: a review. Neurotox Res 1:181-195.

Svarcbahs R, Julku UH, Myohanen TT (2016) Inhibition of Prolyl Oligopeptidase Restores Spontaneous Motor Behavior in the alpha-Synuclein Virus Vector-Based Parkinson's Disease Mouse Model by Decreasing alpha-Synuclein Oligomeric Species in Mouse Brain. J Neurosci 36:12485-12497.

Taguchi K, Watanabe Y, Tsujimura A, Tanaka M (2016) Brain region-dependent differential expression of alpha-synuclein. The Journal of comparative neurology 524:1236-1258.

Takahashi M, Kanuka H, Fujiwara H, Koyama A, Hasegawa M, Miura M, Iwatsubo T (2003) Phosphorylation of alpha-synuclein characteristic of synucleinopathy lesions is recapitulated in alpha-synuclein transgenic Drosophila. Neuroscience letters 336:155-158.
Taylor TN, Caudle WM, Miller GW (2011) VMAT2-Deficient Mice Display Nigral and Extranigral Pathology and Motor and Nonmotor Symptoms of Parkinson's Disease. Parkinsons Dis 2011:124165.
Taymans JM (2012) The GTPase function of LRRK2. Biochemical Society transactions 40:1063-1069.
Teismann P, Tieu K, Cohen O, Choi DK, Wu DC, Marks D, Vila M, Jackson-Lewis V, Przedborski S (2003) Pathogenic role of glial cells in Parkinson's disease. Movement disorders : official journal of the Movement Disorder Society 18:121-129.
Tenreiro S, Eckermann K, Outeiro TF (2014a) Protein phosphorylation in neurodegeneration: friend or foe? Frontiers in molecular neuroscience 7:42.
Tenreiro S, Reimao-Pinto MM, Antas P, Rino J, Wawrzycka D, Macedo D, Rosado-Ramos R, Amen T, Waiss M, Magalhaes F, Gomes A, Santos CN, Kaganovich D, Outeiro TF (2014b) Phosphorylation modulates clearance of alpha-synuclein inclusions in a yeast model of Parkinson's disease. PLoS genetics 10:e1004302.
Tewari R, Bailes E, Bunting KA, Coates JC (2010) Armadillo-repeat protein functions: questions for little creatures. Trends in cell biology 20:470-481.
Thevenet J, Pescini Gobert R, Hooft van Huijsduijnen R, Wiessner C, Sagot YJ (2011) Regulation of LRRK2 expression points to a functional role in human monocyte maturation. PloS one 6:e21519.
Thome AD, Standaert DG, Harms AS (2015) Fractalkine Signaling Regulates the Inflammatory Response in an alpha-Synuclein Model of Parkinson Disease. PLoS One 10:e0140566.
Tong Y, Pisani A, Martella G, Karouani M, Yamaguchi H, Pothos EN, Shen J (2009) R1441C mutation in LRRK2 impairs dopaminergic neurotransmission in mice. Proc Natl Acad Sci U S A 106:14622-14627.
Tozzi A, Durante V, Bastioli G, Mazzocchetti P, Novello S, Mechelli A, Morari M, Costa C, Mancini A, Di Filippo M, Calabresi P (2018) Dopamine D2 receptor activation potently inhibits striatal glutamatergic transmission in a G2019S LRRK2 genetic model of Parkinson's disease. Neurobiology of disease 118:1-8.
Tsika E, Glauser L, Moser R, Fiser A, Daniel G, Sheerin UM, Lees A, Troncoso JC, Lewis PA, Bandopadhyay R, Schneider BL, Moore DJ (2014) Parkinson's disease-linked mutations in VPS35 induce dopaminergic neurodegeneration. Human molecular genetics 23:4621-4638.
Ueda K, Fukushima H, Masliah E, Xia Y, Iwai A, Yoshimoto M, Otero DA, Kondo J, Ihara Y, Saitoh T (1993) Molecular cloning of cDNA encoding an unrecognized component of amyloid in Alzheimer disease. Proceedings of the National Academy of Sciences of the United States of America 90:11282-11286.
Ulusoy A, Decressac M, Kirik D, Bjorklund A (2010) Viral vector-mediated overexpression of alpha-synuclein as a progressive model of Parkinson's disease. Prog Brain Res 184:89-111.
Uversky VN (2003) A protein-chameleon: conformational plasticity of alpha-synuclein, a disordered protein involved in neurodegenerative disorders. Journal of biomolecular structure & dynamics 21:211-234.
Valente EM, Bentivoglio AR, Dixon PH, Ferraris A, Ialongo T, Frontali M, Albanese A, Wood NW (2001) Localization of a novel locus for autosomal recessive early-onset parkinsonism, PARK6, on human chromosome 1p35-p36. American journal of human genetics 68:895-900.
Van der Perren A, Van den Haute C, Baekelandt V (2015) Viral vector-based models of Parkinson's disease. Curr Top Behav Neurosci 22:271-301.
van Egmond WN, van Haastert PJ (2010) Characterization of the Roco protein family in Dictyostelium discoideum. Eukaryotic cell 9:751-761.

Venda LL, Cragg SJ, Buchman VL, Wade-Martins R (2010) alpha-Synuclein and dopamine at the crossroads of Parkinson's disease. Trends in neurosciences 33:559-568.
Vetter IR, Wittinghofer A (2001) The guanine nucleotide-binding switch in three dimensions. Science 294:1299-1304.
Viaro R, Calcagno M, Marti M, Borrelli E, Morari M (2013) Pharmacological and genetic evidence for pre- and postsynaptic D2 receptor involvement in motor responses to nociceptin/orphanin FQ receptor ligands. Neuropharmacology 72:126-138.
Visanji NP, Wislet-Gendebien S, Oschipok LW, Zhang G, Aubert I, Fraser PE, Tandon A (2011) Effect of Ser-129 phosphorylation on interaction of alpha-synuclein with synaptic and cellular membranes. The Journal of biological chemistry 286:35863-35873.
Volpicelli-Daley LA, Abdelmotilib H, Liu Z, Stoyka L, Daher JP, Milnerwood AJ, Unni VK, Hirst WD, Yue Z, Zhao HT, Fraser K, Kennedy RE, West AB (2016) G2019S-LRRK2 Expression Augments alpha-Synuclein Sequestration into Inclusions in Neurons. The Journal of neuroscience : the official journal of the Society for Neuroscience 36:7415-7427.
Volpicelli-Daley LA, Luk KC, Patel TP, Tanik SA, Riddle DM, Stieber A, Meaney DF, Trojanowski JQ, Lee VM (2011) Exogenous alpha-synuclein fibrils induce Lewy body pathology leading to synaptic dysfunction and neuron death. Neuron 72:57-71.
Volta M, Mabrouk OS, Bido S, Marti M, Morari M (2010) Further evidence for an involvement of nociceptin/orphanin FQ in the pathophysiology of Parkinson's disease: a behavioral and neurochemical study in reserpinized mice. Journal of neurochemistry 115:1543-1555.
Volta M, Melrose H (2017) LRRK2 mouse models: dissecting the behavior, striatal neurochemistry and neurophysiology of PD pathogenesis. Biochemical Society transactions 45:113-122.
Wallings R, Manzoni C, Bandopadhyay R (2015) Cellular processes associated with LRRK2 function and dysfunction. The FEBS journal 282:2806-2826.
Wan PT, Garnett MJ, Roe SM, Lee S, Niculescu-Duvaz D, Good VM, Jones CM, Marshall CJ, Springer CJ, Barford D, Marais R, Cancer Genome P (2004) Mechanism of activation of the RAF-ERK signaling pathway by oncogenic mutations of B-RAF. Cell 116:855-867.
Wang L, Das U, Scott DA, Tang Y, McLean PJ, Roy S (2014) alpha-synuclein multimers cluster synaptic vesicles and attenuate recycling. Curr Biol 24:2319-2326.
Wang X, Yan MH, Fujioka H, Liu J, Wilson-Delfosse A, Chen SG, Perry G, Casadesus G, Zhu X (2012) LRRK2 regulates mitochondrial dynamics and function through direct interaction with DLP1. Human molecular genetics 21:1931-1944.
Werner-Allen JW, DuMond JF, Levine RL, Bax A (2016) Toxic Dopamine Metabolite DOPAL Forms an Unexpected Dicatechol Pyrrole Adduct with Lysines of alpha-Synuclein. Angew Chem Int Ed Engl 55:7374-7378.
West AB, Moore DJ, Biskup S, Bugayenko A, Smith WW, Ross CA, Dawson VL, Dawson TM (2005) Parkinson's disease-associated mutations in leucine-rich repeat kinase 2 augment kinase activity. Proceedings of the National Academy of Sciences of the United States of America 102:16842-16847.
West AB, Moore DJ, Choi C, Andrabi SA, Li X, Dikeman D, Biskup S, Zhang Z, Lim KL, Dawson VL, Dawson TM (2007) Parkinson's disease-associated mutations in LRRK2 link enhanced GTP-binding and kinase activities to neuronal toxicity. Human molecular genetics 16:223-232.
Weygant N, Qu D, Berry WL, May R, Chandrakesan P, Owen DB, Sureban SM, Ali N, Janknecht R, Houchen CW (2014) Small molecule kinase inhibitor LRRK2-IN-1 demonstrates potent activity against colorectal and pancreatic cancer through inhibition of doublecortin-like kinase 1. Molecular cancer 13:103.
Winner B, Jappelli R, Maji SK, Desplats PA, Boyer L, Aigner S, Hetzer C, Loher T, Vilar M, Campioni S, Tzitzilonis C, Soragni A, Jessberger S, Mira H, Consiglio A, Pham E, Masliah E, Gage FH, Riek R (2011) In vivo demonstration that alpha-synuclein oligomers are toxic. Proceedings of the National Academy of Sciences of the United States of America 108:4194-4199.
Winslow AR, Chen CW, Corrochano S, Acevedo-Arozena A, Gordon DE, Peden AA, Lichtenberg M, Menzies FM, Ravikumar B, Imarisio S, Brown S, O'Kane CJ, Rubinsztein DC (2010) alpha-

Synuclein impairs macroautophagy: implications for Parkinson's disease. The Journal of cell biology 190:1023-1037.
Wong YC, Krainc D (2016) Lysosomal trafficking defects link Parkinson's disease with Gaucher's disease. Movement disorders : official journal of the Movement Disorder Society 31:1610-1618.
Xia Y, Saitoh T, Ueda K, Tanaka S, Chen X, Hashimoto M, Hsu L, Conrad C, Sundsmo M, Yoshimoto M, Thal L, Katzman R, Masliah E (2001) Characterization of the human alpha-synuclein gene: Genomic structure, transcription start site, promoter region and polymorphisms. Journal of Alzheimer's disease : JAD 3:485-494.
Xilouri M, Stefanis L (2016) Chaperone mediated autophagy in aging: Starve to prosper. Ageing research reviews 32:13-21.
Xilouri M, Vogiatzi T, Vekrellis K, Park D, Stefanis L (2009) Abberant alpha-synuclein confers toxicity to neurons in part through inhibition of chaperone-mediated autophagy. PloS one 4:e5515.
Xiong Y, Neifert S, Karuppagounder SS, Liu Q, Stankowski JN, Lee BD, Ko HS, Lee Y, Grima JC, Mao X, Jiang H, Kang SU, Swing DA, Iacovitti L, Tessarollo L, Dawson TM, Dawson VL (2018) Robust kinase- and age-dependent dopaminergic and norepinephrine neurodegeneration in LRRK2 G2019S transgenic mice. Proceedings of the National Academy of Sciences of the United States of America 115:1635-1640.
Xiong Y, Neifert S, Karuppagounder SS, Stankowski JN, Lee BD, Grima JC, Chen G, Ko HS, Lee Y, Swing D, Tessarollo L, Dawson TM, Dawson VL (2017) Overexpression of Parkinson's Disease-Associated Mutation LRRK2 G2019S in Mouse Forebrain Induces Behavioral Deficits and alpha-Synuclein Pathology. eNeuro 4.
Xu J, Kao SY, Lee FJ, Song W, Jin LW, Yankner BA (2002) Dopamine-dependent neurotoxicity of alpha-synuclein: a mechanism for selective neurodegeneration in Parkinson disease. Nature medicine 8:600-606.
Yaffe MB (2002) How do 14-3-3 proteins work?-- Gatekeeper phosphorylation and the molecular anvil hypothesis. FEBS letters 513:53-57.
Yaffe MB, Rittinger K, Volinia S, Caron PR, Aitken A, Leffers H, Gamblin SJ, Smerdon SJ, Cantley LC (1997) The structural basis for 14-3-3:phosphopeptide binding specificity. Cell 91:961-971.
Yao C, El Khoury R, Wang W, Byrd TA, Pehek EA, Thacker C, Zhu X, Smith MA, Wilson-Delfosse AL, Chen SG (2010) LRRK2-mediated neurodegeneration and dysfunction of dopaminergic neurons in a Caenorhabditis elegans model of Parkinson's disease. Neurobiol Dis 40:73-81.
Yao C, Johnson WM, Gao Y, Wang W, Zhang J, Deak M, Alessi DR, Zhu X, Mieyal JJ, Roder H, Wilson-Delfosse AL, Chen SG (2013) Kinase inhibitors arrest neurodegeneration in cell and C. elegans models of LRRK2 toxicity. Human molecular genetics 22:328-344.
Yin G, Lopes da Fonseca T, Eisbach SE, Anduaga AM, Breda C, Orcellet ML, Szego EM, Guerreiro P, Lazaro DF, Braus GH, Fernandez CO, Griesinger C, Becker S, Goody RS, Itzen A, Giorgini F, Outeiro TF, Zweckstetter M (2014) alpha-Synuclein interacts with the switch region of Rab8a in a Ser129 phosphorylation-dependent manner. Neurobiology of disease 70:149-161.
Yue M, Hinkle KM, Davies P, Trushina E, Fiesel FC, Christenson TA, Schroeder AS, Zhang L, Bowles E, Behrouz B, Lincoln SJ, Beevers JE, Milnerwood AJ, Kurti A, McLean PJ, Fryer JD, Springer W, Dickson DW, Farrer MJ, Melrose HL (2015) Progressive dopaminergic alterations and mitochondrial abnormalities in LRRK2 G2019S knock-in mice. Neurobiol Dis 78:172-195.
Zarranz JJ, Alegre J, Gomez-Esteban JC, Lezcano E, Ros R, Ampuero I, Vidal L, Hoenicka J, Rodriguez O, Atares B, Llorens V, Gomez Tortosa E, del Ser T, Munoz DG, de Yebenes JG (2004) The new mutation, E46K, of alpha-synuclein causes Parkinson and Lewy body dementia. Annals of neurology 55:164-173.
Zheng B, Liao Z, Locascio JJ, Lesniak KA, Roderick SS, Watt ML, Eklund AC, Zhang-James Y, Kim PD, Hauser MA, Grunblatt E, Moran LB, Mandel SA, Riederer P, Miller RM, Federoff HJ,

Wullner U, Papapetropoulos S, Youdim MB, Cantuti-Castelvetri I, Young AB, Vance JM, Davis RL, Hedreen JC, Adler CH, Beach TG, Graeber MB, Middleton FA, Rochet JC, Scherzer CR, Global PDGEC (2010) PGC-1alpha, a potential therapeutic target for early intervention in Parkinson's disease. Science translational medicine 2:52ra73.

Zhou H, Huang C, Tong J, Hong WC, Liu YJ, Xia XG (2011) Temporal expression of mutant LRRK2 in adult rats impairs dopamine reuptake. International journal of biological sciences 7:753-761.

Zimprich A, Biskup S, Leitner P, Lichtner P, Farrer M, Lincoln S, Kachergus J, Hulihan M, Uitti RJ, Calne DB, Stoessl AJ, Pfeiffer RF, Patenge N, Carbajal IC, Vieregge P, Asmus F, Muller-Myhsok B, Dickson DW, Meitinger T, Strom TM, Wszolek ZK, Gasser T (2004) Mutations in LRRK2 cause autosomal-dominant parkinsonism with pleomorphic pathology. Neuron 44:601-607.

ORIGINAL PAPERS

- Longo F, Mercatelli D, **Novello S**, Arcuri L, Brugnoli A, Vincenzi F, Russo I, Berti G, Mabrouk OS, Kennedy RT, Shimshek DR, Varani K, Bubacco L, Greggio E, Morari M (2017) *Age-dependent dopamine transporter dysfunction and Serine129 phospho-alpha-synuclein overload in G2019S LRRK2 mice*. Acta neuropathologica communications 5:22.

- Morari M, Brugnoli A, Pisano CA, **Novello S**, Caccia C, Melloni E, Padoani G, Vailati S, Sardina M (2018) *Safinamide Differentially Modulates In Vivo Glutamate and GABA Release in the Rat Hippocampus and Basal Ganglia*. The Journal of pharmacology and experimental therapeutics 364:198-206.

- Arcuri L, **Novello S**, Frassineti M, Mercatelli D, Pisano CA, Morella I, Fasano S, Journigan BV, Meyer ME, Polgar WE, Brambilla R, Zaveri NT, Morari M (2018) *Anti-Parkinsonian and anti-dyskinetic profiles of two novel potent and selective nociceptin/orphanin FQ receptor agonists*. British journal of pharmacology 175:782-796.

- Tozzi A, Durante V, Bastioli G, Mazzocchetti P, **Novello S**, Mechelli A, Morari M, Costa C, Mancini A, Di Filippo M, Calabresi P (2018) *Dopamine D2 receptor activation potently inhibits striatal glutamatergic transmission in a G2019S LRRK2 genetic model of Parkinson's disease*. Neurobiology of disease 118:1-8.

- **Novello S**, Arcuri L, Dovero S, Dutheil N, Shimshek DR, Bezard E, Morari M (2018) *G2019S LRRK2 mutation facilitates alpha-synuclein neuropathology in aged mice*. Neurobiology of disease 120:21-33.

- Gardoni F, Morari M, Kulisevsky J, Brugnoli A, **Novello S**, Pisano CA, Caccia C, Mellone M, Melloni E, Padoani G, Sosti V, Vailati S, Keywood C (2018) *Safinamide Modulates Striatal Glutamatergic Signaling in a Rat Model of Levodopa-Induced Dyskinesia*. The Journal of pharmacology and experimental therapeutics 367:442-451.

ABBREVIATIONS

PD: Parkinson's Disease

α-syn: α-synuclein

EOPD: early-onset PD

NAC: non-Amyloid-β component

LB: Lewy bodies

HSPs: heat shock proteins

DA: Dopamine

DAT: Dopamine active transporter

ER: endoplasmic reticulum

WT: wild type

SNc: substantia nigra pars compacta

CNS: central nervous system

MAM: mitochondria-associated ER membrane

CMA: chaperone mediated autophagy

GCase: glucocerebrosidase

BBB: blood-brain barrier

DLB: Dementia with Lewy Bodies

MSA: multiple system atrophy

Ser129: Serine-129

pS129: phosphorylation at serine residue 129

UPS: ubiquitin-proteasome system

ALP: autophagic-lysosomal pathway

PLK2: Polo-like kinase 2

PFF: α-synuclein pre-formed fibrils

LRRK2: leucine-rich repeat kinase 2

ARM: armadillo repeats

ANK: ankyrin repeats

LRR: leucine-rich repeats

COR: C-terminal of Roc

ROC: Ras-of-complex

DAPK1: death-associated protein kinases-1

MASL: malignant fibrous histiocytoma amplified sequences with leucine-rich tandem repeats 1

MAP: microtubules-associated proteins

ERM: ezrin/radixin/moesin

VPS35: vacuolar protein sorting 35 ortholog

TLR: Toll-like receptors

DLP1: Dynamin-like protein 1

PBMC: peripheral blood mononuclear cells

LPS: Lipopolysaccharides

VMAT2: Vesicular monoamine transporter 2

KI: Knock-in

KD: Kinase Dead

KO: Knock out